

# Revisiting CPL with sign-switching density: to cross or not to cross the NECB

Mine Gökçen,<sup>1,\*</sup> Özgür Akarsu,<sup>1,†</sup> and Eleonora Di Valentino<sup>2,‡</sup>

<sup>1</sup>*Department of Physics, Istanbul Technical University, Maslak 34469 Istanbul, Türkiye*

<sup>2</sup>*School of Mathematics and Statistics, University of Sheffield,  
Hounsfield Road, Sheffield S3 7RH, United Kingdom*

Recent DESI DR2 BAO measurements, when combined with CMB and SNeIa data, exhibit a  $3.2\sigma$ – $3.4\sigma$  preference for dynamical dark energy described by the Chevallier–Polarski–Linder (CPL)-parametrized equation of state. A particularly striking feature of these reconstructions is an apparent transition from an early-time phantom-like regime to a late-time quintessence-like behavior, whose theoretical realization is highly nontrivial. For positive-definite dark energy densities, this transition is often phrased as a crossing of the phantom divide line (PDL) at  $w(a) = -1$ . Allowing the dark energy density to become negative, however, renders the PDL (in the sense of  $w(a) = -1$ ) non-diagnostic as a global separator: the physically meaningful criterion is instead the null energy condition boundary (NECB),  $\rho_{\text{DE}} + p_{\text{DE}} = 0$ . We therefore test whether the data-driven preference for NECB-crossing in CPL reconstructions persists once alternative realizations of phantom behavior are admitted, specifically through sign-switching dark energy densities. To this end, we introduce and constrain two controlled phenomenological extensions of the CPL framework featuring a negative dark energy phase in the past. In the CPL $\rightarrow$ - $\Lambda$  model, the switching epoch is tied to the CPL-inferred NECB-crossing scale factor, yielding an early-time negative cosmological-constant phase, while the post-switch evolution follows the CPL branch. In the sCPL model, the CPL equation of state is maintained at all times, while the sign switch in the energy density occurs at an independent transition redshift. We find that late-time BAO and SNeIa data drive the negative-density phase beyond their effective redshift coverage, and that this requirement is the primary driver of the inferred parameter behavior. While both models are statistically disfavored relative to the baseline CPL, admitting a negative dark energy phase generally reduces the significance of deviations from a cosmological constant.

## I. INTRODUCTION

The concordance model of cosmology, the  $\Lambda$ CDM model [1, 2], has been subjected to increasingly rigorous scrutiny following the emergence of cosmological tensions [3–18] revealed by the new generation of high-precision observations [19–29]. Over the past decade, a wealth of increasingly precise measurements from a wide range of cosmological probes has become available, opening new avenues for cosmological inference and enabling nearly model-independent determinations of key cosmological parameters. In particular, the growing discrepancy between the value of the Hubble constant  $H_0$  inferred from cosmic microwave background (CMB) observations [20, 22] and that obtained from direct local distance measurements [30–63] has reached a statistically significant level above  $7\sigma$  [61]. As a result, the validity of the  $\Lambda$ CDM framework has begun to be questioned to an unprecedented extent.

A wide variety of potential solutions to the  $H_0$  tension have been proposed over the past decade. These include detailed investigations of possible observational systematics [32, 38, 46, 48, 49, 64–72], modifications of gravity [73–94], extensions of the standard cosmological parameter space [95], scenarios involving vacuum phase

transitions [96], and a broad class of models based on evolving or dynamical dark energy [12, 97–116]. Additional proposals have focused on early-time modifications of the expansion history, often referred to as early dark energy or early-universe solutions [7, 117–139], as well as late-time or local transitions in the expansion rate [140–144]. Other approaches have explored models with negative or sign-switching dark energy densities [92, 99, 106, 145–170], emerging dark energy scenarios [171–173], dark matter or neutrino-based solutions [174–179], and possible revisions of recombination-era physics [161, 180–195].

Among these possibilities, late-time departures from the  $\Lambda$ CDM model have attracted particular attention. This is largely due to the many remaining uncertainties surrounding the dark sector and the dominant role played by dark energy (DE) in shaping the recent expansion history of the Universe. Independent of the current tensions, both parametric and non-parametric reconstructions of the DE evolution [95, 100, 102, 105, 106, 133, 141, 171, 173, 196–265] have long served as important tools for probing deviations from a cosmological constant. In this context, the Chevallier–Polarski–Linder (CPL) parametrization [266, 267] of the dark energy equation of state has become one of the most widely adopted frameworks. Its popularity stems from its simplicity, flexibility, and ability to capture a broad range of time-varying dark energy behaviors within a minimal two-parameter description.

The latest Data Release 2 (DR2) of the Dark Energy Spectroscopic Instrument (DESI) collaboration, based on

\* gokcen23@itu.edu.tr

† akarsuo@itu.edu.tr

‡ e.divalentino@sheffield.ac.uk

baryon acoustic oscillation (BAO) measurements [24], has significantly reshaped the landscape of dynamical dark energy (DDE) studies. When combined with CMB anisotropy data and type Ia supernova (SNeIa) measurements, the DESI BAO results exhibit a greater-than  $3\sigma$  preference for a cold dark matter cosmology with CPL-parametrized dark energy over the standard  $\Lambda$ CDM model [29, 268]. This preference has been confirmed across a variety of data combinations and parametrizations [24, 112, 114–116, 264, 269–319]. At the same time, these results tend to exacerbate the existing  $H_0$  tension, further motivating the exploration of alternative theoretical frameworks. In particular, constructing dark energy models capable of reproducing the specific phenomenological features favored by DESI BAO presents a new set of theoretical challenges. One of the most notable characteristics emerging from CPL-based reconstructions is a transition from an early-time phantom-like regime to a late-time quintessence-like behavior, an evolution that is highly nontrivial to realize within consistent dark energy theories. In the standard setting of positive-definite dark energy density, this is often phrased as a crossing of the phantom divide line (PDL) at  $w_{\text{DE}} = -1$ , or simply “phantom crossing”. In that restricted case ( $\rho_{\text{DE}} > 0$ , as is the case for the standard CPL density by construction), the null energy condition boundary (NECB)  $\rho_{\text{DE}} + p_{\text{DE}} = 0$  is equivalent to  $w_{\text{DE}} = -1$ . Once  $\rho_{\text{DE}}$  is allowed to change sign, however, the PDL in the sense of  $w_{\text{DE}} = -1$  ceases to be a global separator: the physical regime is determined by the sign of  $\rho_{\text{DE}} + p_{\text{DE}}$  (or equivalently  $(1 + w_{\text{DE}})\rho_{\text{DE}}$ ), and  $w_{\text{DE}}$  itself can become non-diagnostic if and when  $\rho_{\text{DE}}$  crosses zero. Accordingly, throughout this work we characterize regime changes in terms of the NECB rather than  $w_{\text{DE}}$  alone [106, 265, 320, 321].

The NECB-crossing behavior inferred within the CPL parametrization was recently examined in Ref. [115], where two restricted versions of CPL dark energy were introduced by enforcing a  $\Lambda$ -like equation of state either before or after reaching the NECB. These constructions were designed to test whether the apparent crossing preferred by the data reflects a genuine physical feature or instead arises as a reconstruction artifact of the linear CPL form. While strong empirical support for an effective NECB-crossing was reported, that analysis was limited to scenarios in which the dark energy density remains positive definite. Motivated by this limitation, the purpose of the present work is to revisit the NECB-crossing preference in a more general setting, allowing the dark energy density itself to change sign. We therefore introduce two phenomenological extensions of CPL-like dark energy that incorporate sign-switching energy densities, remaining positive today while becoming negative in the past. This framework enables a direct test of whether the data-driven preference for NECB-crossing persists once alternative realizations of phantom behavior are admitted, independently of the linear CPL parametrization. Our constructions are further informed by sign-switching

scenarios such as  $\Lambda_s$ CDM [99, 148, 151, 153], which motivate exploring a negative dark energy density phase that can become dynamically relevant at intermediate redshifts.

The  $\Lambda_s$ CDM model [92, 93, 99, 148, 151, 153, 157–159, 163, 164, 166, 167, 322, 323] (see also [154, 156, 165, 324]) has attracted attention due to its ability to yield higher inferred values of  $H_0$  and, in several analyses, improved Bayesian evidences compared to the standard  $\Lambda$ CDM scenario, while also alleviating other minor tensions such as the  $S_8$  discrepancy [325].<sup>1</sup> A defining feature of this model is that the effective energy density associated with the cosmological constant undergoes a sign change, becoming negative at earlier times. The phenomenological success of  $\Lambda_s$ CDM has been attributed to this *negative* DE density phase, which can significantly affect the total cosmic energy budget at intermediate redshifts,  $z \sim 2$ , and lead to a considerable reduction in the Hubble rate at these redshifts. Within the CPL framework, a qualitatively similar effect is produced by a period of phantom-like behavior at comparable redshifts. Motivated by this analogy, we investigate whether introducing a negative-density phase into a more general DDE model can reduce the apparent need for NECB-crossing and bring the evolution closer to that of a constant equation of state.

We emphasize that, in the context of this work, crossing the PDL does not constitute a universal classifier of dark-energy behavior. A central assumption of our analysis is that the effective dark-energy density  $\rho_{\text{DE}}$  is *not* required to be positive definite: within our framework,  $\rho_{\text{DE}}$  is allowed to become negative and may even cross zero. Consequently, the usual intuition based on the condition  $w_{\text{DE}} = -1$  cannot be used as a standalone criterion to distinguish between “quintessence-like” and “phantom-like” regimes [163, 265]. Once sign-changing densities are admitted, the line  $w_{\text{DE}} = -1$  ceases to be a reliable *global* separator in the  $(w, z)$  plane [265]. The physically meaningful discriminator is instead the sign of  $\rho_{\text{DE}} + p_{\text{DE}}$ , where  $p_{\text{DE}}$  denotes the dark-energy pressure, and the corresponding boundary is the NECB, defined by  $\rho_{\text{DE}} + p_{\text{DE}} = 0$ . This follows directly from the continuity equation,

$$\frac{d\rho_{\text{DE}}}{d \ln a} = -3(\rho_{\text{DE}} + p_{\text{DE}}) = -3(1 + w_{\text{DE}})\rho_{\text{DE}}, \quad (1)$$

which shows that “phantom-like” evolution - in the sense that  $\rho_{\text{DE}}$  increases as the Universe expands - corresponds to  $\rho_{\text{DE}} + p_{\text{DE}} < 0$ , or equivalently  $(1 + w_{\text{DE}})\rho_{\text{DE}} < 0$ . This

<sup>1</sup> For further reading on theoretical and observational studies, as well as model-agnostic reconstructions, related to sign-changing dark-energy density in the late Universe, see the following (by no means exhaustive) list of references [77, 86, 88, 91, 94, 96, 97, 105, 107, 110, 113, 145, 147, 149, 150, 152, 160–162, 168, 169, 242, 264, 265, 292, 326–374].

condition implies

$$\rho_{\text{DE}} + p_{\text{DE}} < 0 \iff \begin{cases} w_{\text{DE}} < -1, & \rho_{\text{DE}} > 0, \\ w_{\text{DE}} > -1, & \rho_{\text{DE}} < 0. \end{cases} \quad (2)$$

Therefore, when  $\rho_{\text{DE}} < 0$ , the correspondence between “which side of  $w_{\text{DE}} = -1$ ” and the actual physical regime is reversed. The resulting four kinematic branches - distinguished by the signs of  $\rho_{\text{DE}}$  and  $\rho_{\text{DE}} + p_{\text{DE}}$  - are summarized in Table I. Furthermore, if and when  $\rho_{\text{DE}} \rightarrow 0$  while  $p_{\text{DE}}$  remains finite, the equation-of-state parameter  $w_{\text{DE}} = p_{\text{DE}}/\rho_{\text{DE}}$  develops a kinematic pole. Such a divergence does not signal a physical singularity in the background evolution, but rather reflects the breakdown of  $w_{\text{DE}}$  as a diagnostic at a sign switch. For this reason, to ensure clarity and internal consistency, we formulate our discussion primarily in terms of  $\rho_{\text{DE}}$  and  $\rho_{\text{DE}} + p_{\text{DE}}$  (or equivalently  $(1 + w_{\text{DE}})\rho_{\text{DE}}$ ), and we avoid interpreting regime changes and NECB-crossing based solely on the behavior of  $w_{\text{DE}}(z)$  without explicitly specifying the sign of  $\rho_{\text{DE}}$  [106, 163, 265, 320, 321].

The structure of the paper is as follows. In Section II, we introduce the models considered in this work and describe how CPL-like evolution is combined with a negative dark energy density phase. In Section III, we outline the methodology adopted for cosmological inference and summarize the observational datasets employed. In Section IV, we present the results of our analysis, including parameter constraints, posterior distributions, and quantitative assessments of model performance. We also discuss the broader implications of our findings for future model building and for the interpretation of DDE scenarios. Finally, in Section V, we summarize the main conclusions of this study and place our results in a wider cosmological context.

## II. MODELS

In this work, we consider four cosmological models that introduce late-time departures from the standard  $\Lambda$ CDM scenario within the spatially flat Friedmann-Lemaître-Robertson-Walker (FLRW) framework. We assume a cold dark matter (CDM) cosmology and explore four distinct phenomenological descriptions of DE.

For all models, the cosmic expansion as a function of the scale factor  $a = (1 + z)^{-1}$  is governed by the Friedmann equation

$$\frac{H^2(a)}{H_0^2} = \frac{\Omega_{\text{r}0}}{a^4} + \frac{\Omega_{\text{m}0}}{a^3} + \Omega_{\text{DE}0} \frac{\rho_{\text{DE}}(a)}{\rho_0}, \quad (3)$$

where  $\Omega_{\text{DE}0} \equiv 1 - \Omega_{\text{m}0} - \Omega_{\text{r}0}$  and  $\rho_0 \equiv \rho_{\text{DE}}(a = 1)$  denotes the present-day DE density. Here,  $\Omega_{\text{r}0}$ ,  $\Omega_{\text{m}0}$ , and  $\Omega_{\text{DE}0}$  represent the present-day density parameters of radiation, pressureless matter, and DE, respectively, and  $H(a)$  is the Hubble parameter. Any DE component characterized by an equation-of-state (EoS) parameter

$w_{\text{DE}}(a)$  satisfies the continuity equation

$$\frac{d\rho_{\text{DE}}}{da} = -3 \frac{\rho_{\text{DE}} + p_{\text{DE}}}{a} = -3 \frac{\rho_{\text{DE}}(1 + w_{\text{DE}})}{a}, \quad (4)$$

which leads to the general evolution of the energy density

$$|\rho_{\text{DE}}(a)| = |\rho_{\text{DE}}(a_*)| \exp \left[ -3 \int_{\ln a_*}^{\ln a} [1 + w_{\text{DE}}(a')] d \ln a' \right], \quad (5)$$

relative to a reference scale factor  $a_*$ . This equation holds piecewise on intervals where  $\rho_{\text{DE}}(a) \neq 0$  and therefore determines the magnitude  $|\rho_{\text{DE}}|$ ; if  $\rho_{\text{DE}}$  is allowed to change sign (i.e. cross zero), the sign must be specified separately by the chosen branch in phenomenological sign-switching constructions.

Below, we detail how each of the four models are constructed differently based on these same principal equations.

### A. Baseline CPL

We consider the CPL scenario as our reference for model comparison. The CPL model is defined by its dynamical EoS

$$w_{\text{CPL}}(a) = w_0 + (1 - a)w_a, \quad (6)$$

which implies the standard CPL density evolution

$$\rho_{\text{CPL}}(a) = \rho_0 a^{-3(1+w_0+w_a)} e^{-3(1-a)w_a}. \quad (7)$$

Here,  $w_0$  and  $w_a$  are constants that parametrize the linear EoS of CPL. The parameter  $w_0 \equiv w_{\text{CPL}}(a = 1)$  represents the present-day value of the EoS, while  $w_a$  quantifies the time dependence and controls the rate of deviation from  $w_0$ . The CPL form was originally introduced as a convenient reconstruction ansatz for a DE component whose behavior could be approximated by a Taylor expansion around its present-day value. The validity of this first-order truncation has been discussed and justified in Refs. [375, 376]. Nevertheless, the CPL parametrization is not sufficiently general to describe several classes of DE models, such as those with singular EoS [346] or scenarios involving negative energy densities [99, 100, 106, 114, 153]. Moreover, its linear form is not immune to possible reconstruction artifacts.

### B. $\text{CPL}_{>a_c}$ (restricted-CPL control case)

One potential reconstruction artifact associated with the linear form of  $w_{\text{CPL}}$  is the apparent crossing of  $w_{\text{DE}} = -1$  reported in CPL-based reconstructions of the DESI DR2 results (see Fig. 12 of Ref. [24]). In the standard positive-density setting, this is equivalent to reaching the NECB,  $\rho_{\text{DE}} + p_{\text{DE}} = 0$ . Such NECB

(often phrased as “phantom-divide”) crossing is generally considered problematic because of the difficulties in constructing consistent field-theory models that realize it [377], or because it may point toward modified gravity or brane-world scenarios [378]. For these reasons, any apparent NECB-crossing signal should be interpreted with caution. Recently, two restricted variants of CPL were introduced in Ref. [115] that explicitly prohibit the DE EoS from exhibiting NECB-crossing by construction, with the aim of testing the robustness of the DESI results. In our analysis, we adopt their  $\text{CPL}_{>a_c}$  model as a control case for comparison, for reasons that will become clear in Section II C.

The  $\text{CPL}_{>a_c}$  model employs the scale factor at which the CPL EoS in Eq. (6) reaches the NECB to introduce a *positive* cosmological constant phase in the DE EoS. The condition  $w_{\text{CPL}}(a_c) = -1$  defines the crossing scale factor  $a_c$  as

$$a_c = 1 + \frac{1 + w_0}{w_a} \quad (w_a \neq 0). \quad (8)$$

The EoS is then described by the CPL form after the crossing and fixed to a  $\Lambda$ -like value before it:

$$w(a) = \begin{cases} w_0 + (1 - a)w_a, & a > a_c, \\ -1, & a \leq a_c. \end{cases} \quad (9)$$

Substituting this expression into Eq. (5) yields the corresponding energy density evolution

$$\rho_{\text{DE}}(a) = \begin{cases} \rho_{\text{CPL}}(a), & a > a_c, \\ \rho_{\text{CPL}}(a_c), & a \leq a_c, \end{cases} \quad (10)$$

where continuity of  $\rho_{\text{DE}}$  at  $a_c$  is ensured by construction.

The authors of Ref. [115] concluded that NECB-crossing is indeed preferred, as evidenced by the significantly poorer fits of their restricted models compared to CPL in most cases. In contrast, in this work we investigate whether the phantom-like behavior favored by DESI BAO necessarily requires an evolving EoS that crosses the NECB. Alternative mechanisms capable of producing phantom DE could also reduce the expansion rate in the relevant redshift range and might provide an equally viable explanation. In particular, a negative DE energy density phase in the past can lead to a similar dynamical effect. Consequently, the apparent need for a dynamical EoS at  $a > a_c$  may be alleviated.

Before proceeding, we clarify what we mean by *phantom* behavior. In the standard literature, DE with  $w < -1$  is typically classified as phantom. Since most commonly studied DE models assume positive-definite energy densities, this identification is usually unambiguous. However, defining phantom behavior solely through a condition on the EoS becomes inadequate when DE is allowed to take non-positive values. More generally, phantom behavior corresponds to a DE density that decreases with decreasing redshift, that is,  $d\rho/da > 0$ . In this broader sense, when  $\rho_{\text{DE}} < 0$ , the corresponding

EoS condition is inverted and phantom-like behavior is realized for  $w > -1$ . The theoretical foundations of this reframing, particularly from the perspective of scalar field theory, are discussed in Refs. [163, 265] (see, also Ref. [106]).

In what follows, we introduce a modified version of  $\text{CPL}_{>a_c}$  designed to test whether current data allow for a sign change in the effective DE density at the epoch where the CPL EoS would otherwise cross the NECB.

### C. CPL $\rightarrow -\Lambda$ (NECB-triggered sign-switch)

Denoted as **CPL  $\rightarrow -\Lambda$** , this new model links the onset of a negative  $\Lambda$  phase to the NECB-crossing of the CPL form. The EoS evolution of this model is identical to that of  $\text{CPL}_{>a_c}$  in Eq. (9); however, its energy density undergoes a sign flip at  $a_c$ :

$$\rho_{\text{DE}}(a) = \begin{cases} \rho_{\text{CPL}}(a), & a > a_c, \\ -\rho_{\text{CPL}}(a_c), & a \leq a_c. \end{cases} \quad (11)$$

This abrupt-step sign switch is adopted here as a controlled phenomenological analogue of abrupt implementations of sign-changing vacuum energy, as considered in the abrupt  $\Lambda_s$ CDM literature (see, e.g., Refs. [99, 148, 151, 153]). The switching epoch is fixed by the CPL-inferred NECB-crossing scale factor  $a_c$ , while the post-transition evolution is governed by the CPL branch. This construction realizes an effective negative cosmological constant at early times, while matching the CPL branch in magnitude at the transition. In practice, the model behaves as a CPL DDE at late times and approaches a constant *negative* cosmological constant energy density in the pre-transition era. A limitation of this piecewise prescription is that  $\rho_{\text{DE}}$  is formally discontinuous at  $a = a_c$ . A fully predictive theoretical realization would instead feature a continuous sign switch occurring over a finite interval in  $a$  (or  $z$ ), as discussed, for example, in Refs. [92, 163]. For the purposes of this phenomenological analysis, we adopt this step-like idealization as an effective limit of a sufficiently rapid transition: the likelihoods used here are dominated by background distance observables, which depend on  $H(z)$  and on redshift integrals thereof, and are therefore expected to be largely insensitive to the value of  $\rho_{\text{DE}}$  at an isolated switching point (and, in practice, are further smoothed by the finite redshift resolution of the data). Additional motivation for the abrupt limit comes from the abrupt  $\Lambda_s$ CDM analysis of Ref. [159], where implementing a late-time ( $z \sim 2$ ) AdS-to-dS sign switch as a step-like transition was reported to have only a weak impact on the evolution of bound cosmic structures. Our primary objective is to assess whether the apparent preference for NECB crossing persists, weakens, or changes character once a negative DE density phase is admitted.

Although Ref. [115] introduced an additional variant in which the (positive) cosmological constant phase occurs

after the CPL era, we do not consider that construction here. A negative cosmological constant at the present epoch would lead to a recollapsing universe on timescales incompatible with the observed cosmic age. For this reason, we adopt only their  $\text{CPL}_{>a_c}$  model as a control case and focus instead on the modification outlined above, where the positive cosmological constant phase is replaced by a negative energy density phase.

Both  $\text{CPL} \rightarrow -\Lambda$  and  $\text{CPL}_{>a_c}$  contain CPL-only and  $\mp\Lambda$ -only regimes when  $a_c$  lies outside the physical interval  $[0, 1]$ . If the formal crossing occurs at  $a_c < 0$ , the transition takes place before the onset of the standard cosmological evolution, and the model effectively reduces to the standard CPL scenario with no realized transition. Conversely, if  $a_c > 1$ , the transition is pushed into the future and the model remains entirely in the  $\mp\Lambda$  phase throughout the observable history. Importantly, these non-transitioning regimes cannot be interpreted simply as limits of the free parameters, since  $a_c$  is a nonlinear function of  $(w_0, w_a)$ . Consequently, exploring parameter regions with  $a_c \notin [0, 1]$  complicates the interpretation of model performance and the associated parameter constraints.

To avoid the complications discussed above, we restrict the analysis to scenarios with  $a_c \in [0, 1]$  and exclude the corresponding  $(w_0, w_a)$  combinations that place the transition outside this interval. This procedure necessarily reduces the effective two-dimensional  $w_0$ - $w_a$  parameter space relative to that of  $w_0 w_a$  CDM. However, this restriction does not compromise our objectives, since the purpose of these constructions is specifically to test whether the observed NECB-crossing and dynamical behavior of CPL-parametrized DE represent genuine physical features rather than reconstruction artifacts.

It is also important to emphasize that both  $\text{CPL} \rightarrow -\Lambda$  and  $\text{CPL}_{>a_c}$  cannot simultaneously reproduce an exact cosmological constant behavior at  $a > a_c$  and realize their respective post-transition phases. In particular, since  $a_c \rightarrow \infty$  when  $w_a = 0$ , these models cannot continuously approach the  $\Lambda$  limit while retaining a transition within the physical interval. As a result, they must balance between adopting  $w_a \simeq 0$  at  $a > a_c$  and exhibiting a (negative or positive)  $\Lambda$  phase at  $a < a_c$ . This limitation is especially relevant for the  $\text{CPL} \rightarrow -\Lambda$  construction, which by design cannot smoothly reduce to the  $\Lambda_s$  CDM framework [92, 153]. For this reason, we introduce the sCPL model in the next section, which allows for that limit.

#### D. sCPL (free sign-switch in $\rho_{\text{DE}}$ )

Denoted as **sCPL**, this new model retains the CPL EoS at all times,

$$w(a) = w_0 + (1 - a)w_a \quad \text{for all } a, \quad (12)$$

but introduces an *independent* transition scale factor  $a_\dagger$  (equivalently  $z_\dagger = a_\dagger^{-1} - 1$ ), at which the DE density

$\rho_{\text{DE}}$	$w_{\text{DE}}$	$\rho_{\text{DE}}(1 + w_{\text{DE}})$	Classification
$> 0$	$> -1$	$> 0$	$p$ -quintessence
$< 0$	$< -1$	$> 0$	$n$ -quintessence
$> 0$	$< -1$	$< 0$	$p$ -phantom
$< 0$	$> -1$	$< 0$	$n$ -phantom

TABLE I. Classification of phantom and quintessence branches from the perspective of a single scalar field theory, see, e.g., Refs. [163, 265] (see, also Ref. [106]). The prefixes  $p$  and  $n$  denote  $\rho_{\text{DE}} > 0$  and  $\rho_{\text{DE}} < 0$ , respectively.

changes sign:

$$\rho_{\text{DE}}(a) = \begin{cases} \rho_{\text{CPL}}(a), & a > a_\dagger, \\ -\rho_{\text{CPL}}(a), & a \leq a_\dagger, \end{cases} \quad (13)$$

an abrupt-step idealization reminiscent of the abrupt  $\Lambda_s$  CDM scenario [148], which may be written schematically as  $\Lambda_s(a) = \Lambda_{s0} \text{sgn}(a - a_\dagger)$ , where  $\Lambda_{s0}$  denotes the post-transition (i.e. present-day) value. In the limit  $w_0 \rightarrow -1$  and  $w_a \rightarrow 0$ , this construction reduces to the abrupt  $\Lambda_s$  CDM framework [99, 148, 151, 153]. As in the  $\text{CPL} \rightarrow -\Lambda$  case, the sign flip at  $a = a_\dagger$  formally introduces a discontinuity in  $\rho_{\text{DE}}$ . A fully predictive realization would instead implement the sign switch continuously over a finite interval in  $a$  (or  $z$ ); here we adopt the same sharp-step idealization and justification discussed in Section II C, to be understood as the effective limit of a sufficiently rapid transition.

Fig. 1 illustrates the distinct behaviors of the proposed models for identical parameter choices. Compared to  $\text{CPL} \rightarrow -\Lambda$ , the key conceptual difference is that the switching epoch in sCPL is treated as an independent free parameter,  $a_\dagger$  (or equivalently  $z_\dagger$ ), and is not tied to the NECB-crossing of the CPL EoS. We impose priors such that the transition occurs in the past, thereby avoiding a negative DE density today, and that it lies approximately within the redshift range probed by late-time observations, as detailed in Section III. If the transition is pushed sufficiently early (i.e.  $a_\dagger \ll 1$ , or equivalently  $z_\dagger$  is large), the model effectively reduces to CPL behavior over the redshift range probed by the data, rendering the analysis insensitive to the underlying sign-switch mechanism.

Within the framework of our clarified definition of phantom DE, the sCPL model can exhibit a nontrivial history characterized by alternating quintessence (q) and phantom (p) regimes. Since the sign-switch is decoupled from the NECB-crossing, the ordering of events can lead to either  $p \rightarrow q \rightarrow p$  or  $q \rightarrow p \rightarrow q$  behavior, where the arrows denote increasing redshift. We further subdivide the phantom and quintessence regimes according to the sign of  $\rho_{\text{DE}}$  and the position of  $w_{\text{DE}}$  relative to the NECB, as summarized in Table I. For example, if  $w_0 > -1$ ,  $w_a < 0$ , and  $z_c < z_\dagger$ , the model follows a  $p$ -quintessence  $\rightarrow p$ -phantom  $\rightarrow n$ -quintessence sequence. Conversely, if  $w_0 < -1$ ,  $w_a > 0$ , and  $z_c < z_\dagger$ , the evolution becomes  $p$ -

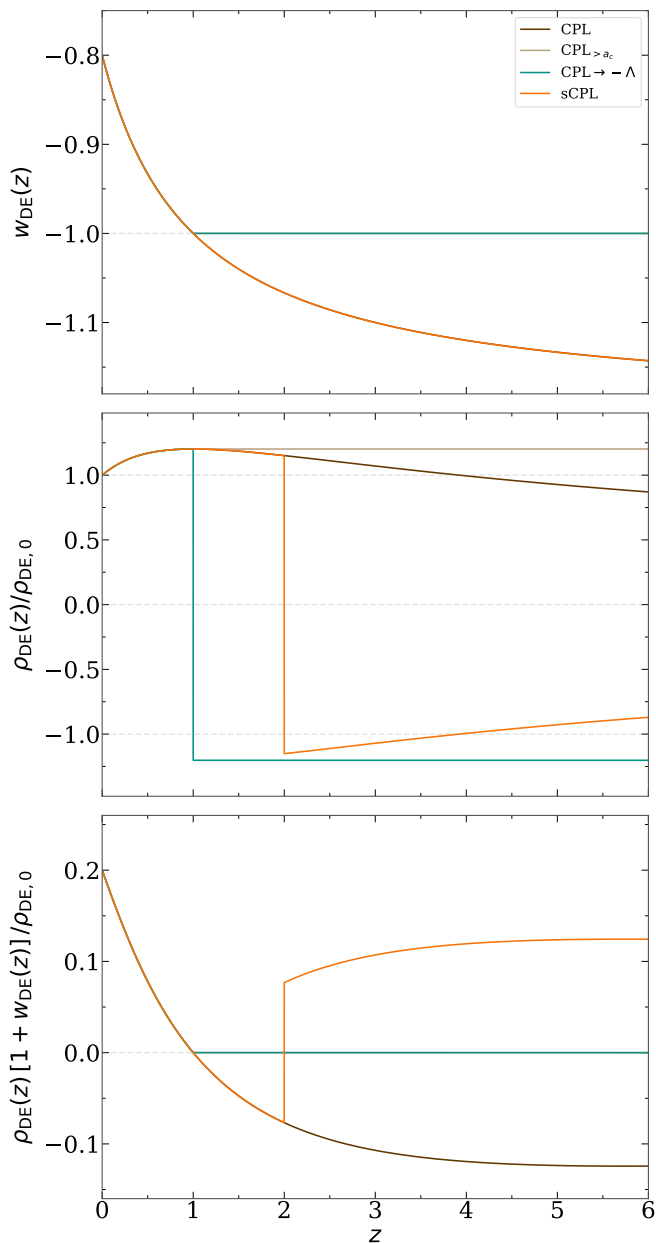


FIG. 1. Evolution of the DE EoS (**top panel**), energy density (**middle panel**), and  $\rho_{\text{DE}} + p_{\text{DE}}$  (**bottom panel**) for the models considered, assuming  $w_0 = -0.8$ ,  $w_a = -0.4$ , and  $z_{\dagger} = 2$ . In the top panel, the CPL and  $\text{CPL}_{>a_c}$  curves are indistinguishable from those of sCPL and  $\text{CPL} \rightarrow -\Lambda$ , respectively, and are therefore not separately visible. Likewise, in the bottom panel,  $\text{CPL}_{>a_c}$  and  $\text{CPL} \rightarrow -\Lambda$  exhibit identical evolutions.

phantom  $\rightarrow p$ -quintessence  $\rightarrow n$ -phantom. This possible alternation of regimes is illustrated in the bottom panel of Fig. 1. For the representative parameter choices shown, the sCPL model exhibits a sequence of  $p$ -quintessence at  $z \simeq 0$ -1, followed by  $p$ -phantom behavior at  $z \simeq 1$ -2, and finally  $n$ -quintessence at  $z \gtrsim 2$ . This example demonstrates that the equation-of-state parameter  $w_{\text{DE}}$  alone

is insufficient to characterize phantom or quintessence behavior, and highlights the fundamentally misleading nature of interpreting the condition  $w_{\text{DE}} = -1$  as a universal “phantom divide line”.

### III. DATA AND METHODOLOGY

We perform cosmological inference for the aforementioned models using the Monte Carlo Markov Chain (MCMC) sampling method implemented within the Cobaya framework [379]. Theoretical predictions are computed with the CAMB code [380, 381], where DE perturbations are treated using the parametrized post-Friedmann (PPF) prescription [382]. Convergence of the MCMC chains is assessed using the Gelman–Rubin criterion [383], requiring  $R - 1 < 0.01$ . The resulting chains are analyzed and visualized with the GetDist package [384].

In addition to the six free parameters of the  $\Lambda$ CDM model,  $w_0 w_a$ CDM introduces two extra parameters,  $w_0$  and  $w_a$ , to describe a dynamical DE EoS.  $\text{CPL} \rightarrow -\Lambda$  model is characterized by the same set of free parameters as  $w_0 w_a$ CDM. sCPL model, however, extends the parameter space by introducing the additional transition parameter  $z_{\dagger}$ , allowing for an independent sign-switch epoch. For all models, we adopt flat priors over the parameter ranges specified in Table II.

TABLE II. Model parameters and the corresponding flat prior ranges used in the cosmological inference.

Parameter	Prior
$\Omega_b h^2$	[0.005, 0.1]
$\Omega_c h^2$	[0.001, 0.99]
$\tau_{\text{reio}}$	[0.01, 0.8]
$\ln(10^{10} A_s)$	[1.61, 3.91]
$n_s$	[0.8, 1.2]
$\theta_s$	[0.5, 10]
$w_0$	[-3, 1]
$w_a$	[-3, 2]
$z_{\dagger}$	[1, 3]

For the observational datasets, we incorporate both early- and late-time measurements in various combinations.

For CMB anisotropies and lensing, we use the Planck 2018 [385, 386] power spectra. Specifically, we include the low- $\ell$  ( $\ell < 30$ ) *TT* Commander likelihood, the low- $\ell$  *EE* SimAll likelihood, and the high- $\ell$  ( $\ell \geq 30$ ) CamSpec likelihood [387, 388], together with the NPIPE PR4 lensing likelihood [389].

BAO distance measurements from DESI DR2 [24] play a central role in our analysis. Covering an effective redshift range of  $0.295 < z < 2.330$ , the DESI BAO data probe the expansion history and large-scale structure, where the dark sector contributes significantly [390].

We also include three independent SNeIa compilations to assess how the models describe the recent expansion history. The **Pantheon+** sample [25] contains 1550 objects in the range  $0.001 < z < 2.26$ . The Dark Energy Survey Year 5 (DESY5) dataset [391] comprises 1635 SNeIa from a single survey spanning  $0.10 < z < 1.13$ ; we adopt the latest **Dovekie** recalibration [28, 29]. Finally, the **Union3** compilation [27] includes 2087 objects. Although these datasets share a substantial number of supernovae, they remain statistically distinct due to differences in calibration strategies, systematic treatments, and light-curve fitting methodologies.

After the data analysis is complete, we calculate the Akaike information criterion (AIC) [392, 393]

$$\text{AIC}_{\text{model}} \equiv -2 \ln \mathcal{L}_{\text{max}} + 2k = \chi_{\text{min}}^2 + 2k \quad (14)$$

for each model and dataset combination as a measure of relative goodness of fit, where  $\mathcal{L}_{\text{max}}$  is the maximum likelihood achieved by the model,  $k$  is the number of free parameters, and  $\chi_{\text{min}}^2$  is the minimum chi-square value. By explicitly accounting for  $k$ , the AIC allows for a fair comparison between models with different numbers of parameters, as is the case for sCPL relative to the other constructions. A positive  $\Delta\text{AIC} \equiv \text{AIC}_{\text{model}} - \text{AIC}_{\text{CPL}}$  indicates a worse fit to the data with respect to the reference CPL model.

In addition to the AIC, we compute the Bayesian evidence

$$\mathcal{Z}_i = \mathcal{Z}(d | \mathcal{M}_i) \equiv \int d\theta p(d | \theta, \mathcal{M}_i) p(\theta | \mathcal{M}_i) \quad (15)$$

using a modified version of the **MCEvidence**<sup>2,3</sup> package [394, 395], fully compatible with **Cobaya**. Here,  $\mathcal{L} = p(d | \theta, \mathcal{M}_i)$  denotes the likelihood and  $p(\theta | \mathcal{M}_i)$  the prior distribution. The quantities  $d$ ,  $\theta$ , and  $\mathcal{M}_i$  represent the observational data, the model parameters, and a specific model, respectively. The Bayes factor  $\mathcal{B}_{ij}$  is then defined as

$$\ln \mathcal{B}_{ij} \equiv \ln \mathcal{Z}_i - \ln \mathcal{Z}_j \quad (16)$$

with respect to the reference CPL model, denoted by the subscript  $j$ . We interpret  $\mathcal{B}_{ij}$  using the Jeffreys scale, as summarized in Tab. 1 of Ref. [396]. A Bayes factor satisfying  $|\ln \mathcal{B}_{ij}| < 1$  corresponds to inconclusive evidence, meaning that the two models perform comparably. If  $1 \lesssim |\ln \mathcal{B}_{ij}| \lesssim 2.5$ ,  $2.5 \lesssim |\ln \mathcal{B}_{ij}| \lesssim 5$ , or  $|\ln \mathcal{B}_{ij}| \gtrsim 5$ , the evidence against the model under consideration is weak, moderate, or strong, respectively. In our convention, negative values of  $\ln \mathcal{B}_{ij}$  indicate poorer performance of  $\mathcal{M}_i$  relative to CPL. Although the Bayesian evidence provides a more comprehensive assessment of model performance by accounting for prior volume effects and the full

posterior structure, compared to  $\chi^2$ -based criteria, the AIC remains a useful indicator of relative goodness of fit. For this reason, we consider both  $\Delta\text{AIC}$  and  $\mathcal{B}_{ij}$  in our model comparison.

## IV. RESULTS

Table III summarizes the marginalized parameter constraints, reported as posterior means with 68% credible intervals (CI), for the four models considered: CPL $\rightarrow -\Lambda$  (introduced in Section II C), sCPL (introduced in Section II D), the restricted CPL $_{>a_c}$  control case, and the reference CPL model. We also report the derived NECB-crossing redshift  $z_c = a_c^{-1} - 1$ , where  $a_c = 1 + (1 + w_0)/w_a$ . Near  $w_a \simeq 0$ , this mapping becomes ill-conditioned and  $z_c$  may develop strongly non-Gaussian tails; therefore, percentile-based summaries are generally more robust than mean-based estimates. We further quote the best-fit  $\Delta\text{AIC}$  (Eq. (14)) and Bayes factors (Eq. (16)) to assess model performance relative to the reference CPL.

Triangular posterior plots for the free parameters are shown in Figs. 2 and 9, illustrating the impact of each dataset combination on individual models and the relative performance of different models under the same dataset combination, respectively. The corresponding one-dimensional posteriors of the derived parameter  $z_c$  are displayed in Figs. 3 and 10. The following subsections highlight the main trends in the parameter constraints for each model and discuss the principal findings of our analysis.

### A. Baseline CPL

We first examine the impact of different dataset combinations on the inferred cosmological parameters. When DESI BAO data are included, our results are broadly consistent with those reported in Tab. V of the DESI DR2 analysis [24], with minor differences arising from our use of Planck 2018 measurements alone for CMB anisotropies and the updated **Dovekie** likelihood [28] for DESY5. In addition, we present results obtained from CMB and SNeIa combinations without BAO data, which allow us to isolate parameter tendencies driven specifically by BAO information.

Planck-only constraints on  $(w_0, w_a)$  remain broad and largely degeneracy dominated, permitting a wide range of  $(H_0, \Omega_{m0})$ . In the base combination, where DESI BAO data are added to Planck CMB, the CPL model favors a more dynamical region with  $w_0 = -0.44 \pm 0.21$  and  $w_a = -1.66 \pm 0.59$ , accompanied by lower  $H_0$  and higher  $\Omega_{m0}$  compared to SNeIa-only combinations. Including low-redshift SNeIa distance data (Pantheon+, DESY5, Union3) significantly tightens the CPL constraints and correspondingly reduces parameter uncertainties in the extended models. With or without DESI BAO, analyses incorporating SNeIa data generally yield higher  $H_0$  and

<sup>2</sup> [github.com/williamgiare/wgcosmo/tree/main](https://github.com/williamgiare/wgcosmo/tree/main)

<sup>3</sup> [github.com/yabebalFantaye/MCEvidence](https://github.com/yabebalFantaye/MCEvidence)

TABLE III. Constraints for the models considered. We report the best-fit  $\Delta\text{AIC} \equiv \text{AIC}_{\text{model}} - \text{AIC}_{\text{CPL}}$  and the Bayes factors  $\mathcal{B}_{ij}$ , defined as  $\ln \mathcal{B}_{ij} = \ln \mathcal{Z}_{\text{model}} - \ln \mathcal{Z}_{\text{CPL}}$ , where CPL is the reference model. Positive  $\Delta\text{AIC}$  values indicate worse fits to the data, whereas negative values of  $\ln \mathcal{B}_{ij}$  indicate poorer performance of model  $\mathcal{M}_i$  relative to CPL. The quantity  $z_c$  denotes the (derived) redshift of NECB-crossing, i.e. the redshift corresponding to  $a_c$  when such a crossing occurs within the relevant domain. For  $z_c$  entries marked by \*, we report the upper and lower 68% confidence bounds around the posterior peak (rather than the mean) when the mean lies outside the credible interval, which can occur for distributions with long tails. For one-sided constraints, we quote the 95% confidence interval.

Model / Dataset	$w_0$	$w_a$	$z_{\dagger}$	$\Omega_{m0}$	$H_0$ [km/s/Mpc]	$z_c$	$\Delta\text{AIC}$	$\ln \mathcal{B}_{ij}$
<b>CPL <math>\rightarrow -\Lambda</math></b>								
Planck	$-1.83^{+0.14}_{-0.40}$	$1.12^{+0.58}_{-0.33}$	—	$0.1864^{+0.0070}_{-0.044}$	$> 73.4$	$2.04^{+6.22}_{-0.31}$ *	0.55	-2.19
Planck+Pantheon+	$-0.904^{+0.040}_{-0.055}$	$-0.138^{+0.097}_{-0.056}$	—	$0.309^{+0.020}_{-0.012}$	$67.9^{+1.1}_{-2.1}$	$2.02^{+3.80}_{-0.22}$ *	1.25	-3.28
Planck+DESY5	$-0.882^{+0.048}_{-0.067}$	$-0.177^{+0.13}_{-0.070}$	—	$0.304^{+0.022}_{-0.014}$	$68.5^{+1.3}_{-2.4}$	$1.83^{+2.37}_{-0.19}$ *	2.30	-4.10
Planck+Union3	$-0.820^{+0.062}_{-0.081}$	$-0.257^{+0.15}_{-0.088}$	—	$0.322^{+0.022}_{-0.016}$	$66.6^{+1.4}_{-2.3}$	$1.90^{+3.59}_{-0.14}$ *	2.71	-3.99
Base: Planck+DESI	$-0.99 \pm 0.11$	$-0.02 \pm 0.15$	—	$0.303 \pm 0.016$	$68.5 \pm 1.8$	$2.67^{+1.34}_{-0.15}$ *	5.51	-6.19
Base+Pantheon+	$-0.925 \pm 0.033$	$-0.102^{+0.046}_{-0.040}$	—	$0.3119 \pm 0.0054$	$67.43 \pm 0.56$	$2.61^{+0.76}_{-0.12}$ *	1.15	-4.29
Base+DESY5	$-0.921^{+0.028}_{-0.032}$	$-0.107^{+0.045}_{-0.038}$	—	$0.3124 \pm 0.0050$	$67.38 \pm 0.52$	$2.57^{+0.76}_{-0.08}$ *	2.87	-5.20
Base+Union3	$-0.881 \pm 0.045$	$-0.163^{+0.065}_{-0.058}$	—	$0.3184 \pm 0.0070$	$66.75 \pm 0.73$	$2.58^{+0.59}_{-0.12}$ *	5.46	-6.51
<b>sCPL</b>								
Planck	$-1.19^{+0.44}_{-0.61}$	$< 1.29$	—	$0.220^{+0.019}_{-0.078}$	$> 63.3$	$-0.033^{+0.694}_{-0.564}$ *	3.36	-0.30
Planck+Pantheon+	$-0.859 \pm 0.090$	$-0.48 \pm 0.49$	$> 1.70$	$0.302^{+0.011}_{-0.010}$	$68.6^{+1.0}_{-1.3}$	$0.330^{+0.244}_{-0.329}$ *	3.46	-0.80
Planck+DESY5	$-0.772 \pm 0.099$	$-0.89 \pm 0.51$	$> 1.58$	$0.302^{+0.010}_{-0.0084}$	$68.66^{+0.81}_{-1.1}$	$0.302^{+0.12}_{-0.060}$	4.29	-0.75
Planck+Union3	$-0.64 \pm 0.14$	$-1.30 \pm 0.67$	$> 1.58$	$0.313 \pm 0.013$	$67.5 \pm 1.3$	$0.379^{+0.095}_{-0.11}$	2.23	-0.76
Base: Planck+DESI	$-0.50 \pm 0.23$	$-1.45 \pm 0.67$	$> 2.37$	$0.346 \pm 0.023$	$64.3^{+1.9}_{-2.3}$	$0.5 \pm 4.3$	3.82	-1.13
Base+Pantheon+	$-0.870 \pm 0.058$	$-0.42 \pm 0.23$	$> 2.38$	$0.3112 \pm 0.0057$	$67.68 \pm 0.60$	$0.45^{+0.22}_{-0.14}$	2.89	-0.63
Base+DESY5	$-0.837 \pm 0.060$	$-0.55 \pm 0.25$	$> 2.38$	$0.3128 \pm 0.0053$	$67.52 \pm 0.54$	$0.359^{+0.15}_{-0.062}$	2.40	-0.93
Base+Union3	$-0.704 \pm 0.093$	$-0.91 \pm 0.32$	$> 2.38$	$0.3261 \pm 0.0088$	$66.14 \pm 0.87$	$0.545^{+0.063}_{-0.14}$	2.20	-1.13
<b>CPL<math>_{&gt;a_c}</math> (control)</b>								
Planck	$-1.17^{+0.77}_{-1.0}$	—	—	$0.286^{+0.078}_{-0.14}$	$73^{+20}_{-20}$	$< 7.22$	0.97	-0.58
Planck+Pantheon+	$-0.864^{+0.087}_{-0.11}$	$< 0.392$	—	$0.3208 \pm 0.0069$	$66.69 \pm 0.57$	$< 0.273$	0.13	2.17
Planck+DESY5	$-0.792^{+0.12}_{-0.091}$	$< -0.456$	—	$0.3236 \pm 0.0069$	$66.37 \pm 0.59$	$0.149^{+0.050}_{-0.10}$	1.31	1.59
Planck+Union3	$-0.67^{+0.16}_{-0.12}$	$< -0.455$	—	$0.336 \pm 0.011$	$65.19^{+0.94}_{-1.1}$	$0.282^{+0.044}_{-0.16}$	0.57	0.76
Base: Planck+DESI	$-0.79 \pm 0.23$	$< 0.939$	—	$0.314^{+0.013}_{-0.017}$	$67.0^{+1.7}_{-1.5}$	$< 0.517$	10.96	-2.59
Base+Pantheon+	$-0.821^{+0.11}_{-0.094}$	$< -0.272$	—	$0.3097^{+0.0052}_{-0.0060}$	$67.39^{+0.61}_{-0.52}$	$0.159^{+0.026}_{-0.12}$	7.12	-0.28
Base+DESY5	$-0.738^{+0.11}_{-0.080}$	$< -0.559$	—	$0.3140 \pm 0.0057$	$66.90^{+0.53}_{-0.60}$	$0.191^{+0.041}_{-0.094}$	5.62	-0.37
Base+Union3	$-0.63^{+0.15}_{-0.11}$	$< -0.625$	—	$0.3246 \pm 0.0094$	$65.80^{+0.83}_{-1.0}$	$0.272^{+0.069}_{-0.12}$	8.50	-2.06
<b>CPL (reference)</b>								
Planck	$-1.16^{+0.49}_{-0.67}$	—	—	$0.237^{+0.025}_{-0.094}$	$80^{+20}_{-7}$	$-0.11^{+0.88}_{-0.63}$	0.00	0.00
Planck+Pantheon+	$-0.878 \pm 0.097$	$-0.51^{+0.51}_{-0.43}$	—	$0.313^{+0.011}_{-0.013}$	$67.5 \pm 1.2$	$0.227^{+0.24}_{-0.096}$	0.00	0.00
Planck+DESY5	$-0.79 \pm 0.10$	$-0.90 \pm 0.50$	—	$0.3100^{+0.0087}_{-0.0099}$	$67.78 \pm 0.94$	$0.377^{+0.020}_{-0.122}$	0.00	0.00
Planck+Union3	$-0.66 \pm 0.14$	$-1.28 \pm 0.66$	—	$0.320^{+0.012}_{-0.014}$	$66.7 \pm 1.3$	$0.395^{+0.108}_{-0.098}$ *	0.00	0.00
Base: Planck+DESI	$-0.44 \pm 0.21$	$-1.66 \pm 0.59$	—	$0.351 \pm 0.021$	$63.8^{+1.7}_{-2.1}$	$0.500^{+0.069}_{-0.054}$	0.00	0.00
Base+Pantheon+	$-0.842 \pm 0.054$	$-0.59^{+0.21}_{-0.19}$	—	$0.3111 \pm 0.0057$	$67.50 \pm 0.59$	$0.38 \pm 0.53$	0.00	0.00
Base+DESY5	$-0.812 \pm 0.056$	$-0.69^{+0.23}_{-0.20}$	—	$0.3131 \pm 0.0053$	$67.32 \pm 0.55$	$0.385^{+0.052}_{-0.085}$	0.00	0.00
Base+Union3	$-0.674 \pm 0.088$	$-1.05^{+0.31}_{-0.27}$	—	$0.3270 \pm 0.0088$	$65.91 \pm 0.85$	$0.462^{+0.055}_{-0.081}$	0.00	0.00

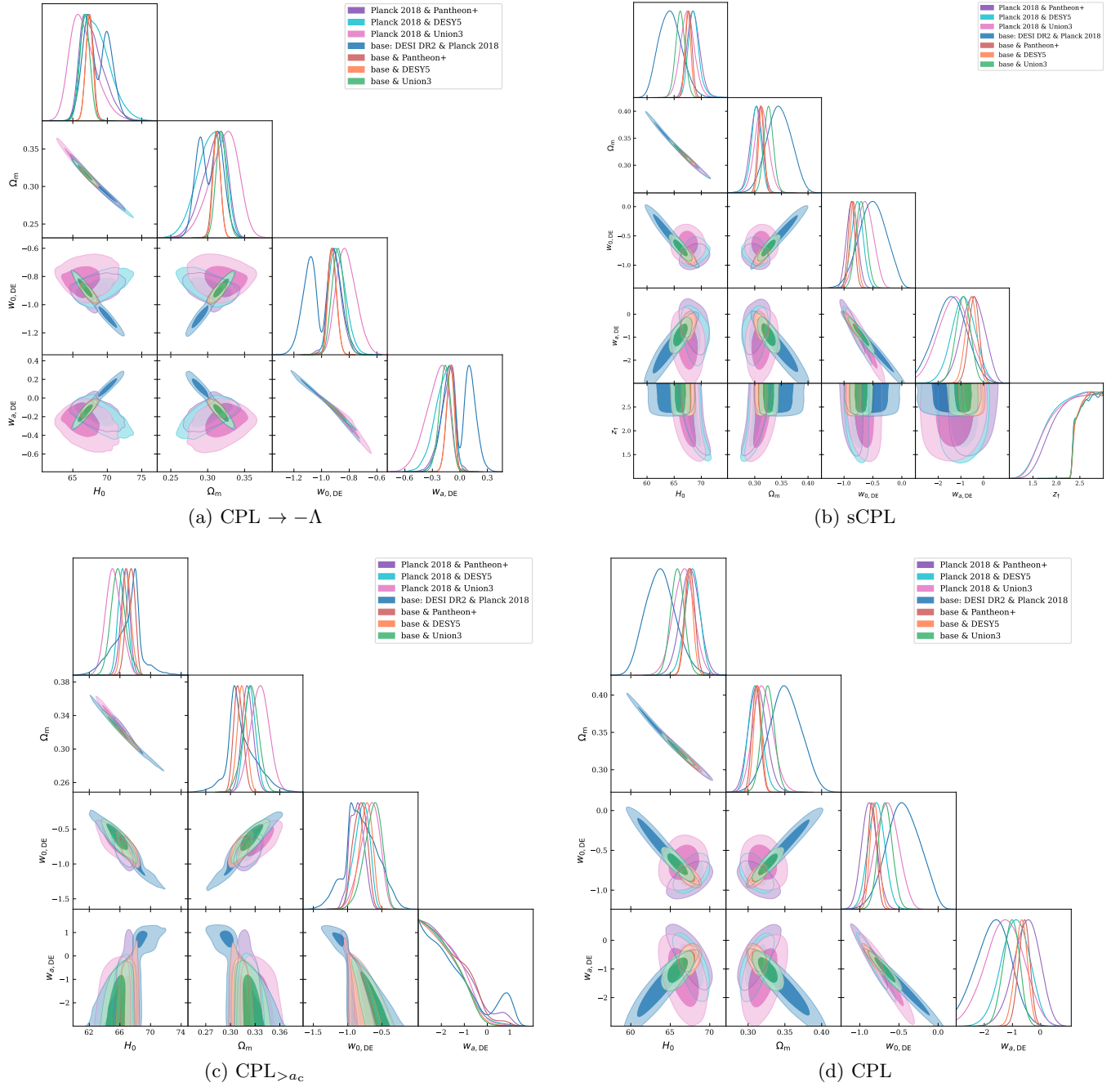


FIG. 2. One- and two-dimensional marginalized posterior distributions of the model parameters for the four models considered, obtained using various dataset combinations.

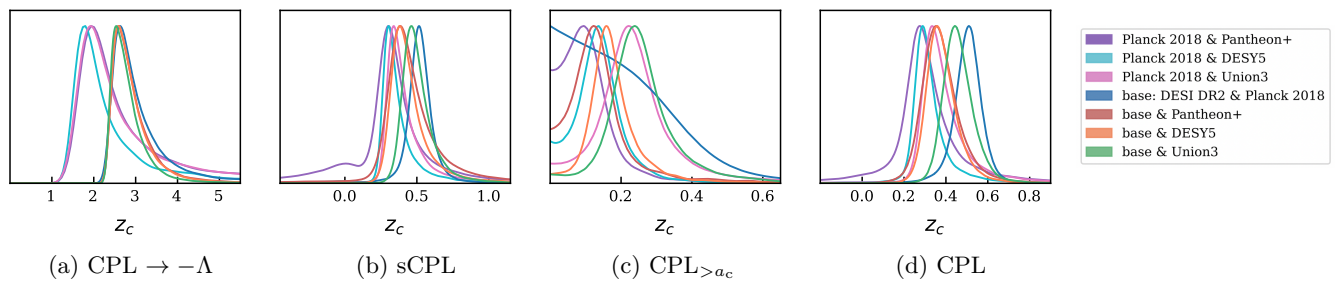


FIG. 3. One-dimensional posterior distributions of the derived parameter  $z_c$  for the models considered. Colors correspond to the various dataset combinations labeled in Fig. 2.

lower  $\Omega_{m0}$  relative to the base (Planck + DESI) combination. These trends are illustrated in Fig. 2(d).

Overall, we observe a relatively well-defined preferred range for the NECB-crossing redshift  $z_c$  (Fig. 3(d)). Aside from the Planck-only case, which remains weakly constrained, the CPL model tends to predict crossing within the redshift interval probed by current observations. If CPL provides the best effective description of the data, this suggests that the inferred crossing captures a feature of the reconstructed DE density evolution from Eq. (7) in that redshift range. Whether this behavior reflects a genuine physical transition or instead arises as an artifact of the CPL parametrization remains an open question, motivating the alternative constructions explored in this work.

### B. $\text{CPL}_{>a_c}$ (restricted-CPL control case)

The  $\text{CPL}_{>a_c}$  case restricts the CPL parameter space by replacing the dynamical CPL evolution with a cosmological constant at the location of a NECB-crossing, provided that  $a_c \in [0, 1]$ . This restriction is strongly disfavored for DESI-inclusive datasets, as reflected by large penalties of  $\Delta\text{AIC} \simeq 11$  for the base combination and  $\Delta\text{AIC} \simeq 5\text{--}9$  for the base + SNeIa combinations. When DESI BAO data are excluded, however, the fits improve substantially, even though the corresponding parameter constraints do not change dramatically. This behavior indicates that the preference for NECB-crossing is primarily driven by the DESI BAO information. In the absence of DESI, the data no longer favor the region  $w(a) < -1$ , and the tension with the  $\text{CPL}_{>a_c}$  construction—which forbids NECB-crossing by design—is effectively removed. As a result, the restricted model becomes compatible with the remaining datasets and yields improved goodness of fit.

Another noteworthy feature emerges in the constraints on  $w_a$ . Across all dataset combinations, an upper bound of  $w_a \lesssim -1.60$  at 68% confidence level is required, enforcing a strictly attenuating DE density toward the past. Since NECB-crossing is forbidden by construction in this model, the slowing-down effect preferred by the expansion history is instead accommodated by reaching

the NECB earlier than in the CPL case, as illustrated in Fig. 10. This mechanism, however, comes at a cost. Such early phantom-limiting behavior is not well supported by the data, as reflected by the systematically worse  $\Delta\text{AIC}$  values. This tension arises because the DE density is forced to remain constant for  $a < a_c$ , yielding an energy density that is lower than its present-day value but still insufficiently suppressed at intermediate redshifts  $z \sim 0.5\text{--}1$ , where a reduced expansion rate is preferred. The authors of Ref. [115] similarly note that the constraints on  $w_a$  are largely prior dominated, particularly at the lower boundary, and that extending the prior range does not lead to improved fits. In addition, we find that allowing more negative values of  $w_a$  would merely push  $a_c$  further outside the physical interval  $[0, 1]$ , causing those regions of parameter space to be effectively excluded from the analysis.

Overall, the  $\text{CPL}_{>a_c}$  construction provides an essential baseline for interpreting our subsequent results for the  $\text{CPL} \rightarrow -\Lambda$  model, in which the energy density of the cosmological constant phase is taken to be negative. This progression allows us to disentangle the effects of introducing a negative DE density from those arising solely due to the imposed restriction on the CPL evolution.

### C. $\text{CPL} \rightarrow -\Lambda$ (NECB-triggered sign-switch)

At first glance, the  $\text{CPL} \rightarrow -\Lambda$  model (introduced in Section II C) appears to yield only modest improvements. However, a closer inspection of the DE parameters reveals a more informative picture. In all dataset combinations, the  $(w_0, w_a)$  constraints are driven systematically toward their  $\Lambda$  limits, namely  $w_0 \rightarrow -1$  and  $w_a \rightarrow 0$ . For instance, for the base (Planck + DESI) combination we obtain  $w_0 = -0.99 \pm 0.11$  and  $w_a = -0.02 \pm 0.15$ , in stark contrast to the reference CPL constraints  $w_0 = -0.44 \pm 0.21$  and  $w_a = -1.66 \pm 0.59$ . This behavior is illustrated in Fig. 4, where we compare the DE EoS parameter constraints of CPL and  $\text{CPL} \rightarrow -\Lambda$ . The introduction of a negative DE density phase in the past effectively tilts the reconstructed  $w(z)$  evolution, forcing the model to mimic a less dynamical, nearly constant equation of state parameter in order to remain com-

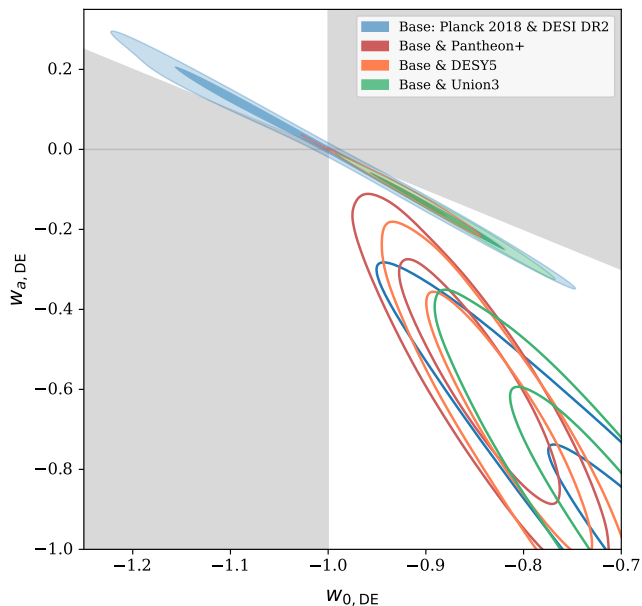


FIG. 4. Comparison of dark energy parameter constraints for  $\text{CPL} \rightarrow -\Lambda$  (filled contours) and the reference CPL model (solid contours). Shaded regions indicate scenarios with  $w < -1$  or  $w > -1$  at all times, corresponding to the absence of a transition within  $a \in [0, 1]$ . In these regions, the model effectively reduces to CPL.

patible with the data. In this sense, the apparent shift toward  $\Lambda$ -like values is not a genuine preference of the data, but rather a consequence of the imposed negative-density phase compensating for the expansion history otherwise achieved through phantom-like dynamics in CPL. Despite this enforced convergence toward  $\Lambda$ -like behavior, the preference for a genuinely dynamical EoS remains evident in the Bayesian model comparison. For analyses including DESI BAO, CPL is strongly favored over  $\text{CPL} \rightarrow -\Lambda$ , while for Planck + SNeIa-only combinations the evidence ranges from mild to strong in favor of CPL.

Moreover, the constraints on both  $w_0$  and  $w_a$ , and in particular on  $w_a$ , become significantly tighter (Fig. 9), while the contours for  $H_0$  and  $\Omega_{m0}$  remain comparably broad. We first note that the forbidden regions with  $a_c \notin [0, 1]$ , shaded in Fig. 4, play only a minor role in this tightening, as the 95% confidence contours barely approach these boundaries. Instead, fixing the DE density to a negative  $\Lambda$  phase at intermediate-to-high redshifts imposes a more constrained expansion history, directly restricting the range of  $(w_0, w_a)$  combinations that can reproduce the observed distance measures. This effect is therefore the primary driver of the tighter posteriors. The tightening is further enhanced by the data preference for a specific range of the derived parameter  $a_c$ , which sets the location of the DE density sign switch in the  $\text{CPL} \rightarrow -\Lambda$  model. As shown in Fig. 3(a), the inferred values of  $z_c$  remain consistent across the two main classes of dataset combinations, namely CMB + SNeIa

and CMB + BAO + SNeIa. This behavior contrasts with that of other models, either lacking a sign switch altogether or featuring an additional free parameter controlling it. Notably, we find  $z_c \gtrsim 2.46$  for all combinations that include DESI BAO. This is not accidental. The  $\text{CPL} \rightarrow -\Lambda$  model exhibits a sharp reduction in  $\chi_{\text{DESI}}^2$  immediately beyond  $z = 2.33$ , corresponding to the highest effective redshift probed by DESI BAO. In other words, negative DE densities are strongly disfavored within the redshift range directly constrained by BAO measurements. Finally, Fig. 10 shows that the  $z_c$  posteriors are relatively broad for this model, which is reflected in the tight constraints on  $w_a$ . Although  $w_a$  is the primary free parameter and  $z_c$  is derived, the combined evidence indicates that the tightening of the DE EoS constraints ultimately originates from the data preference for a restricted range of  $z_c$ .

In principle, as  $w_0 \rightarrow -1$  and  $w_a \rightarrow 0$ , tensions with a cosmological constant would be expected to diminish. However, the simultaneous reduction in parameter uncertainties limits the extent to which the inferred significances decrease. To quantify the proximity of our constraints to  $\Lambda$ , we adopt the null hypothesis  $w_0 = -1$  and  $w_a = 0$  and compute the significance of deviations from these values in units of equivalent Gaussian standard deviations  $\sigma$ . We evaluate the one-dimensional significances  $N_{w_0}$  and  $N_{w_a}$  using a two-tailed test [397], which remains applicable in the presence of non-Gaussian posteriors. For the joint two-dimensional significance  $N_\Lambda$ , we perform an analogous test in the  $(w_0, w_a)$  posterior space and apply Wilks' theorem [398] to express the probability of obtaining a non-null result in terms of Gaussian-equivalent sigmas. The resulting values are reported in Table IV. For the base combination, we find  $N_\Lambda = 0.8\sigma$ , indicating that the tension with  $\Lambda$  is fully resolved. For the remaining dataset combinations, despite the constraints moving closer to the cosmological constant limit and their associated significances being reduced,  $(w_0, w_a)$  remain mildly displaced from  $\Lambda$ , with  $N_\Lambda$  in the range  $2.3\sigma - 2.9\sigma$ .

Unfortunately, the  $\text{CPL} \rightarrow -\Lambda$  model does not improve the overall fit to the data. The corresponding  $\Delta\text{AIC}$  values are positive for all dataset combinations, indicating worse performance than CPL, since both models have the same number of free parameters. This degradation is more pronounced for DESI-inclusive analyses. This behavior can be understood as a consequence of the model construction: both  $\text{CPL} \rightarrow -\Lambda$  and  $\text{CPL}_{>a_c}$  exclude a pure cosmological constant as a viable realization within their CPL-parametrized regime. This interpretation is supported by the systematic shifts observed in the  $(w_0, w_a)$  constraints. In particular, as  $w_a \rightarrow 0$ , the crossing scale factor  $a_c \rightarrow \infty$ , and the transition to the (negative) cosmological constant phase never occurs within the physically relevant redshift range. Enforcing  $w_a \neq 0$  therefore impacts the inferred constraints, leading to visibly non-Gaussian posteriors in cases where the parameter space approaches  $w_a \simeq 0$ . This non-Gaussianity is most

TABLE IV. Significance of deviations from  $w_0 = -1$  and  $w_a = 0$ , expressed in terms of equivalent Gaussian standard deviations  $\sigma$ . The one-dimensional significances are reported as  $N_{w_0}$  and  $N_{w_a}$ , while the joint two-dimensional significance is denoted by  $N_\Lambda$ . For a detailed discussion of one- and two-dimensional significances, see the Appendix (Section A).

Model	Dataset	$N_{w_0}$	$N_{w_a}$	$N_\Lambda$
CPL $\rightarrow -\Lambda$	Planck	1.9 $\sigma$	1.9 $\sigma$	2.7 $\sigma$
CPL $\rightarrow -\Lambda$	Planck+Pantheon+	2.1 $\sigma$	2.1 $\sigma$	2.3 $\sigma$
CPL $\rightarrow -\Lambda$	Planck+DESY5	2.5 $\sigma$	2.5 $\sigma$	2.5 $\sigma$
CPL $\rightarrow -\Lambda$	Planck+Union3	2.9 $\sigma$	2.9 $\sigma$	2.9 $\sigma$
CPL $\rightarrow -\Lambda$	Base (Planck+DESI)	0.1 $\sigma$	0.1 $\sigma$	0.8 $\sigma$
CPL $\rightarrow -\Lambda$	Base+Pantheon+	2.3 $\sigma$	2.3 $\sigma$	2.3 $\sigma$
CPL $\rightarrow -\Lambda$	Base+DESY5	2.6 $\sigma$	2.6 $\sigma$	2.6 $\sigma$
CPL $\rightarrow -\Lambda$	Base+Union3	2.7 $\sigma$	2.7 $\sigma$	2.6 $\sigma$
sCPL	Planck	0.4 $\sigma$	0.7 $\sigma$	2.3 $\sigma$
sCPL	Planck+Pantheon+	1.6 $\sigma$	0.9 $\sigma$	2.0 $\sigma$
sCPL	Planck+DESY5	2.4 $\sigma$	1.7 $\sigma$	2.7 $\sigma$
sCPL	Planck+Union3	2.7 $\sigma$	2.0 $\sigma$	3.0 $\sigma$
sCPL	Base (Planck+DESI)	2.1 $\sigma$	2.2 $\sigma$	2.2 $\sigma$
sCPL	Base+Pantheon+	2.2 $\sigma$	1.8 $\sigma$	2.3 $\sigma$
sCPL	Base+DESY5	2.8 $\sigma$	2.3 $\sigma$	2.8 $\sigma$
sCPL	Base+Union3	3.4 $\sigma$	3.0 $\sigma$	3.3 $\sigma$
CPL $_{>a_c}$	Planck	0.0 $\sigma$	0.0 $\sigma$	2.5 $\sigma$
CPL $_{>a_c}$	Planck+Pantheon+	1.6 $\sigma$	1.6 $\sigma$	2.1 $\sigma$
CPL $_{>a_c}$	Planck+DESY5	2.1 $\sigma$	2.1 $\sigma$	2.4 $\sigma$
CPL $_{>a_c}$	Planck+Union3	2.2 $\sigma$	2.2 $\sigma$	2.6 $\sigma$
CPL $_{>a_c}$	Base (Planck+DESI)	1.1 $\sigma$	1.1 $\sigma$	2.0 $\sigma$
CPL $_{>a_c}$	Base+Pantheon+	1.9 $\sigma$	1.9 $\sigma$	2.4 $\sigma$
CPL $_{>a_c}$	Base+DESY5	2.5 $\sigma$	2.5 $\sigma$	2.9 $\sigma$
CPL $_{>a_c}$	Base+Union3	2.6 $\sigma$	2.6 $\sigma$	3.0 $\sigma$
CPL	Planck	0.3 $\sigma$	0.7 $\sigma$	2.2 $\sigma$
CPL	Planck+Pantheon+	1.3 $\sigma$	1.1 $\sigma$	1.3 $\sigma$
CPL	Planck+DESY5	2.0 $\sigma$	1.9 $\sigma$	2.0 $\sigma$
CPL	Planck+Union3	2.4 $\sigma$	2.0 $\sigma$	2.5 $\sigma$
CPL	Base (Planck+DESI)	2.7 $\sigma$	3.1 $\sigma$	3.3 $\sigma$
CPL	Base+Pantheon+	3.0 $\sigma$	3.1 $\sigma$	3.2 $\sigma$
CPL	Base+DESY5	3.5 $\sigma$	3.7 $\sigma$	3.7 $\sigma$
CPL	Base+Union3	3.9 $\sigma$	3.8 $\sigma$	3.9 $\sigma$

pronounced for the base combination, where we observe a clear bimodality that warrants a dedicated discussion in Section IV E.

Concerning the  $H_0$  tension, the CPL $\rightarrow -\Lambda$  model does not substantially outperform the other scenarios. Nevertheless, an interesting exception arises for the base (Planck + DESI) dataset combination. While CPL $_{>a_c}$  already raises the CPL value of  $H_0 =$

$63.8^{+1.7}_{-2.1} \text{ km s}^{-1} \text{ Mpc}^{-1}$  to  $H_0 = 67.0^{+1.7}_{-1.5} \text{ km s}^{-1} \text{ Mpc}^{-1}$ , the inclusion of a negative DE density phase in CPL $\rightarrow -\Lambda$  further increases the inferred value to  $H_0 = 68.5 \pm 1.8 \text{ km s}^{-1} \text{ Mpc}^{-1}$ , the highest among the models considered. Although this shift remains insufficient to reconcile the inferred value with the local distance ladder measurement,  $H_0^{\text{LD}} = 73.50 \pm 0.81 \text{ km s}^{-1} \text{ Mpc}^{-1}$  [32, 61], the results obtained with CPL $\rightarrow -\Lambda$  nevertheless provide valuable insight into how modifications of the DE sector influence late-time expansion and point toward directions for future model building.

#### D. sCPL (free sign-switch in $\rho_{\text{DE}}$ )

We introduced the sCPL model in Section II D with a free sign-switch redshift  $z_\dagger$  in order to superpose the dynamical CPL EoS with a sign-switching feature in a more flexible manner. Unlike CPL $\rightarrow -\Lambda$ , the sCPL construction admits a limit in which it reduces to the  $\Lambda_s$ CDM model [99, 148, 151, 153]. A key result for sCPL is that, across all dataset combinations, the inferred posteriors closely track those of CPL for DESI-inclusive analyses and differ only mildly when DESI BAO data are excluded. When the lower bound on  $z_\dagger$  exceeds the maximum redshift probed by a given dataset, the analysis becomes insensitive to the presence of the sign switch, rendering sCPL effectively indistinguishable from CPL. In particular, DESI BAO data drive  $z_\dagger \gtrsim 2.38$ , placing the transition entirely beyond the redshift range probed by BAO measurements. In contrast, SNeIa data alone allow the switch to occur, but typically near the upper end of the prior range specified in Section III, reflecting their more limited constraining power. We note that the upper prior bound on  $z_\dagger$  lies relatively close to the inferred lower limits. While standard practice would suggest extending the prior range, doing so would be inconsequential in this case. The posteriors plateau once the transition is pushed beyond the observationally accessible redshift range, where no data are available to break the degeneracy between CPL and sCPL.

Despite yielding parameter constraints that closely resemble those of CPL, the sCPL model incurs larger  $\Delta\text{AIC}$  values due to the penalty associated with its additional free parameter. For the Planck + SNeIa combinations, sCPL therefore fits the data slightly worse than CPL. These degraded  $\Delta\text{AIC}$  values can be partially attributed to the “sandwich” behavior permitted by the model. Across all dataset combinations, the preferred solutions correspond to a  $p$ -phantom  $\rightarrow p$ -quintessence  $\rightarrow n$ -phantom evolution. We also note that sCPL is subject to the same limitations as CPL, namely the abundance of low-redshift data relative to intermediate-redshift information, as well as reconstruction artifacts inherent to a linear EoS parametrization. In the absence of higher-redshift BAO measurements, it remains difficult to determine whether CPL is favored because it effectively mimics a slowly sign-switching DE [163] or

because the DE EoS is genuinely dynamical.

Furthermore, while the DE parameters retain their preference for dynamical behavior, the inclusion of negative DE densities at early times leads only to modest increases in the inferred values of  $H_0$ . As a result, the anticipated alleviation of the  $H_0$  tension is not realized. Nevertheless, the sCPL model remains valuable for interpreting the results obtained with  $\text{CPL} \rightarrow -\Lambda$ . In particular, when comparing the constraints on  $z_{\dagger}$  in sCPL with the derived  $z_c$  constraints in  $\text{CPL} \rightarrow -\Lambda$ , we find a striking similarity between the two. Since  $z_{\dagger}$  and  $z_c$  respectively mark the redshifts at which the transition to negative DE densities occurs, this correspondence suggests that the location of the sign switch plays a decisive role in shaping the  $(w_0, w_a)$  constraints in the  $\text{CPL} \rightarrow -\Lambda$  model. This observation also helps explain why the inferred  $z_c$  values in  $\text{CPL} \rightarrow -\Lambda$  differ markedly from those of the other models. The DESI BAO data exhibit a strong disfavoring of negative DE densities within their effective redshift range, to the extent that the model selects less favorable  $(w_0, w_a)$  values rather than allowing a sign switch to occur where BAO measurements are active. With these considerations in mind, we now proceed to the next section, where we elaborate on one of the core findings of this work.

### E. Bimodality in the base constraints of $\text{CPL} \rightarrow -\Lambda$

As noted earlier, in the limit  $w_a \rightarrow 0$  the crossing scale factor  $a_c$  becomes ill defined. For models in which  $a_c$  plays a central role in characterizing the DE behavior—namely  $\text{CPL} \rightarrow -\Lambda$  and  $\text{CPL}_{>a_c}$ —this leads to non-Gaussian features in the posterior distributions (Fig. 2(a) and (c)). In dataset combinations including SNeIa, these deviations are relatively mild and primarily appear as skewness and extended tails. In contrast, for the base (Planck + DESI) combination, we observe highly irregular posteriors for  $\text{CPL}_{>a_c}$  and a pronounced bimodality with nearly resolved peaks for the  $\text{CPL} \rightarrow -\Lambda$  model. In this section, we investigate the origin of the bimodality observed in the base results for  $\text{CPL} \rightarrow -\Lambda$  and discuss its cosmological implications.

We begin by separating the two modes of the bimodal posterior in order to study each regime independently. Following standard practice, we impose a cut in post-processing and reweight the chains to implement the split illustrated in Fig. 5. We find that the bimodality observed across all parameters is consistently resolved by a cut at  $w_a = 0$ . The two resulting regions are treated as independent chains, from which we derive the parameter constraints reported in Table V. The posterior separates into two mirror branches across the  $w_a = 0$  boundary: a “red” mode characterized by  $w_0 < -1$  and  $w_a > 0$ , and a “blue” mode with  $w_0 > -1$  and  $w_a < 0$ . Despite their different locations in the  $(w_0, w_a)$  plane, both branches correspond to comparable NECB-crossing redshifts,  $z_c \sim 3$ . From the bottom panel of Fig. 6, we identify the red

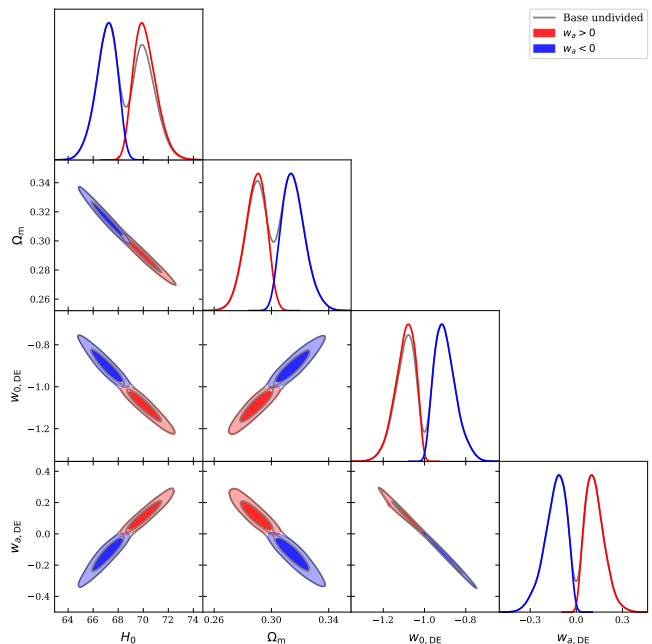


FIG. 5. The base (Planck 2018 + DESI DR2) analysis chain is divided at  $w_a = 0$  into two regions in order to investigate the bimodality observed in the  $\text{CPL} \rightarrow -\Lambda$  posteriors.

TABLE V. The base (Planck 2018 + DESI DR2) analysis chain is divided at  $w_a = 0$  into two regions to investigate the bimodality observed in the  $\text{CPL} \rightarrow -\Lambda$  posteriors. The table reports the posterior mean and the 68% CI for each region.

	Whole Chain	$w_a > 0$	$w_a < 0$
$w_0$	$-0.99 \pm 0.11$	$-1.095^{+0.060}_{-0.036}$	$-0.899^{+0.038}_{-0.063}$
$w_a$	$-0.02 \pm 0.15$	$0.121^{+0.045}_{-0.077}$	$-0.138^{+0.088}_{-0.051}$
$H_0$	$68.5 \pm 1.8$	$70.17^{+0.72}_{-1.1}$	$67.04^{+0.97}_{-0.69}$
$\Omega_{m0}$	$0.303 \pm 0.016$	$0.2888^{+0.0084}_{-0.0065}$	$0.3157^{+0.0066}_{-0.0094}$
$z_c$ *	$2.67^{+1.34}_{-0.15}$	$2.79^{+2.80}_{-0.15}$	$2.60^{+0.68}_{-0.14}$
$\Delta\chi^2_{\min}$ **	0.0000	0.2766	0.0000

\* For the derived parameter  $z_c$ , we report the posterior peak rather than the mean. For distributions with long tails, the mean may lie outside the 68% confidence interval, which is the case here.

\*\*  $\Delta\chi^2_{\min} \equiv \chi^2_{\min, \text{region}} - \chi^2_{\min, \text{whole-chain}}$

mode as a thawing-like phantom and the blue mode as a freezing-like quintessence scenario *at late times*, based on which side of the NECB these evolutions occupy. However, for a sign-switching scenario to be physically realized with a smooth transition in  $\rho_{\text{DE}}$ , both modes must exhibit phantom behavior at  $a = a_c$  in order to satisfy the continuity equation in Eq. (4). The absence of bimodality in the control  $\text{CPL}_{>a_c}$  case, together with the unimodal base  $z_c$  posteriors (Fig. 9(a)), indicates that the presence of negative energy densities and the location of the transition to that regime play a central role in shaping the  $(w_0, w_a)$  constraints. To illustrate this, we show

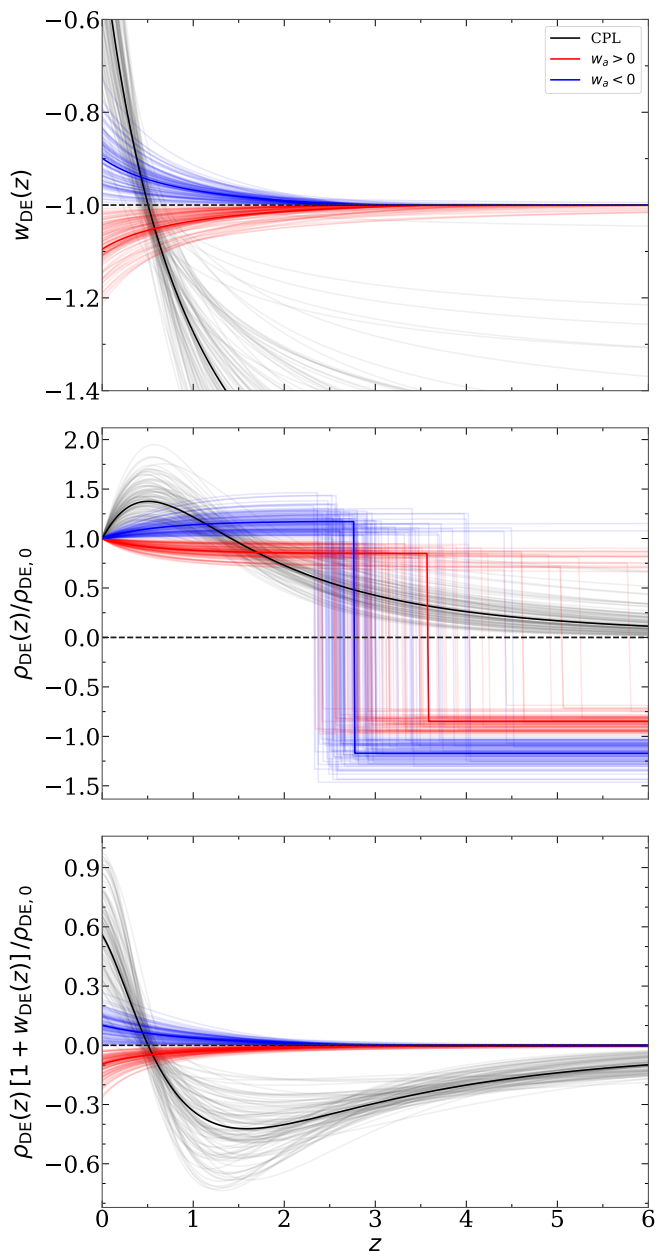


FIG. 6. Dark energy EoS evolution (**top panel**), energy density evolution (**middle panel**), and  $\rho_{\text{DE}} + p_{\text{DE}}$  (**bottom panel**) for the two regions identified in Fig. 5, compared with the CPL-parametrized dark energy constraints from the base analysis. Multiple evolution histories are generated using the `fgivenx` package [399], with fainter lines corresponding to samples further from the posterior mean.

the corresponding DE EoS and energy density evolutions for the two bimodal branches in Fig. 6. The asymptotic behavior of the EoS in both regimes approaches the  $\Lambda$  limit, suggesting that each branch tends toward a  $\Lambda_s$ CDM-like scenario, even though the model cannot reduce to it by construction. Technically, the model does not forbid  $w_a = 0$ . Rather, it enforces a choice between remaining in a CPL phase with  $w_a = 0$  or undergoing a

transition to a negative-density era. This tension naturally raises the question of why the sCPL model does not converge to its  $\Lambda_s$ CDM limit. While a definitive answer lies beyond the scope of this phenomenological study, we can state with certainty that once a negative cosmological constant phase is imposed in the past, consistency of the CPL branch at  $a < a_c$  requires the equation of state parameter to approach  $w = -1$ .

We examine the impact of different combinations of Planck, DESI, and Pantheon+ data on the posterior distributions in Fig. 7. The Pantheon+ data exhibit a strong preference for the blue ( $w_a < 0$ ) branch over the red one, both with and without the inclusion of DESI BAO. As SNeIa provide dense low-redshift distance information, they break the near symmetry between the ( $w_0 < -1, w_a > 0$ ) and ( $w_0 > -1, w_a < 0$ ) solutions, which can otherwise reproduce integrated high-redshift distance constraints with comparable accuracy. DESI BAO alone remain largely insensitive to the distinction between the two DE regimes. However, when combined with SNeIa data, the parameter space corresponding to the red ( $w_a > 0$ ) branch becomes increasingly suppressed. In contrast to the CPL case, SNeIa-only combinations favor lower values of  $H_0$ , whereas the base combination allows for higher values, reaching  $H_0 = 70.17^{+0.72}_{-1.1} \text{ km s}^{-1} \text{ Mpc}^{-1}$  within the red ( $w_a > 0$ ) region. The resultant expansion rates, viz., comoving Hubble parameters  $\dot{a} = H(z)/(1+z)$ , inferred from the different dataset combinations are shown in Fig. 8, alongside the corresponding CPL predictions. Beyond  $z \simeq 0.2$ , the expansion histories are largely indistinguishable across models. The most pronounced differences emerge in the redshift interval  $z \simeq 0.2-1.2$ , where the six scenarios display the greatest diversity in their expansion behavior. At higher redshifts, CPL generally predicts lower expansion rates. The sensitivity of the models to the expansion dynamics within this intermediate-redshift window suggests that their relative performance is strongly influenced by how accurately they capture the evolution during this phase of slowed expansion.

To summarize, splitting the base chain at  $w_a = 0$  cleanly isolates the two modes and simultaneously removes the apparent bimodality in the remaining parameters (Fig. 5 and Table V). While the two branches lead to distinct late-time parameter shifts, most notably in  $H_0$  and  $\Omega_{m0}$ , they share an identical early-time behavior. In both cases,  $w(z) \rightarrow -1$  at high redshift (Fig. 6 (top)), reflecting the fact that the CPL  $\rightarrow -\Lambda$  construction enforces a vacuum-like phase prior to  $a_c$ , with the pre-transition energy density fixed to a constant negative plateau. Consequently, the observed bimodality should not be interpreted as evidence for two qualitatively different early-time cosmological histories. Rather, it reflects the likelihood exploring two comparable ways of positioning the NECB-triggered transition while remaining close to a  $\Lambda$ -like evolution away from the switching epoch.

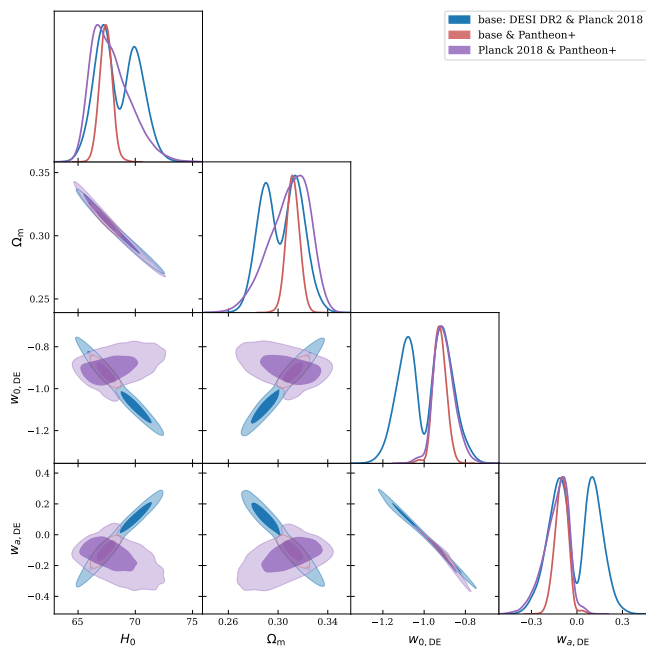


FIG. 7. One- and two-dimensional posterior distributions of the  $\text{CPL} \rightarrow -\Lambda$  model parameters for various combinations of three datasets.

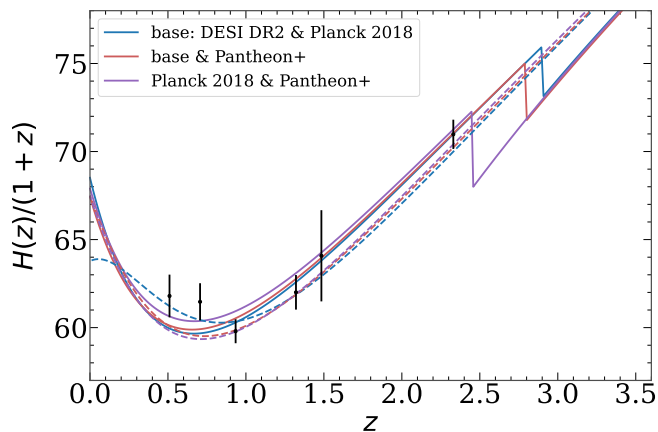


FIG. 8. Redshift evolution of the comoving Hubble parameter  $\dot{a} = H(z)/(1+z)$  for  $\text{CPL} \rightarrow -\Lambda$  (solid lines) and CPL (dashed lines). The evolutions are computed using the posterior mean parameter values. Black points correspond to DESI BAO Hubble distance measurements  $D_H(z)/r_d$  from Tab. IV of Ref. [24], assuming  $r_d = 147.05$  Mpc. Note how the inclusion of SNe data strongly influences which peak of the base posterior is preferred.

## V. CONCLUSIONS

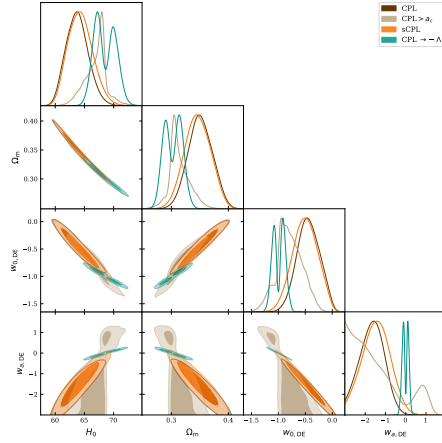
In this work, we have examined whether the apparent preference for phantom behavior inferred from current data (traditionally identified through an EoS crossing of  $w = -1$ ) persists when DE is described in its most general form, allowing for sign changes in the energy density

and hence NECB-crossing. Our goal was deliberately narrow: to test whether the dynamical EoS behavior favored by DESI BAO remains necessary once alternative realizations of phantom behavior are permitted. To this end, we adopted a generalized definition of phantom evolution and introduced two phenomenological models that allow the DE energy density to switch sign, remaining positive today while becoming negative in the past. The motivation for considering a negative DE density phase is informed by scenarios in which such a transition occurs at intermediate redshifts, comparable to those where the expansion rate  $\dot{a}$  is observed to be suppressed. In particular, models such as  $\Lambda_s$ CDM exhibit a spontaneous sign switch in the DE density around  $z \sim 2$ , preceding the epoch  $z \simeq 0.5-1$  where the expansion history deviates most strongly from a pure  $\Lambda$  behavior.

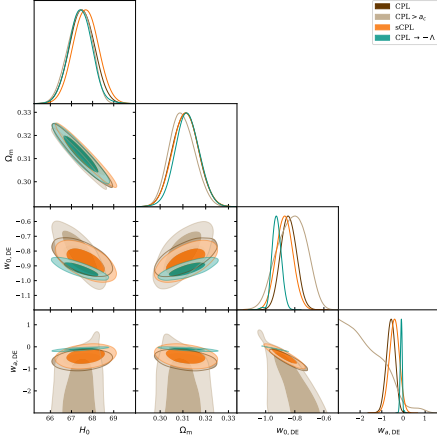
We constructed  $\text{CPL} \rightarrow -\Lambda$  (Section II C) inspired by the work of Ref. [115], where the  $\text{CPL}_{>a_c}$  model was introduced to assess whether NECB-crossing of the EoS is a reconstruction artifact of the linear CPL parametrization or an effective physical feature. We adopted  $\text{CPL}_{>a_c}$  as a control case, retaining its prescription of a cosmological constant phase beyond the NECB-crossing at a redshift implicitly determined by  $(w_0, w_a)$ , but replacing the positive cosmological constant with a negative one. Complementarily, in sCPL (Section II D), we decoupled the location of the sign switch from NECB-crossing by introducing an explicit transition redshift and allowing the EoS to cross the NECB freely. Together, these constructions enabled us to disentangle which model ingredients are actually favored by the data, within the set of four models considered: CPL,  $\text{CPL}_{>a_c}$ ,  $\text{CPL} \rightarrow -\Lambda$ , and sCPL.

The results convey a clear message: DESI BAO data do not permit negative DE densities within the redshift range they probe. In both sign-switching models, the redshift parameter determining the transition is driven beyond the effective redshift of the highest- $z$  DESI BAO measurement ( $z = 2.33$ , corresponding to  $a = 0.300$ ). In sCPL, this manifests as a lower bound on the free parameter  $z_{\dagger}$ , while in  $\text{CPL} \rightarrow -\Lambda$  it appears through the derived NECB-crossing redshift  $z_c$ . Consequently, sCPL effectively reduces to CPL from a data analysis perspective, with nearly indistinguishable parameter constraints. In contrast, enforcing  $a_c = 1 + (1 + w_0)/w_a > 0.300$  in the  $\text{CPL} \rightarrow -\Lambda$  model has nontrivial implications for the  $(w_0, w_a)$  posteriors. This requirement is effectively equivalent to imposing  $(1 + w_0)/w_a < -0.700$ . A similar constraint arises in Planck + SNeIa-only analyses, where the transition is pushed to  $z_c \gtrsim 1.7$ , corresponding to  $(1 + w_0)/w_a \lesssim -0.630$ . These additional practical restrictions, together with the requirement  $w_a \neq 0$  inherent to the  $\text{CPL} \rightarrow -\Lambda$  construction, lead to a significant tightening of the  $(w_0, w_a)$  constraints while leaving  $(\Omega_{m0}, H_0)$  largely unaffected.

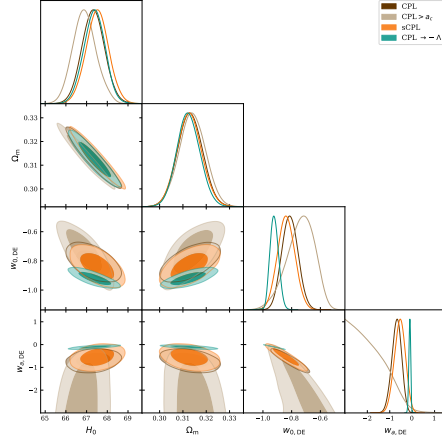
Moreover, the presence of a negative DE density phase in the  $\text{CPL} \rightarrow -\Lambda$  model naturally drives the EoS parameters toward a less dynamical regime. This effect is most



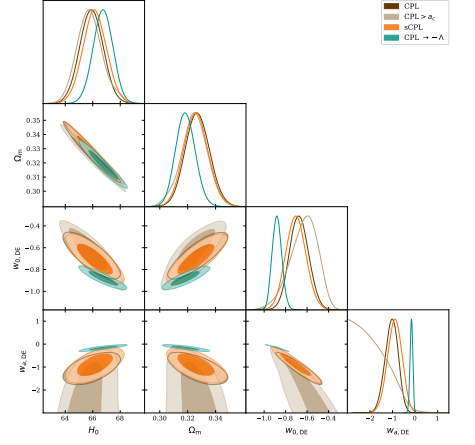
(a) Base: Planck 2018 &amp; DESI DR2



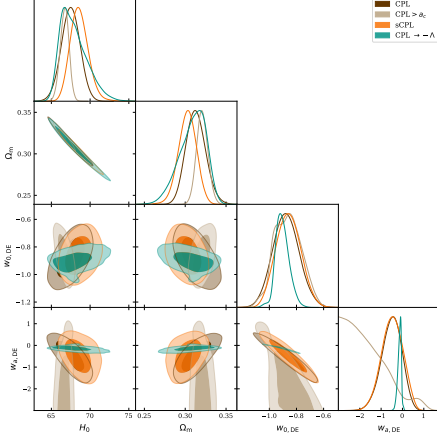
(b) Base &amp; Pantheon+



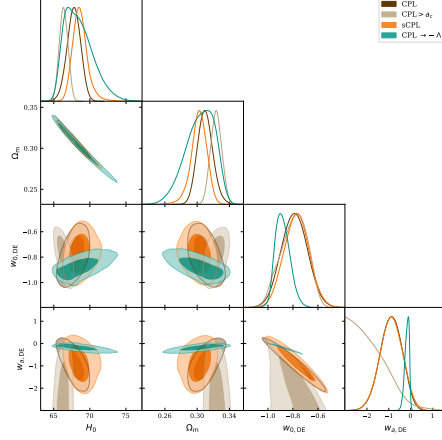
(c) Base &amp; DESY5



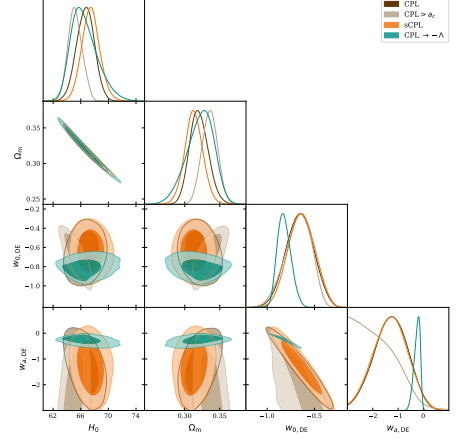
(d) Base &amp; Union3



(e) Planck 2018 &amp; Pantheon+



(f) Planck 2018 &amp; DESY5



(g) Planck 2018 &amp; Union3

FIG. 9. One- and two-dimensional marginalized posterior distributions for the four models, presented for each dataset combination.

pronounced for the base (Planck + DESI) combination, where the 68% confidence contours clearly encompass the cosmological constant limits ( $w_0 \rightarrow -1$  and  $w_a \rightarrow 0$ ). Nevertheless, owing to the simultaneous tightening of the

EoS constraints, the statistical preference for a dynamical DE component does not vanish, with the notable exception of the base case. From the bimodal structure observed in the base posteriors, we identify an important

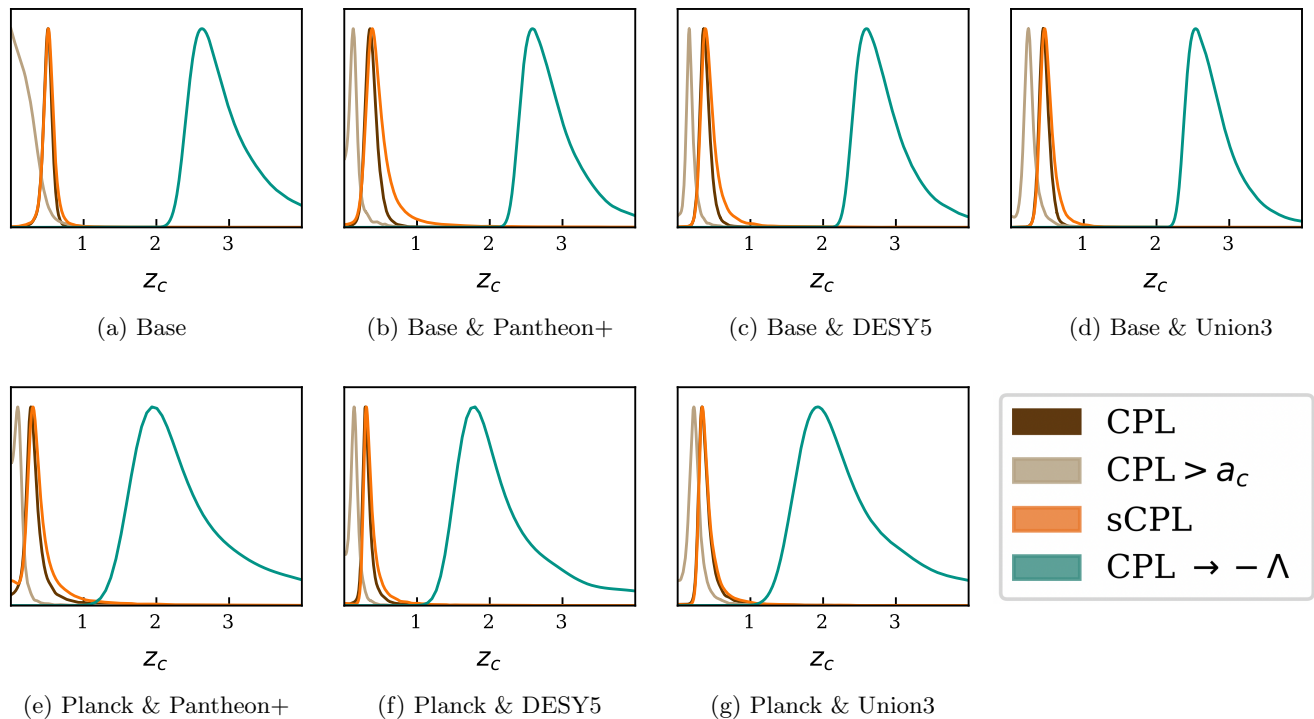


FIG. 10. One-dimensional posterior distributions of the derived parameter  $z_c$  for the four models, shown separately for each dataset combination. Colors correspond to the models labeled in Fig. 9.

limitation of the  $\text{CPL} \rightarrow -\Lambda$  construction and, more generally, of model building within the baseline CPL EoS framework. Any model that explicitly ties the onset of NECB-crossing to its location in redshift space (through a parameter such as  $z_c$ ) inevitably disfavors behavior arbitrarily close to a cosmological constant, since it requires  $w_a \neq 0$  by construction. We further emphasize that DESI BAO data, even when combined with Planck, are insufficient on their own to fully break degeneracies in the EoS parameters, highlighting the essential role of SNeIa data in constraining late-time DE properties.

Overall, none of the models explored in this work outperform CPL, as indicated by their consistently positive  $\Delta\text{AIC}$  values. Nor do they provide a compelling pathway toward resolving the  $H_0$  tension. Several factors contribute to these outcomes, including the effective penalization of near- $\Lambda$  behavior in the  $\text{CPL} \rightarrow -\Lambda$  model and the presence of an additional free parameter in sCPL. Nonetheless, within the scope of the scenarios considered here, the dynamical CPL parametrization remains the most effective phenomenological framework for capturing the phantom-like behavior suggested by current cosmological observations.

#### ACKNOWLEDGMENTS

The authors are grateful to Emre Özüiker and Luis Escamilla for their insightful comments and valuable suggestions. M.G. acknowledges partial support from

TÜBİTAK through a fellowship associated with Grant No. 124N627. Ö.A. acknowledges the support by the Turkish Academy of Sciences in the scheme of the Outstanding Young Scientist Award (TÜBA-GEBİP). E.D.V. is supported by a Royal Society Dorothy Hodgkin Research Fellowship. This article is based upon work from COST Action CA21136 Addressing observational tensions in cosmology with systematics and fundamental physics (CosmoVerse) supported by COST (European Cooperation in Science and Technology). The authors acknowledge the use of High-Performance Computing resources from the IT Services at the University of Sheffield.

#### Appendix A: On the interpretation of one- and two-dimensional parameter constraints

It is useful to clarify a well-known but sometimes counterintuitive feature of multi-parameter inference, which plays a role in the interpretation of our results. In particular, it is possible for two parameters to be individually consistent with a reference value at the one-dimensional level, while their joint constraints exclude that same reference point in the two-dimensional parameter space. This effect is purely geometric and arises from the projection of a correlated posterior distribution. In a multi-parameter analysis, the marginalized one-dimensional posterior for a parameter is obtained

by integrating the full posterior over all other parameters. As a result, one-dimensional confidence intervals reflect agreement with a reference value after averaging over degeneracies with other parameters. By contrast, two-dimensional confidence regions encode information about correlations between parameters and therefore test whether a specific *pair* of values is jointly compatible with the data. When parameters are correlated, the posterior probability density can be elongated along a degeneracy direction. In such cases, a reference point may lie well within the one-dimensional marginalized intervals of each parameter separately, yet fall outside the high-probability region of their joint distribution. This situation does not represent an inconsistency or tension in the data, but rather reflects the fact that the data constrain a particular *combination* of parameters more tightly than the individual parameters themselves. In practical terms, this means that agreement with a reference model should not be assessed solely from one-dimensional constraints. A full assessment requires examining the joint posterior, especially when correlations are present. Throughout this work, we therefore report both one-dimensional significances and two-dimensional joint significances, and we emphasize that apparent agreement at the level of individual parameters does not guarantee compatibility in the full parameter space. Fig. 11 provides a concrete illustration of this projection effect using the sCPL model constrained by Planck-only data. In this case, the one-dimensional constraints show only mild deviations from a cosmological constant, with tensions of  $0.4\sigma$  in  $w_0$  and  $0.7\sigma$  in  $w_a$ , while the joint two-dimensional constraint

excludes the  $(w_0, w_a) = (-1, 0)$  point at the  $2.3\sigma$  level. This discrepancy arises purely from parameter correlations and does not indicate an inconsistency between the one- and two-dimensional results.

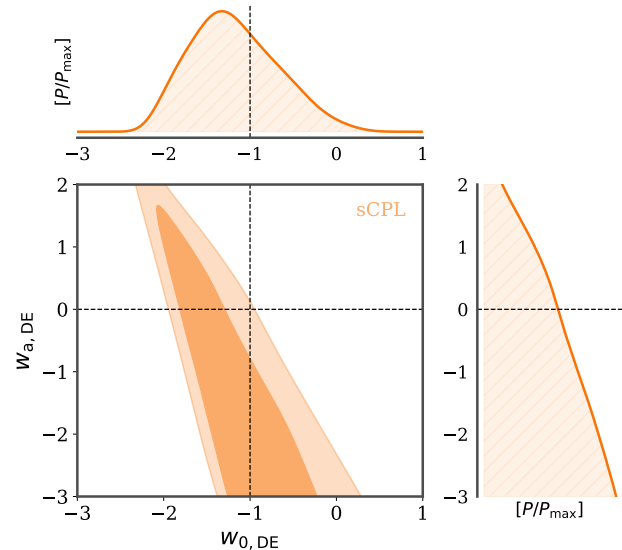


FIG. 11. The projection effect on the measurement significances  $N_\Lambda$  illustrated using marginalized one- and two-dimensional posteriors of the  $w_0$  and  $w_a$  parameters from Planck 2018 analyses.<sup>a</sup>

<sup>a</sup> [github.com/williamgiare/wgcosmo/tree/main](https://github.com/williamgiare/wgcosmo/tree/main)

- 
- [1] P. J. E. Peebles and B. Ratra, The Cosmological Constant and Dark Energy, *Rev. Mod. Phys.* **75**, 559 (2003), [arXiv:astro-ph/0207347](https://arxiv.org/abs/astro-ph/0207347).
  - [2] E. J. Copeland, M. Sami, and S. Tsujikawa, Dynamics of dark energy, *Int. J. Mod. Phys. D* **15**, 1753 (2006), [arXiv:hep-th/0603057](https://arxiv.org/abs/hep-th/0603057).
  - [3] L. Verde, T. Treu, and A. G. Riess, Tensions between the Early and the Late Universe, *Nature Astron.* **3**, 891 (2019), [arXiv:1907.10625](https://arxiv.org/abs/1907.10625) [[astro-ph.CO](https://arxiv.org/abs/astro-ph.CO)].
  - [4] E. Di Valentino *et al.*, Snowmass2021 - Letter of interest cosmology intertwined II: The Hubble constant tension, *Astropart. Phys.* **131**, 102605 (2021), [arXiv:2008.11284](https://arxiv.org/abs/2008.11284) [[astro-ph.CO](https://arxiv.org/abs/astro-ph.CO)].
  - [5] E. Di Valentino, O. Mena, S. Pan, L. Visinelli, W. Yang, A. Melchiorri, D. F. Mota, A. G. Riess, and J. Silk, In the realm of the Hubble tension—a review of solutions, *Class. Quant. Grav.* **38**, 153001 (2021), [arXiv:2103.01183](https://arxiv.org/abs/2103.01183) [[astro-ph.CO](https://arxiv.org/abs/astro-ph.CO)].
  - [6] L. Perivolaropoulos and F. Skara, Challenges for  $\Lambda$ CDM: An update, *New Astron. Rev.* **95**, 101659 (2022), [arXiv:2105.05208](https://arxiv.org/abs/2105.05208) [[astro-ph.CO](https://arxiv.org/abs/astro-ph.CO)].
  - [7] N. Schöneberg, G. Franco Abellán, A. Pérez Sánchez, S. J. Witte, V. Poulin, and J. Lesgourgues, The H0 Olympics: A fair ranking of proposed models, *Phys. Rept.* **984**, 1 (2022), [arXiv:2107.10291](https://arxiv.org/abs/2107.10291) [[astro-ph.CO](https://arxiv.org/abs/astro-ph.CO)].
  - [8] P. Shah, P. Lemos, and O. Lahav, A buyer’s guide to the Hubble constant, *Astron. Astrophys. Rev.* **29**, 9 (2021), [arXiv:2109.01161](https://arxiv.org/abs/2109.01161) [[astro-ph.CO](https://arxiv.org/abs/astro-ph.CO)].
  - [9] E. Abdalla *et al.*, Cosmology intertwined: A review of the particle physics, astrophysics, and cosmology associated with the cosmological tensions and anomalies, *JHEAp* **34**, 49 (2022), [arXiv:2203.06142](https://arxiv.org/abs/2203.06142) [[astro-ph.CO](https://arxiv.org/abs/astro-ph.CO)].
  - [10] E. Di Valentino, Challenges of the Standard Cosmological Model, *Universe* **8**, 399 (2022).
  - [11] M. Kamionkowski and A. G. Riess, The Hubble Tension and Early Dark Energy, *Ann. Rev. Nucl. Part. Sci.* **73**, 153 (2023), [arXiv:2211.04492](https://arxiv.org/abs/2211.04492) [[astro-ph.CO](https://arxiv.org/abs/astro-ph.CO)].
  - [12] W. Giarè, CMB Anomalies and the Hubble Tension (2023), [arXiv:2305.16919](https://arxiv.org/abs/2305.16919) [[astro-ph.CO](https://arxiv.org/abs/astro-ph.CO)].
  - [13] J.-P. Hu and F.-Y. Wang, Hubble Tension: The Evidence of New Physics, *Universe* **9**, 94 (2023), [arXiv:2302.05709](https://arxiv.org/abs/2302.05709) [[astro-ph.CO](https://arxiv.org/abs/astro-ph.CO)].
  - [14] L. Verde, N. Schöneberg, and H. Gil-Marín, A tale of many  $H_0$  (2023), [arXiv:2311.13305](https://arxiv.org/abs/2311.13305) [[astro-ph.CO](https://arxiv.org/abs/astro-ph.CO)].
  - [15] O. Akarsu, E. O. Colgáin, A. A. Sen, and M. M. Sheikh-Jabbari,  $\Lambda$ CDM Tensions: Localising Missing Physics through Consistency Checks, *Universe* **10**, 305 (2024), [arXiv:2402.04767](https://arxiv.org/abs/2402.04767) [[astro-ph.CO](https://arxiv.org/abs/astro-ph.CO)].
  - [16] E. Di Valentino and D. Brout, eds., *The Hubble Constant Tension*, Springer Series in Astrophysics and Cos-

- mology (Springer, 2024).
- [17] E. Di Valentino *et al.* (CosmoVerse Network), The CosmoVerse White Paper: Addressing observational tensions in cosmology with systematics and fundamental physics, *Phys. Dark Univ.* **49**, 101965 (2025), [arXiv:2504.01669 \[astro-ph.CO\]](#).
- [18] D. D. Y. Ong and W. Handley, *unimpeded*: A Public Grid of Nested Sampling Chains for Cosmological Model Comparison and Tension Analysis (2025), [arXiv:2511.04661 \[astro-ph.CO\]](#).
- [19] N. Aghanim *et al.* (Planck), Planck 2018 results. I. Overview and the cosmological legacy of Planck, *Astron. Astrophys.* **641**, A1 (2020), [arXiv:1807.06205 \[astro-ph.CO\]](#).
- [20] N. Aghanim *et al.* (Planck), Planck 2018 results. VI. Cosmological parameters, *Astron. Astrophys.* **641**, A6 (2020), [Erratum: *Astron. Astrophys.* 652, C4 (2021)], [arXiv:1807.06209 \[astro-ph.CO\]](#).
- [21] T. Louis *et al.* (Atacama Cosmology Telescope), The Atacama Cosmology Telescope: DR6 power spectra, likelihoods and  $\Lambda$ CDM parameters, *JCAP* **11**, 062, [arXiv:2503.14452 \[astro-ph.CO\]](#).
- [22] E. Camphuis *et al.* (SPT-3G), SPT-3G D1: CMB temperature and polarization power spectra and cosmology from 2019 and 2020 observations of the SPT-3G Main field (2025), [arXiv:2506.20707 \[astro-ph.CO\]](#).
- [23] S. Alam *et al.* (eBOSS), Completed SDSS-IV extended Baryon Oscillation Spectroscopic Survey: Cosmological implications from two decades of spectroscopic surveys at the Apache Point Observatory, *Phys. Rev. D* **103**, 083533 (2021), [arXiv:2007.08991 \[astro-ph.CO\]](#).
- [24] M. Abdul Karim *et al.* (DESI), DESI DR2 results. II. Measurements of baryon acoustic oscillations and cosmological constraints, *Phys. Rev. D* **112**, 083515 (2025), [arXiv:2503.14738 \[astro-ph.CO\]](#).
- [25] D. Scolnic *et al.*, The Pantheon+ Analysis: The Full Data Set and Light-curve Release, *Astrophys. J.* **938**, 113 (2022), [arXiv:2112.03863 \[astro-ph.CO\]](#).
- [26] D. Brout *et al.*, The Pantheon+ Analysis: Cosmological Constraints, *Astrophys. J.* **938**, 110 (2022), [arXiv:2202.04077 \[astro-ph.CO\]](#).
- [27] D. Rubin *et al.*, Union Through UNITY: Cosmology with 2,000 SNe Using a Unified Bayesian Framework, *Astrophys. J.* **986**, 231 (2025), [arXiv:2311.12098 \[astro-ph.CO\]](#).
- [28] B. Popovic *et al.*, A Reassessment of the Pantheon+ and DES 5YR Calibration Uncertainties: Dovekie, (2025), [arXiv:2506.05471 \[astro-ph.CO\]](#).
- [29] B. Popovic *et al.* (DES), The Dark Energy Survey Supernova Program: A Reanalysis Of Cosmology Results And Evidence For Evolving Dark Energy With An Updated Type Ia Supernova Calibration (2025), [arXiv:2511.07517 \[astro-ph.CO\]](#).
- [30] W. L. Freedman, B. F. Madore, T. Hoyt, I. S. Jang, R. Beaton, M. G. Lee, A. Monson, J. Neeley, and J. Rich, Calibration of the Tip of the Red Giant Branch (TRGB), *Astrophys. J.* **891**, 57 (2020), [arXiv:2002.01550 \[astro-ph.GA\]](#).
- [31] S. Birrer *et al.*, TDCOSMO - IV. Hierarchical time-delay cosmography – joint inference of the Hubble constant and galaxy density profiles, *Astron. Astrophys.* **643**, A165 (2020), [arXiv:2007.02941 \[astro-ph.CO\]](#).
- [32] A. G. Riess *et al.*, A Comprehensive Measurement of the Local Value of the Hubble Constant with 1 km  $s^{-1}$  Mpc $^{-1}$  Uncertainty from the Hubble Space Telescope and the SH0ES Team, *Astrophys. J. Lett.* **934**, L7 (2022), [arXiv:2112.04510 \[astro-ph.CO\]](#).
- [33] R. I. Anderson, N. W. Koblishke, and L. Eyer, Small-amplitude Red Giants Elucidate the Nature of the Tip of the Red Giant Branch as a Standard Candle, *Astrophys. J. Lett.* **963**, L43 (2024), [arXiv:2303.04790 \[astro-ph.CO\]](#).
- [34] D. Scolnic, A. G. Riess, J. Wu, S. Li, G. S. Anand, R. Beaton, S. Casertano, R. I. Anderson, S. Dhawan, and X. Ke, CATS: The Hubble Constant from Standardized TRGB and Type Ia Supernova Measurements, *Astrophys. J. Lett.* **954**, L31 (2023), [arXiv:2304.06693 \[astro-ph.CO\]](#).
- [35] D. O. Jones *et al.*, Cosmological Results from the RAISIN Survey: Using Type Ia Supernovae in the Near Infrared as a Novel Path to Measure the Dark Energy Equation of State, *Astrophys. J.* **933**, 172 (2022), [arXiv:2201.07801 \[astro-ph.CO\]](#).
- [36] G. S. Anand, R. B. Tully, L. Rizzi, A. G. Riess, and W. Yuan, Comparing Tip of the Red Giant Branch Distance Scales: An Independent Reduction of the Carnegie-Chicago Hubble Program and the Value of the Hubble Constant, *Astrophys. J.* **932**, 15 (2022), [arXiv:2108.00007 \[astro-ph.CO\]](#).
- [37] W. L. Freedman, Measurements of the Hubble Constant: Tensions in Perspective, *Astrophys. J.* **919**, 16 (2021), [arXiv:2106.15656 \[astro-ph.CO\]](#).
- [38] S. A. Uddin *et al.*, Carnegie Supernova Project I and II: Measurements of  $H_0$  Using Cepheid, Tip of the Red Giant Branch, and Surface Brightness Fluctuation Distance Calibration to Type Ia Supernovae\*, *Astrophys. J.* **970**, 72 (2024), [arXiv:2308.01875 \[astro-ph.CO\]](#).
- [39] C. D. Huang *et al.*, The Mira Distance to M101 and a 4% Measurement of  $H_0$ , *Astrophys. J.* **963**, 83 (2024), [arXiv:2312.08423 \[astro-ph.CO\]](#).
- [40] S. Li, A. G. Riess, S. Casertano, G. S. Anand, D. M. Scolnic, W. Yuan, L. Breuval, and C. D. Huang, Reconnaissance with JWST of the J-region Asymptotic Giant Branch in Distance Ladder Galaxies: From Irregular Luminosity Functions to Approximation of the Hubble Constant, *Astrophys. J.* **966**, 20 (2024), [arXiv:2401.04777 \[astro-ph.CO\]](#).
- [41] D. W. Pesce *et al.*, The Megamaser Cosmology Project. XIII. Combined Hubble constant constraints, *Astrophys. J. Lett.* **891**, L1 (2020), [arXiv:2001.09213 \[astro-ph.CO\]](#).
- [42] E. Kourkchi, R. B. Tully, G. S. Anand, H. M. Courtois, A. Dupuy, J. D. Neill, L. Rizzi, and M. Seibert, Cosmicflows-4: The Calibration of Optical and Infrared Tully–Fisher Relations, *Astrophys. J.* **896**, 3 (2020), [arXiv:2004.14499 \[astro-ph.GA\]](#).
- [43] J. Schombert, S. McGaugh, and F. Lelli, Using the Baryonic Tully–Fisher Relation to Measure  $H_0$ , *Astron. J.* **160**, 71 (2020), [arXiv:2006.08615 \[astro-ph.CO\]](#).
- [44] J. P. Blakeslee, J. B. Jensen, C.-P. Ma, P. A. Milne, and J. E. Greene, The Hubble Constant from Infrared Surface Brightness Fluctuation Distances, *Astrophys. J.* **911**, 65 (2021), [arXiv:2101.02221 \[astro-ph.CO\]](#).
- [45] T. de Jaeger, L. Galbany, A. G. Riess, B. E. Stahl, B. J. Shappee, A. V. Filippenko, and W. Zheng, A 5 per cent measurement of the Hubble–Lemaître constant from Type II supernovae, *Mon. Not. Roy. Astron. Soc.* **514**, 4620 (2022), [arXiv:2203.08974 \[astro-ph.CO\]](#).

- [46] Y. S. Murakami, A. G. Riess, B. E. Stahl, W. D. Kenworthy, D.-M. A. Pluck, A. Macoreta, D. Brout, D. O. Jones, D. M. Scolnic, and A. V. Filippenko, Leveraging SN Ia spectroscopic similarity to improve the measurement of  $H_0$ , *JCAP* **11**, 046, [arXiv:2306.00070 \[astro-ph.CO\]](#).
- [47] L. Breuval, A. G. Riess, S. Casertano, W. Yuan, L. M. Macri, M. Romaniello, Y. S. Murakami, D. Scolnic, G. S. Anand, and I. Soszyński, Small Magellanic Cloud Cepheids Observed with the Hubble Space Telescope Provide a New Anchor for the SH0ES Distance Ladder, *Astrophys. J.* **973**, 30 (2024), [arXiv:2404.08038 \[astro-ph.CO\]](#).
- [48] W. L. Freedman, B. F. Madore, T. J. Hoyt, I. S. Jang, A. J. Lee, and K. A. Owens, Status Report on the Chicago-Carnegie Hubble Program (CCHP): Measurement of the Hubble Constant Using the Hubble and James Webb Space Telescopes, *Astrophys. J.* **985**, 203 (2025), [arXiv:2408.06153 \[astro-ph.CO\]](#).
- [49] A. G. Riess *et al.*, JWST Validates HST Distance Measurements: Selection of Supernova Subsample Explains Differences in JWST Estimates of Local  $H_0$ , *Astrophys. J.* **977**, 120 (2024), [arXiv:2408.11770 \[astro-ph.CO\]](#).
- [50] C. Vogl *et al.*, No rungs attached: A distance-ladder free determination of the Hubble constant through type II supernova spectral modelling (2024), [arXiv:2411.04968 \[astro-ph.CO\]](#).
- [51] D. Scolnic *et al.*, The Hubble Tension in Our Own Backyard: DESI and the Nearness of the Coma Cluster, *Astrophys. J. Lett.* **979**, L9 (2025), [arXiv:2409.14546 \[astro-ph.CO\]](#).
- [52] K. Said *et al.*, DESI Peculiar Velocity Survey – Fundamental Plane, *Mon. Not. Roy. Astron. Soc.* **539**, 3627 (2025), [arXiv:2408.13842 \[astro-ph.CO\]](#).
- [53] P. Boubel, M. Colless, K. Said, and L. Staveley-Smith, An improved Tully–Fisher estimate of  $H_0$ , *Mon. Not. Roy. Astron. Soc.* **533**, 1550 (2024), [arXiv:2408.03660 \[astro-ph.CO\]](#).
- [54] D. Scolnic, P. Boubel, J. Byrne, A. G. Riess, and G. S. Anand, Calibrating the Tully–Fisher Relation to Measure the Hubble Constant (2024), [arXiv:2412.08449 \[astro-ph.CO\]](#).
- [55] S. Li, A. G. Riess, D. Scolnic, S. Casertano, and G. S. Anand, JAGB 2.0: Improved Constraints on the J-region Asymptotic Giant Branch–based Hubble Constant from an Expanded Sample of JWST Observations, *Astrophys. J.* **988**, 97 (2025), [arXiv:2502.05259 \[astro-ph.CO\]](#).
- [56] J. B. Jensen, J. P. Blakeslee, M. Cantiello, M. Cowles, G. S. Anand, R. B. Tully, E. Kourkchi, and G. Raimondo, The TRGB-SBF Project. III. Refining the HST Surface Brightness Fluctuation Distance Scale Calibration with JWST (2025), [arXiv:2502.15935 \[astro-ph.CO\]](#).
- [57] A. G. Riess *et al.*, The Perfect Host: JWST Cepheid Observations in a Background-free Type Ia Supernova Host Confirm No Bias in Hubble-constant Measurements, *Astrophys. J. Lett.* **992**, L34 (2025), [arXiv:2509.01667 \[astro-ph.CO\]](#).
- [58] D. Benisty, J. Wagner, S. Haridasu, and P. Salucci, Unveiling the Coma Cluster Structure: From the Core to the Hubble Flow (2025), [arXiv:2504.04135 \[astro-ph.CO\]](#).
- [59] M. J. B. Newman *et al.*, Tip of the Red Giant Branch Distances to NGC 1316, NGC 1380, NGC 1404, & NGC 4457: A Pilot Study of a Parallel Distance Ladder Using Type Ia Supernovae in Early-Type Host Galaxies (2025), [arXiv:2508.20023 \[astro-ph.CO\]](#).
- [60] R. Stiskalek, H. Desmond, E. Tsaprazi, A. Heavens, G. Lavaux, S. McAlpine, and J. Jasche, 1.8 per cent measurement of  $H_0$  from Cepheids alone (2025), [arXiv:2509.09665 \[astro-ph.CO\]](#).
- [61] S. Casertano *et al.* (H0DN), The Local Distance Network: a community consensus report on the measurement of the Hubble constant at 1% precision (2025), [arXiv:2510.23823 \[astro-ph.CO\]](#).
- [62] A. Agrawal *et al.*, Testing Lens Models of PLCK G165.7+67.0 Using Lensed SN H0pe (2025), [arXiv:2510.07637 \[astro-ph.CO\]](#).
- [63] A. Bhardwaj, N. Matsunaga, C. D. Huang, A. G. Riess, and M. Rejkuba, Absolute Calibration of Cluster Mira Variables to Provide a New Anchor for the Hubble Constant Determination, *Astrophys. J.* **990**, 63 (2025), [arXiv:2507.10658 \[astro-ph.GA\]](#).
- [64] G. Efstathiou, A Lockdown Perspective on the Hubble Tension (with comments from the SH0ES team) (2020), [arXiv:2007.10716 \[astro-ph.CO\]](#).
- [65] E. Mortsell, A. Goobar, J. Johansson, and S. Dhawan, Sensitivity of the Hubble Constant Determination to Cepheid Calibration, *Astrophys. J.* **933**, 212 (2022), [arXiv:2105.11461 \[astro-ph.CO\]](#).
- [66] E. Mortsell, A. Goobar, J. Johansson, and S. Dhawan, The Hubble Tension Revisited: Additional Local Distance Ladder Uncertainties, *Astrophys. J.* **935**, 58 (2022), [arXiv:2106.09400 \[astro-ph.CO\]](#).
- [67] A. Sharon, D. Kushnir, W. Yuan, L. Macri, and A. Riess, Reassessing the constraints from SH0ES extragalactic Cepheid amplitudes on systematic blending bias, *Mon. Not. Roy. Astron. Soc.* **528**, 6861 (2024), [arXiv:2305.14435 \[astro-ph.CO\]](#).
- [68] A. G. Riess, G. S. Anand, W. Yuan, S. Casertano, A. Dolphin, L. M. Macri, L. Breuval, D. Scolnic, M. Perin, and R. I. Anderson, Crowded No More: The Accuracy of the Hubble Constant Tested with High-resolution Observations of Cepheids by JWST, *Astrophys. J. Lett.* **956**, L18 (2023), [arXiv:2307.15806 \[astro-ph.CO\]](#).
- [69] A. Bhardwaj *et al.*, High-resolution Spectroscopic Metallicities of Milky Way Cepheid Standards and Their Impact on the Leavitt Law and the Hubble Constant, *Astrophys. J. Lett.* **955**, L13 (2023), [arXiv:2309.03263 \[astro-ph.SR\]](#).
- [70] D. Brout and A. Riess, The Impact of Dust on Cepheid and Type Ia Supernova Distances (2023), [arXiv:2311.08253 \[astro-ph.CO\]](#).
- [71] A. M. Dwomoh, E. R. Peterson, D. Scolnic, C. Ashall, J. M. DerKacy, A. Do, J. Johansson, D. O. Jones, A. G. Riess, and B. J. Shappee, Evaluating the Consistency of Cosmological Distances Using Supernova Siblings in the Near-infrared, *Astrophys. J.* **965**, 90 (2024), [arXiv:2311.06178 \[astro-ph.CO\]](#).
- [72] A. G. Riess, G. S. Anand, W. Yuan, S. Casertano, A. Dolphin, L. M. Macri, L. Breuval, D. Scolnic, M. Perin, and I. R. Anderson, JWST Observations Reject Unrecognized Crowding of Cepheid Photometry as an Explanation for the Hubble Tension at  $8\sigma$  Confidence, *Astrophys. J. Lett.* **962**, L17 (2024), [arXiv:2401.04773](#)

- [astro-ph.CO].
- [73] E. Di Valentino, A. Melchiorri, and J. Silk, Cosmological hints of modified gravity?, *Phys. Rev. D* **93**, 023513 (2016), arXiv:1509.07501 [astro-ph.CO].
- [74] M. Zumalacarregui, Gravity in the Era of Equality: Towards solutions to the Hubble problem without fine-tuned initial conditions, *Phys. Rev. D* **102**, 023523 (2020), arXiv:2003.06396 [astro-ph.CO].
- [75] S. D. Odintsov, D. Sáez-Chillón Gómez, and G. S. Sharov, Analyzing the  $H_0$  tension in  $F(R)$  gravity models, *Nucl. Phys. B* **966**, 115377 (2021), arXiv:2011.03957 [gr-qc].
- [76] T. Adi and E. D. Kovetz, Can conformally coupled modified gravity solve the Hubble tension?, *Phys. Rev. D* **103**, 023530 (2021), arXiv:2011.13853 [astro-ph.CO].
- [77] A. De Felice, S. Mukohyama, and M. C. Pookkillath, Addressing  $H_0$  tension by means of  $\Lambda$ CDM, *Phys. Lett. B* **816**, 136201 (2021), [Erratum: *Phys. Lett. B* **818**, 136364 (2021)], arXiv:2009.08718 [astro-ph.CO].
- [78] L. Pogosian, M. Raveri, K. Koyama, M. Martinelli, A. Silvestri, G.-B. Zhao, J. Li, S. Peirone, and A. Zucca, Imprints of cosmological tensions in reconstructed gravity, *Nature Astron.* **6**, 1484 (2022), arXiv:2107.12992 [astro-ph.CO].
- [79] Y. Akrami *et al.* (CANTATA), *Modified Gravity and Cosmology. An Update by the CANTATA Network*, edited by E. N. Saridakis, R. Lazkoz, V. Salzano, P. Vargas Moniz, S. Capozziello, J. Beltrán Jiménez, M. De Laurentis, and G. J. Olmo (Springer, 2021) arXiv:2105.12582 [gr-qc].
- [80] T. Schiavone, G. Montani, and F. Bombacigno,  $f(R)$  gravity in the Jordan frame as a paradigm for the Hubble tension, *Mon. Not. Roy. Astron. Soc.* **522**, L72 (2023), arXiv:2211.16737 [gr-qc].
- [81] M. Ishak *et al.*, Modified Gravity Constraints from the Full Shape Modeling of Clustering Measurements from DESI 2024 (2024), arXiv:2411.12026 [astro-ph.CO].
- [82] E. Specogna, E. Di Valentino, J. Levi Said, and N.-M. Nguyen, Exploring the growth index  $\gamma_L$ : Insights from different CMB dataset combinations and approaches, *Phys. Rev. D* **109**, 043528 (2024), arXiv:2305.16865 [astro-ph.CO].
- [83] E. Specogna, W. Giarè, and E. Di Valentino, Planck-PR4 anisotropy spectra show (better) consistency with General Relativity (2024), arXiv:2411.03896 [astro-ph.CO].
- [84] E. Calabrese *et al.* (Atacama Cosmology Telescope), The Atacama Cosmology Telescope: DR6 constraints on extended cosmological models, *JCAP* **11**, 063, arXiv:2503.14454 [astro-ph.CO].
- [85] W. Giarè, O. Mena, E. Specogna, and E. Di Valentino, Neutrino mass tension or suppressed growth rate of matter perturbations? (2025), arXiv:2507.01848 [astro-ph.CO].
- [86] Y. Tiwari, B. Ghosh, and R. K. Jain, Towards a possible solution to the Hubble tension with Horndeski gravity, *Eur. Phys. J. C* **84**, 220 (2024), arXiv:2301.09382 [astro-ph.CO].
- [87] M. Högås and E. Mörtsell, Hubble tension and fifth forces, *Phys. Rev. D* **108**, 124050 (2023), arXiv:2309.01744 [astro-ph.CO].
- [88] R. Y. Wen, L. T. Hergt, N. Afshordi, and D. Scott, A cosmic glitch in gravity, *JCAP* **03**, 045, arXiv:2311.03028 [astro-ph.CO].
- [89] C. Pitrou and J.-P. Uzan, Hubble Tension as a Window on the Gravitation of the Dark Matter Sector, *Phys. Rev. Lett.* **132**, 191001 (2024), arXiv:2312.12493 [astro-ph.CO].
- [90] G. Montani, N. Carlevaro, L. A. Escamilla, and E. Di Valentino, Kinetic model for dark energy—dark matter interaction: Scenario for the hubble tension, *Phys. Dark Univ.* **48**, 101848 (2025), arXiv:2404.15977 [gr-qc].
- [91] S. Dwivedi and M. Högås, 2D BAO vs 3D BAO: solving the Hubble tension with alternative cosmological models (2024), arXiv:2407.04322 [astro-ph.CO].
- [92] Ö. Akarsu, A. De Felice, E. Di Valentino, S. Kumar, R. C. Nunes, E. Özüiker, J. A. Vazquez, and A. Yadav,  $\Lambda_s$ CDM cosmology from a type-II minimally modified gravity (2024), arXiv:2402.07716 [astro-ph.CO].
- [93] O. Akarsu, B. Bulduk, A. De Felice, N. Katırcı, and N. M. Uzun, Unexplored regions in teleparallel  $f(T)$  gravity: Sign-changing dark energy density, *Phys. Rev. D* **112**, 083532 (2025), arXiv:2410.23068 [gr-qc].
- [94] M. Högås and E. Mörtsell, Bimetric gravity improves the fit to DESI BAO and eases the Hubble tension, *Phys. Rev. D* **112**, 103515 (2025), arXiv:2507.03743 [astro-ph.CO].
- [95] E. Di Valentino, A. Melchiorri, and J. Silk, Reconciling Planck with the local value of  $H_0$  in extended parameter space, *Phys. Lett. B* **761**, 242 (2016), arXiv:1606.00634 [astro-ph.CO].
- [96] E. Di Valentino, E. V. Linder, and A. Melchiorri, Vacuum phase transition solves the  $H_0$  tension, *Phys. Rev. D* **97**, 043528 (2018), arXiv:1710.02153 [astro-ph.CO].
- [97] K. Dutta, Ruchika, A. Roy, A. A. Sen, and M. M. Sheikh-Jabbari, Beyond  $\Lambda$ CDM with low and high redshift data: implications for dark energy, *Gen. Rel. Grav.* **52**, 15 (2020), arXiv:1808.06623 [astro-ph.CO].
- [98] R. von Martens, L. Lombriser, M. Kunz, V. Marra, L. Casarini, and J. Alcaniz, Dark degeneracy I: Dynamical or interacting dark energy?, *Phys. Dark Univ.* **28**, 100490 (2020), arXiv:1911.02618 [astro-ph.CO].
- [99] Ö. Akarsu, J. D. Barrow, L. A. Escamilla, and J. A. Vazquez, Graduated dark energy: Observational hints of a spontaneous sign switch in the cosmological constant, *Phys. Rev. D* **101**, 063528 (2020), arXiv:1912.08751 [astro-ph.CO].
- [100] E. Di Valentino, A. Mukherjee, and A. A. Sen, Dark Energy with Phantom Crossing and the  $H_0$  Tension, *Entropy* **23**, 404 (2021), arXiv:2005.12587 [astro-ph.CO].
- [101] E. Di Valentino, A combined analysis of the  $H_0$  late time direct measurements and the impact on the Dark Energy sector, *Mon. Not. Roy. Astron. Soc.* **502**, 2065 (2021), arXiv:2011.00246 [astro-ph.CO].
- [102] W. Yang, E. Di Valentino, S. Pan, Y. Wu, and J. Lu, Dynamical dark energy after Planck CMB final release and  $H_0$  tension, *Mon. Not. Roy. Astron. Soc.* **501**, 5845 (2021), arXiv:2101.02168 [astro-ph.CO].
- [103] E. Di Valentino, S. Gariazzo, C. Giunti, O. Mena, S. Pan, and W. Yang, Minimal dark energy: Key to sterile neutrino and Hubble constant tensions?, *Phys. Rev. D* **105**, 103511 (2022), arXiv:2110.03990 [astro-ph.CO].
- [104] L. Heisenberg, H. Villarrubia-Rojo, and J. Zosso, Simultaneously solving the  $H_0$  and  $\sigma_8$  tensions with late dark energy, *Phys. Dark Univ.* **39**, 101163 (2023), arXiv:2201.11623 [astro-ph.CO].

- [105] O. Akarsu, E. O. Colgain, E. Özulker, S. Thakur, and L. Yin, Inevitable manifestation of wiggles in the expansion of the late Universe, *Phys. Rev. D* **107**, 123526 (2023), [arXiv:2207.10609 \[astro-ph.CO\]](#).
- [106] S. A. Adil, Ö. Akarsu, E. Di Valentino, R. C. Nunes, E. Özulker, A. A. Sen, and E. Specogna, Omnipotent dark energy: A phenomenological answer to the Hubble tension, *Phys. Rev. D* **109**, 023527 (2024), [arXiv:2306.08046 \[astro-ph.CO\]](#).
- [107] A. Gómez-Valent, A. Favale, M. Migliaccio, and A. A. Sen, Late-time phenomenology required to solve the  $H_0$  tension in view of the cosmic ladders and the anisotropic and angular BAO datasets, *Phys. Rev. D* **109**, 023525 (2024), [arXiv:2309.07795 \[astro-ph.CO\]](#).
- [108] A. Lapi, L. Boco, M. M. Cueli, B. S. Haridasu, T. Ronconi, C. Baccigalupi, and L. Danese, Little Ado about Everything:  $\eta$ CDM, a Cosmological Model with Fluctuation-driven Acceleration at Late Times, *Astrophys. J.* **959**, 83 (2023), [arXiv:2310.06028 \[astro-ph.CO\]](#).
- [109] A. Krolewski, W. J. Percival, and A. Woodfinden, A new method to determine  $H_0$  from cosmological energy-density measurements (2024), [arXiv:2403.19227 \[astro-ph.CO\]](#).
- [110] D. Bousis and L. Perivolaropoulos, Hubble tension tomography: BAO vs SN Ia distance tension, *Phys. Rev. D* **110**, 103546 (2024), [arXiv:2405.07039 \[astro-ph.CO\]](#).
- [111] X. Tang, Y.-Z. Ma, W.-M. Dai, and H.-J. He, Constraining holographic dark energy and analyzing cosmological tensions, *Phys. Dark Univ.* **46**, 101568 (2024), [arXiv:2407.08427 \[astro-ph.CO\]](#).
- [112] J.-Q. Jiang, D. Pedrotti, S. S. da Costa, and S. Vagnozzi, Non-parametric late-time expansion history reconstruction and implications for the Hubble tension in light of DESI (2024), [arXiv:2408.02365 \[astro-ph.CO\]](#).
- [113] M. T. Manoharan, Insights on Granda–Oliveros holographic dark energy: possibility of negative dark energy at  $z \gtrsim 2$ , *Eur. Phys. J. C* **84**, 552 (2024).
- [114] E. Specogna, S. A. Adil, E. Ozulker, E. Di Valentino, R. C. Nunes, O. Akarsu, and A. A. Sen, Updated Constraints on Omnipotent Dark Energy: A Comprehensive Analysis with CMB and BAO Data (2025), [arXiv:2504.17859 \[gr-qc\]](#).
- [115] E. Özulker, E. Di Valentino, and W. Giarè, Dark Energy Crosses the Line: Quantifying and Testing the Evidence for Phantom Crossing (2025), [arXiv:2506.19053 \[astro-ph.CO\]](#).
- [116] D. H. Lee, W. Yang, E. Di Valentino, S. Pan, and C. van de Bruck, The Shape of Dark Energy: Constraining Its Evolution with a General Parametrization (2025), [arXiv:2507.11432 \[astro-ph.CO\]](#).
- [117] V. Poulin, T. L. Smith, T. Karwal, and M. Kamionkowski, Early Dark Energy Can Resolve The Hubble Tension, *Phys. Rev. Lett.* **122**, 221301 (2019), [arXiv:1811.04083 \[astro-ph.CO\]](#).
- [118] T. L. Smith, V. Poulin, and M. A. Amin, Oscillating scalar fields and the Hubble tension: a resolution with novel signatures, *Phys. Rev. D* **101**, 063523 (2020), [arXiv:1908.06995 \[astro-ph.CO\]](#).
- [119] F. Niedermann and M. S. Sloth, New early dark energy, *Phys. Rev. D* **103**, L041303 (2021), [arXiv:1910.10739 \[astro-ph.CO\]](#).
- [120] C. Krishnan, E. Ó. Colgáin, Ruchika, A. A. Sen, M. M. Sheikh-Jabbari, and T. Yang, Is there an early Universe solution to Hubble tension?, *Phys. Rev. D* **102**, 103525 (2020), [arXiv:2002.06044 \[astro-ph.CO\]](#).
- [121] G. Ye, J. Zhang, and Y.-S. Piao, Alleviating both  $H_0$  and  $S_8$  tensions: Early dark energy lifts the CMB-lockdown on ultralight axion, *Phys. Lett. B* **839**, 137770 (2023), [arXiv:2107.13391 \[astro-ph.CO\]](#).
- [122] V. Poulin, T. L. Smith, and A. Bartlett, Dark energy at early times and ACT data: A larger Hubble constant without late-time priors, *Phys. Rev. D* **104**, 123550 (2021), [arXiv:2109.06229 \[astro-ph.CO\]](#).
- [123] F. Niedermann and M. S. Sloth, Hot new early dark energy, *Phys. Rev. D* **105**, 063509 (2022), [arXiv:2112.00770 \[hep-ph\]](#).
- [124] D. H. F. de Souza and R. Rosenfeld, Can neutrino-assisted early dark energy models ameliorate the  $H_0$  tension in a natural way?, *Phys. Rev. D* **108**, 083512 (2023), [arXiv:2302.04644 \[astro-ph.CO\]](#).
- [125] V. Poulin, T. L. Smith, and T. Karwal, The Ups and Downs of Early Dark Energy solutions to the Hubble tension: A review of models, hints and constraints circa 2023, *Phys. Dark Univ.* **42**, 101348 (2023), [arXiv:2302.09032 \[astro-ph.CO\]](#).
- [126] J. S. Cruz, F. Niedermann, and M. S. Sloth, Cold New Early Dark Energy pulls the trigger on the  $H_0$  and  $S_8$  tensions: a simultaneous solution to both tensions without new ingredients, *JCAP* **11**, 033, [arXiv:2305.08895 \[astro-ph.CO\]](#).
- [127] F. Niedermann and M. S. Sloth, *New Early Dark Energy as a solution to the  $H_0$  and  $S_8$  tensions* (2023), [arXiv:2307.03481 \[hep-ph\]](#).
- [128] S. Vagnozzi, Seven Hints That Early-Time New Physics Alone Is Not Sufficient to Solve the Hubble Tension, *Universe* **9**, 393 (2023), [arXiv:2308.16628 \[astro-ph.CO\]](#).
- [129] G. Efstathiou, E. Rosenberg, and V. Poulin, Improved Planck Constraints on Axionlike Early Dark Energy as a Resolution of the Hubble Tension, *Phys. Rev. Lett.* **132**, 221002 (2024), [arXiv:2311.00524 \[astro-ph.CO\]](#).
- [130] T. Simon, T. Adi, J. L. Bernal, E. D. Kovetz, V. Poulin, and T. L. Smith, Toward alleviating the  $H_0$  and  $S_8$  tensions with early dark energy-dark matter drag, *Phys. Rev. D* **111**, 023523 (2025), [arXiv:2410.21459 \[astro-ph.CO\]](#).
- [131] J. L. Cervantes-Cota, S. Galindo-Uribarri, and G. F. Smoot, The Unsettled Number: Hubble’s Tension, *Universe* **9**, 501 (2023), [arXiv:2311.07552 \[physics.hist-ph\]](#).
- [132] M. Garny, F. Niedermann, H. Rubira, and M. S. Sloth, Hot new early dark energy bridging cosmic gaps: Supercooled phase transition reconciles stepped dark radiation solutions to the Hubble tension with BBN, *Phys. Rev. D* **110**, 023531 (2024), [arXiv:2404.07256 \[astro-ph.CO\]](#).
- [133] W. Giarè, Inflation, the Hubble tension, and early dark energy: An alternative overview, *Phys. Rev. D* **109**, 123545 (2024), [arXiv:2404.12779 \[astro-ph.CO\]](#).
- [134] W. Giarè, J. Betts, C. van de Bruck, and E. Di Valentino, A model-independent test of pre-recombination New Physics: Machine Learning based estimate of the Sound Horizon from Gravitational Wave Standard Sirens and the Baryon Acoustic Oscillation Angular Scale (2024), [arXiv:2406.07493 \[astro-ph.CO\]](#).
- [135] V. Poulin, T. L. Smith, R. Calderón, and T. Simon, Implications of the cosmic calibration tension be-

- yond  $H_0$  and the synergy between early- and late-time new physics, *Phys. Rev. D* **111**, 083552 (2025), [arXiv:2407.18292 \[astro-ph.CO\]](#).
- [136] D. Pedrotti, J.-Q. Jiang, L. A. Escamilla, S. S. da Costa, and S. Vagnozzi, Multidimensionality of the Hubble tension: the roles of  $\Omega_m$  and  $\omega_c$  (2024), [arXiv:2408.04530 \[astro-ph.CO\]](#).
- [137] J. Kochappan, L. Yin, B.-H. Lee, and T. Ghosh, Observational evidence for early dark energy as a unified explanation for cosmic birefringence and the Hubble tension, *Phys. Rev. D* **112**, 063562 (2025), [arXiv:2408.09521 \[astro-ph.CO\]](#).
- [138] V. Poulin, T. L. Smith, R. Calderón, and T. Simon, Impact of ACT DR6 and DESI DR2 for Early Dark Energy and the Hubble tension (2025), [arXiv:2505.08051 \[astro-ph.CO\]](#).
- [139] T. L. Smith and N. Schöneberg, Predictions for new physics in the CMB damping tail, *Phys. Rev. D* **112**, 083559 (2025), [arXiv:2503.20002 \[astro-ph.CO\]](#).
- [140] E. Di Valentino, R. Z. Ferreira, L. Visinelli, and U. Danielsson, Late time transitions in the quintessence field and the  $H_0$  tension, *Phys. Dark Univ.* **26**, 100385 (2019), [arXiv:1906.11255 \[astro-ph.CO\]](#).
- [141] G. Alestas, D. Camarena, E. Di Valentino, L. Kazantzidis, V. Marra, S. Nesseris, and L. Perivolaropoulos, Late-transition versus smooth  $H(z)$ -deformation models for the resolution of the Hubble crisis, *Phys. Rev. D* **105**, 063538 (2022), [arXiv:2110.04336 \[astro-ph.CO\]](#).
- [142] Ruchika, H. Rathore, S. Roy Choudhury, and V. Rentala, A gravitational constant transition within cepheids as supernovae calibrators can solve the Hubble tension, *JCAP* **06**, 056, [arXiv:2306.05450 \[astro-ph.CO\]](#).
- [143] E. Frion, D. Camarena, L. Giani, T. Miranda, D. Bertacca, V. Marra, and O. F. Piattella, *Bayesian analysis of a Unified Dark Matter model with transition: can it alleviate the  $H_0$  tension?* (2023), [arXiv:2307.06320 \[astro-ph.CO\]](#).
- [144] Ruchika, L. Perivolaropoulos, and A. Melchiorri, Effects of a local physics change on the SH0ES determination of  $H_0$  (2024), [arXiv:2408.03875 \[astro-ph.CO\]](#).
- [145] L. Visinelli, S. Vagnozzi, and U. Danielsson, Revisiting a negative cosmological constant from low-redshift data, *Symmetry* **11**, 1035 (2019), [arXiv:1907.07953 \[astro-ph.CO\]](#).
- [146] G. Ye and Y.-S. Piao, Is the Hubble tension a hint of AdS phase around recombination?, *Phys. Rev. D* **101**, 083507 (2020), [arXiv:2001.02451 \[astro-ph.CO\]](#).
- [147] R. Calderón, R. Gannouji, B. L’Huillier, and D. Polarski, Negative cosmological constant in the dark sector?, *Phys. Rev. D* **103**, 023526 (2021), [arXiv:2008.10237 \[astro-ph.CO\]](#).
- [148] O. Akarsu, S. Kumar, E. Özüiker, and J. A. Vazquez, Relaxing cosmological tensions with a sign switching cosmological constant, *Phys. Rev. D* **104**, 123512 (2021), [arXiv:2108.09239 \[astro-ph.CO\]](#).
- [149] A. A. Sen, S. A. Adil, and S. Sen, Do cosmological observations allow a negative  $\Lambda$ ?, *Mon. Not. Roy. Astron. Soc.* **518**, 1098 (2022), [arXiv:2112.10641 \[astro-ph.CO\]](#).
- [150] S. Di Gennaro and Y. C. Ong, Sign Switching Dark Energy from a Running Barrow Entropy, *Universe* **8**, 541 (2022), [arXiv:2205.09311 \[gr-qc\]](#).
- [151] O. Akarsu, S. Kumar, E. Özüiker, J. A. Vazquez, and A. Yadav, Relaxing cosmological tensions with a sign switching cosmological constant: Improved results with Planck, BAO, and Pantheon data, *Phys. Rev. D* **108**, 023513 (2023), [arXiv:2211.05742 \[astro-ph.CO\]](#).
- [152] Y. C. Ong, An Effective Sign Switching Dark Energy: Lotka–Volterra Model of Two Interacting Fluids, *Universe* **9**, 437 (2023), [arXiv:2212.04429 \[gr-qc\]](#).
- [153] O. Akarsu, E. Di Valentino, S. Kumar, R. C. Nunes, J. A. Vazquez, and A. Yadav,  $\Lambda_s$ CDM model: A promising scenario for alleviation of cosmological tensions (2023), [arXiv:2307.10899 \[astro-ph.CO\]](#).
- [154] L. A. Anchordoqui, I. Antoniadis, and D. Lust, Anti-de Sitter  $\rightarrow$  de Sitter transition driven by Casimir forces and mitigating tensions in cosmological parameters, *Phys. Lett. B* **855**, 138775 (2024), [arXiv:2312.12352 \[hep-th\]](#).
- [155] S. Halder, J. de Haro, T. Saha, and S. Pan, Phase space analysis of sign-shifting interacting dark energy models, *Phys. Rev. D* **109**, 083522 (2024), [arXiv:2403.01397 \[gr-qc\]](#).
- [156] L. A. Anchordoqui, I. Antoniadis, D. Lust, N. T. Noble, and J. F. Soriano, From infinite to infinitesimal: Using the Universe as a dataset to probe Casimir corrections to the vacuum energy from fields inhabiting the dark dimension, *Phys. Dark Univ.* **46**, 101715 (2024), [arXiv:2404.17334 \[astro-ph.CO\]](#).
- [157] O. Akarsu, A. De Felice, E. Di Valentino, S. Kumar, R. C. Nunes, E. Ozulker, J. A. Vazquez, and A. Yadav, Cosmological constraints on  $\Lambda_s$ CDM scenario in a type II minimally modified gravity (2024), [arXiv:2406.07526 \[astro-ph.CO\]](#).
- [158] A. Yadav, S. Kumar, C. Kibris, and O. Akarsu,  $\Lambda_s$ CDM cosmology: Alleviating major cosmological tensions by predicting standard neutrino properties (2024), [arXiv:2406.18496 \[astro-ph.CO\]](#).
- [159] E. A. Paraskevas, A. Cam, L. Perivolaropoulos, and O. Akarsu, Transition dynamics in the  $\Lambda_s$ CDM model: Implications for bound cosmic structures, *Phys. Rev. D* **109**, 103522 (2024), [arXiv:2402.05908 \[astro-ph.CO\]](#).
- [160] A. Gomez-Valent and J. Solà Peracaula, Phantom Matter: A Challenging Solution to the Cosmological Tensions, *Astrophys. J.* **975**, 64 (2024), [arXiv:2404.18845 \[astro-ph.CO\]](#).
- [161] Y. Toda, W. Giarè, E. Özüiker, E. Di Valentino, and S. Vagnozzi, Combining pre- and post-recombination new physics to address cosmological tensions: case study with varying electron mass and a sign-switching cosmological constant (2024), [arXiv:2407.01173 \[astro-ph.CO\]](#).
- [162] A. Gómez-Valent and J. Solà Peracaula, Composite dark energy and the cosmological tensions, *Phys. Lett. B* **864**, 139391 (2025), [arXiv:2412.15124 \[astro-ph.CO\]](#).
- [163] Ö. Akarsu, L. Perivolaropoulos, A. Tsikoundoura, A. E. Yükselci, and A. Zhuk, Dynamical dark energy with AdS-to-dS and dS-to-dS transitions: Implications for the  $H_0$  tension (2025), [arXiv:2502.14667 \[astro-ph.CO\]](#).
- [164] M. S. Souza, A. M. Barcelos, R. C. Nunes, Ö. Akarsu, and S. Kumar, Mapping the  $\Lambda_s$ CDM Scenario to  $f(T)$  Modified Gravity: Effects on Structure Growth Rate, *Universe* **11**, 2 (2025), [arXiv:2501.18031 \[astro-ph.CO\]](#).
- [165] J. F. Soriano, S. Wohlberg, and L. A. Anchordoqui, New insights on a sign-switching  $\Lambda$ , *Phys. Dark Univ.* **48**,

- 101911 (2025), [arXiv:2502.19239 \[astro-ph.CO\]](#).
- [166] Ö. Akarsu, A. Çam, E. A. Paraskevas, and L. Perivolaropoulos, Linear matter density perturbations in the  $\Lambda_s$ CDM model: Examining growth dynamics and addressing the  $S_8$  tension, *JCAP* **08**, 089, [arXiv:2502.20384 \[astro-ph.CO\]](#).
- [167] L. A. Escamilla, Ö. Akarsu, E. Di Valentino, E. Özülker, and J. A. Vazquez, Exploring the Growth-Index ( $\gamma$ ) Tension with  $\Lambda_s$ CDM (2025), [arXiv:2503.12945 \[astro-ph.CO\]](#).
- [168] M. Bouhmadi-López and B. Ibarra-Uriondo, Cosmographical analysis of sign-switching dark energy (2025), [arXiv:2506.12139 \[gr-qc\]](#).
- [169] P. Ghafari, M. Najafi, M. Ghodsi Yengejeh, E. Özülker, E. Di Valentino, and J. T. Firouzjaee, A Multi-Probe ISW Study of Dark Energy Models with Negative Energy Density: Galaxy Correlations, Lensing Bispectrum, and Planck ISW-Lensing Likelihood (2025), [arXiv:2512.07060 \[astro-ph.CO\]](#).
- [170] B. Ibarra-Uriondo and M. Bouhmadi-López, Sign-Switching Dark Energy: Smooth Transitions with Recent `textit`DESI DR2 Observations (2026), [arXiv:2602.12347 \[astro-ph.CO\]](#).
- [171] S. Pan, W. Yang, E. Di Valentino, A. Shafieloo, and S. Chakraborty, Reconciling  $H_0$  tension in a six parameter space?, *JCAP* **06** (06), 062, [arXiv:1907.12551 \[astro-ph.CO\]](#).
- [172] W. Yang, E. Di Valentino, S. Pan, S. Basilakos, and A. Paliathanasis, Metastable dark energy models in light of *Planck* 2018 data: Alleviating the  $H_0$  tension, *Phys. Rev. D* **102**, 063503 (2020), [arXiv:2001.04307 \[astro-ph.CO\]](#).
- [173] W. Yang, E. Di Valentino, S. Pan, A. Shafieloo, and X. Li, Generalized emergent dark energy model and the Hubble constant tension, *Phys. Rev. D* **104**, 063521 (2021), [arXiv:2103.03815 \[astro-ph.CO\]](#).
- [174] E. Di Valentino, C. Bøehm, E. Hivon, and F. R. Bouchet, Reducing the  $H_0$  and  $\sigma_8$  tensions with Dark Matter-neutrino interactions, *Phys. Rev. D* **97**, 043513 (2018), [arXiv:1710.02559 \[astro-ph.CO\]](#).
- [175] L. A. Anchordoqui, V. Barger, D. Marfatia, and J. F. Soriano, Decay of multiple dark matter particles to dark radiation in different epochs does not alleviate the Hubble tension, *Phys. Rev. D* **105**, 103512 (2022), [arXiv:2203.04818 \[astro-ph.CO\]](#).
- [176] S. Pan, O. Seto, T. Takahashi, and Y. Toda, Constraints on sterile neutrinos and the cosmological tensions, *Phys. Rev. D* **110**, 083524 (2024), [arXiv:2312.15435 \[astro-ph.CO\]](#).
- [177] I. J. Allali, D. Aloni, and N. Schöneberg, Cosmological probes of Dark Radiation from Neutrino Mixing, *JCAP* **09**, 019, [arXiv:2404.16822 \[astro-ph.CO\]](#).
- [178] R. T. Co, N. Fernandez, A. Ghalsasi, K. Harigaya, and J. Shelton, Axion baryogenesis puts a new spin on the Hubble tension, *Phys. Rev. D* **110**, 083534 (2024), [arXiv:2405.12268 \[hep-ph\]](#).
- [179] A. Aboubrahim and P. Nath, Interacting ultralight dark matter and dark energy and fits to cosmological data in a field theory approach, *JCAP* **09**, 076, [arXiv:2406.19284 \[astro-ph.CO\]](#).
- [180] L. Hart and J. Chluba, New constraints on time-dependent variations of fundamental constants using Planck data, *Mon. Not. Roy. Astron. Soc.* **474**, 1850 (2018), [arXiv:1705.03925 \[astro-ph.CO\]](#).
- [181] L. Hart and J. Chluba, Updated fundamental constant constraints from Planck 2018 data and possible relations to the Hubble tension, *Mon. Not. Roy. Astron. Soc.* **493**, 3255 (2020), [arXiv:1912.03986 \[astro-ph.CO\]](#).
- [182] T. Sekiguchi and T. Takahashi, Early recombination as a solution to the  $H_0$  tension, *Phys. Rev. D* **103**, 083507 (2021), [arXiv:2007.03381 \[astro-ph.CO\]](#).
- [183] L. Hart and J. Chluba, Varying fundamental constants principal component analysis: additional hints about the Hubble tension, *Mon. Not. Roy. Astron. Soc.* **510**, 2206 (2022), [arXiv:2107.12465 \[astro-ph.CO\]](#).
- [184] N. Lee, Y. Ali-Haïmoud, N. Schöneberg, and V. Poulin, What It Takes to Solve the Hubble Tension through Modifications of Cosmological Recombination, *Phys. Rev. Lett.* **130**, 161003 (2023), [arXiv:2212.04494 \[astro-ph.CO\]](#).
- [185] J. Chluba and L. Hart, Varying fundamental constants meet Hubble (2023), [arXiv:2309.12083 \[astro-ph.CO\]](#).
- [186] K. L. Greene and F.-Y. Cyr-Racine, Thomson scattering: one rate to rule them all, *JCAP* **10**, 065, [arXiv:2306.06165 \[astro-ph.CO\]](#).
- [187] K. Greene and F.-Y. Cyr-Racine, Ratio-preserving approach to cosmological concordance, *Phys. Rev. D* **110**, 043524 (2024), [arXiv:2403.05619 \[astro-ph.CO\]](#).
- [188] M. Baryakhtar, O. Simon, and Z. J. Weiner, Cosmology with varying fundamental constants from hyperlight, coupled scalars, *Phys. Rev. D* **110**, 083505 (2024), [arXiv:2405.10358 \[astro-ph.CO\]](#).
- [189] O. Seto and Y. Toda, DESI constraints on the varying electron mass model and axionlike early dark energy, *Phys. Rev. D* **110**, 083501 (2024), [arXiv:2405.11869 \[astro-ph.CO\]](#).
- [190] S. H. Mirpoorian, K. Jedamzik, and L. Pogosian, Modified recombination and the Hubble tension, *Phys. Rev. D* **111**, 083519 (2025), [arXiv:2411.16678 \[astro-ph.CO\]](#).
- [191] G. P. Lynch, L. Knox, and J. Chluba, DESI observations and the Hubble tension in light of modified recombination, *Phys. Rev. D* **110**, 083538 (2024), [arXiv:2406.10202 \[astro-ph.CO\]](#).
- [192] N. Schöneberg and L. Vacher, The mass effect – Variations of masses and their impact on cosmology (2024), [arXiv:2407.16845 \[astro-ph.CO\]](#).
- [193] A. Smith, M. Mylova, C. van de Bruck, C. P. Burgess, and E. Di Valentino, The Serendipitous Axiodilaton: A Self-Consistent Recombination-Era Solution to the Hubble Tension (2025), [arXiv:2512.13544 \[astro-ph.CO\]](#).
- [194] H. García Escudero, S. H. Mirpoorian, and L. Pogosian, Sound-Horizon-Agnostic Inference of the Hubble Constant and Neutrino Mass from BAO, CMB Lensing, and Galaxy Weak Lensing and Clustering (2025), [arXiv:2509.16202 \[astro-ph.CO\]](#).
- [195] Y. Toda and O. Seto, Constraints on the varying electron mass and early dark energy in light of ACT DR6 and DESI DR2 and the implications for inflation (2025), [arXiv:2508.09025 \[astro-ph.CO\]](#).
- [196] A. R. Cooray and D. Huterer, Gravitational lensing as a probe of quintessence, *Astrophys. J. Lett.* **513**, L95 (1999), [arXiv:astro-ph/9901097](#).
- [197] G. Efstathiou, Constraining the equation of state of the universe from distant type Ia supernovae and cosmic microwave background anisotropies, *Mon. Not. Roy. Astron. Soc.* **310**, 842 (1999), [arXiv:astro-ph/9904356](#).

- [198] C. Wetterich, Phenomenological parameterization of quintessence, *Phys. Lett. B* **594**, 17 (2004), [arXiv:astro-ph/0403289](#).
- [199] P. S. Corasaniti and E. J. Copeland, A Model independent approach to the dark energy equation of state, *Phys. Rev. D* **67**, 063521 (2003), [arXiv:astro-ph/0205544](#).
- [200] B. A. Bassett, M. Kunz, D. Parkinson, and C. Ungarelli, Condensate cosmology - Dark energy from dark matter, *Phys. Rev. D* **68**, 043504 (2003), [arXiv:astro-ph/0211303](#).
- [201] U. Alam, V. Sahni, and A. A. Starobinsky, The Case for dynamical dark energy revisited, *JCAP* **06**, 008, [arXiv:astro-ph/0403687](#).
- [202] E. V. Linder and D. Huterer, How many dark energy parameters?, *Phys. Rev. D* **72**, 043509 (2005), [arXiv:astro-ph/0505330](#).
- [203] A. Melchiorri, B. Paciello, P. Serra, and A. Slosar, Constraints on dynamical dark energy: an update, *New J. Phys.* **8**, 325 (2006).
- [204] J.-F. Zhang, X. Zhang, and H.-Y. Liu, Reconstructing generalized ghost condensate model with dynamical dark energy parametrizations and observational datasets, *Mod. Phys. Lett. A* **23**, 139 (2008), [arXiv:astro-ph/0612642](#).
- [205] H. Li and X. Zhang, Constraining dynamical dark energy with a divergence-free parametrization in the presence of spatial curvature and massive neutrinos, *Phys. Lett. B* **713**, 160 (2012), [arXiv:1202.4071 \[astro-ph.CO\]](#).
- [206] B. Novosyadlyj, O. Sergijenko, R. Durrer, and V. Pełykh, Constraining the dynamical dark energy parameters: Planck-2013 vs WMAP9, *JCAP* **05**, 030, [arXiv:1312.6579 \[astro-ph.CO\]](#).
- [207] M. Rezaei, M. Malekjani, S. Basilakos, A. Mehrabi, and D. F. Mota, Constraints to Dark Energy Using PADE Parameterizations, *Astrophys. J.* **843**, 65 (2017), [arXiv:1706.02537 \[astro-ph.CO\]](#).
- [208] D. Wang and X.-H. Meng, No evidence for dynamical dark energy in two models, *Phys. Rev. D* **96**, 103516 (2017), [arXiv:1709.01074 \[astro-ph.CO\]](#).
- [209] M. Rezaei, Structure formation in dark energy cosmologies described by PADE parametrization, *Mon. Not. Roy. Astron. Soc.* **485**, 4841 (2019), [arXiv:1904.02785 \[gr-qc\]](#).
- [210] R. K. Sharma, K. L. Pandey, and S. Das, Implications of an Extended Dark Energy Model with Massive Neutrinos, *Astrophys. J.* **934**, 113 (2022), [arXiv:2202.01749 \[astro-ph.CO\]](#).
- [211] R. von Martens, D. Barbosa, and J. Alcaniz, One-parameter dynamical dark-energy from the generalized Chaplygin gas, *JCAP* **04**, 052, [arXiv:2208.06302 \[astro-ph.CO\]](#).
- [212] T.-Y. Yao, R.-Y. Guo, and X.-Y. Zhao, Constraining neutrino mass in dynamical dark energy cosmologies with the logarithm parametrization and the oscillating parametrization (2022), [arXiv:2211.05956 \[gr-qc\]](#).
- [213] B. Feng, M. Li, Y.-S. Piao, and X. Zhang, Oscillating quintom and the recurrent universe, *Phys. Lett. B* **634**, 101 (2006), [arXiv:astro-ph/0407432](#).
- [214] S. Hannestad and E. Mortsell, Cosmological constraints on the dark energy equation of state and its evolution, *JCAP* **09**, 001, [arXiv:astro-ph/0407259](#).
- [215] J.-Q. Xia, B. Feng, and X.-M. Zhang, Constraints on oscillating quintom from supernova, microwave background and galaxy clustering, *Mod. Phys. Lett. A* **20**, 2409 (2005), [arXiv:astro-ph/0411501](#).
- [216] Y.-g. Gong and Y.-Z. Zhang, Probing the curvature and dark energy, *Phys. Rev. D* **72**, 043518 (2005), [arXiv:astro-ph/0502262](#).
- [217] H. K. Jassal, J. S. Bagla, and T. Padmanabhan, Observational constraints on low redshift evolution of dark energy: How consistent are different observations?, *Phys. Rev. D* **72**, 103503 (2005), [arXiv:astro-ph/0506748](#).
- [218] S. Nesseris and L. Perivolaropoulos, Comparison of the legacy and gold snia dataset constraints on dark energy models, *Phys. Rev. D* **72**, 123519 (2005), [arXiv:astro-ph/0511040](#).
- [219] D.-J. Liu, X.-Z. Li, J. Hao, and X.-H. Jin, Revisiting the parametrization of Equation of State of Dark Energy via SNIa Data, *Mon. Not. Roy. Astron. Soc.* **388**, 275 (2008), [arXiv:0804.3829 \[astro-ph\]](#).
- [220] E. M. Barboza, Jr. and J. S. Alcaniz, A parametric model for dark energy, *Phys. Lett. B* **666**, 415 (2008), [arXiv:0805.1713 \[astro-ph\]](#).
- [221] E. M. Barboza, J. S. Alcaniz, Z. H. Zhu, and R. Silva, A generalized equation of state for dark energy, *Phys. Rev. D* **80**, 043521 (2009), [arXiv:0905.4052 \[astro-ph.CO\]](#).
- [222] J.-Z. Ma and X. Zhang, Probing the dynamics of dark energy with novel parametrizations, *Phys. Lett. B* **699**, 233 (2011), [arXiv:1102.2671 \[astro-ph.CO\]](#).
- [223] I. Sendra and R. Lazkoz, SN and BAO constraints on (new) polynomial dark energy parametrizations: current results and forecasts, *Mon. Not. Roy. Astron. Soc.* **422**, 776 (2012), [arXiv:1105.4943 \[astro-ph.CO\]](#).
- [224] L. Feng and T. Lu, A new equation of state for dark energy model, *JCAP* **11**, 034, [arXiv:1203.1784 \[astro-ph.CO\]](#).
- [225] E. M. Barboza, Jr. and J. S. Alcaniz, Probing the time dependence of dark energy, *JCAP* **02**, 042, [arXiv:1103.0257 \[astro-ph.CO\]](#).
- [226] A. De Felice, S. Nesseris, and S. Tsujikawa, Observational constraints on dark energy with a fast varying equation of state, *JCAP* **05**, 029, [arXiv:1203.6760 \[astro-ph.CO\]](#).
- [227] C.-J. Feng, X.-Y. Shen, P. Li, and X.-Z. Li, A New Class of Parametrization for Dark Energy without Divergence, *JCAP* **09**, 023, [arXiv:1206.0063 \[astro-ph.CO\]](#).
- [228] H. Wei, X.-P. Yan, and Y.-N. Zhou, Cosmological Applications of Padé Approximant, *JCAP* **01**, 045, [arXiv:1312.1117 \[astro-ph.CO\]](#).
- [229] J. Magaña, V. H. Cárdenas, and V. Motta, Cosmic slowing down of acceleration for several dark energy parametrizations, *JCAP* **10**, 017, [arXiv:1407.1632 \[astro-ph.CO\]](#).
- [230] O. Akarsu, T. Dereli, and J. A. Vazquez, A divergence-free parametrization for dynamical dark energy, *JCAP* **06**, 049, [arXiv:1501.07598 \[astro-ph.CO\]](#).
- [231] S. Pan, J. de Haro, A. Paliathanasis, and R. J. Slagter, Evolution and Dynamics of a Matter creation model, *Mon. Not. Roy. Astron. Soc.* **460**, 1445 (2016), [arXiv:1601.03955 \[gr-qc\]](#).
- [232] R. C. Nunes, A. Bonilla, S. Pan, and E. N. Saridakis, Observational Constraints on  $f(T)$  gravity from varying fundamental constants, *Eur. Phys. J. C* **77**, 230 (2017), [arXiv:1608.01960 \[gr-qc\]](#).
- [233] R. C. Nunes, S. Pan, E. N. Saridakis, and E. M. C. Abreu, New observational constraints on  $f(R)$  gravity from cosmic chronometers, *JCAP* **01**, 005,

- arXiv:1610.07518 [astro-ph.CO].
- [234] J. Magana, V. Motta, V. H. Cardenas, and G. Foex, Testing cosmic acceleration for  $w(z)$  parameterizations using  $f_{gas}$  measurements in galaxy clusters, *Mon. Not. Roy. Astron. Soc.* **469**, 47 (2017), arXiv:1703.08521 [astro-ph.CO].
- [235] W. Yang, S. Pan, and A. Paliathanasis, Latest astronomical constraints on some non-linear parametric dark energy models, *Mon. Not. Roy. Astron. Soc.* **475**, 2605 (2018), arXiv:1708.01717 [gr-qc].
- [236] S. Pan, E. N. Saridakis, and W. Yang, Observational Constraints on Oscillating Dark-Energy Parametrizations, *Phys. Rev. D* **98**, 063510 (2018), arXiv:1712.05746 [astro-ph.CO].
- [237] G. Panotopoulos and A. Rincón, Growth index and statefinder diagnostic of Oscillating Dark Energy, *Phys. Rev. D* **97**, 103509 (2018), arXiv:1804.11208 [astro-ph.CO].
- [238] W. Yang, S. Pan, E. Di Valentino, E. N. Saridakis, and S. Chakraborty, Observational constraints on one-parameter dynamical dark-energy parametrizations and the  $H_0$  tension, *Phys. Rev. D* **99**, 043543 (2019), arXiv:1810.05141 [astro-ph.CO].
- [239] L. G. Jaime, M. Jaber, and C. Escamilla-Rivera, New parametrized equation of state for dark energy surveys, *Phys. Rev. D* **98**, 083530 (2018), arXiv:1804.04284 [astro-ph.CO].
- [240] A. Das, A. Banerjee, S. Chakraborty, and S. Pan, Perfect Fluid Cosmological Universes: One equation of state and the most general solution, *Pramana* **90**, 19 (2018), arXiv:1706.08145 [gr-qc].
- [241] W. Yang, S. Pan, E. Di Valentino, and E. N. Saridakis, Observational constraints on dynamical dark energy with pivoting redshift, *Universe* **5**, 219 (2019), arXiv:1811.06932 [astro-ph.CO].
- [242] X. Li and A. Shafieloo, A Simple Phenomenological Emergent Dark Energy Model can Resolve the Hubble Tension, *Astrophys. J. Lett.* **883**, L3 (2019), arXiv:1906.08275 [astro-ph.CO].
- [243] W. Yang, S. Pan, A. Paliathanasis, S. Ghosh, and Y. Wu, Observational constraints of a new unified dark fluid and the  $H_0$  tension, *Mon. Not. Roy. Astron. Soc.* **490**, 2071 (2019), arXiv:1904.10436 [gr-qc].
- [244] D. Tamayo and J. A. Vazquez, Fourier-series expansion of the dark-energy equation of state, *Mon. Not. Roy. Astron. Soc.* **487**, 729 (2019), arXiv:1901.08679 [astro-ph.CO].
- [245] S. Pan, W. Yang, and A. Paliathanasis, Imprints of an extended Chevallier–Polarski–Linder parametrization on the large scale of our universe, *Eur. Phys. J. C* **80**, 274 (2020), arXiv:1902.07108 [astro-ph.CO].
- [246] M. Rezaei, T. Naderi, M. Malekjani, and A. Mehrabi, A Bayesian comparison between  $\Lambda$ CDM and phenomenologically emergent dark energy models, *Eur. Phys. J. C* **80**, 374 (2020), arXiv:2004.08168 [astro-ph.CO].
- [247] D. Perkovic and H. Stefancic, Barotropic fluid compatible parametrizations of dark energy, *Eur. Phys. J. C* **80**, 629 (2020), arXiv:2004.05342 [gr-qc].
- [248] A. Banihashemi, N. Khosravi, and A. Shafieloo, Dark energy as a critical phenomenon: a hint from Hubble tension, *JCAP* **06**, 003, arXiv:2012.01407 [astro-ph.CO].
- [249] M. Jaber-Bravo, E. Almaraz, and A. de la Macorra, Imprint of a Steep Equation of State in the growth of structure, *Astropart. Phys.* **115**, 102388 (2020), arXiv:1906.09522 [astro-ph.CO].
- [250] H. B. Benaoum, W. Yang, S. Pan, and E. Di Valentino, Modified emergent dark energy and its astronomical constraints, *Int. J. Mod. Phys. D* **31**, 2250015 (2022), arXiv:2008.09098 [gr-qc].
- [251] M. Jaber, G. Arciniega, L. G. Jaime, and O. A. Rodríguez-López, A single parameterization for dark energy and modified gravity models, *Phys. Dark Univ.* **37**, 101069 (2022), arXiv:2102.08561 [astro-ph.CO].
- [252] J. Yang, X.-Y. Fan, C.-J. Feng, and X.-H. Zhai, Latest Data Constraint of Some Parameterized Dark Energy Models, *Chin. Phys. Lett.* **40**, 019801 (2023), arXiv:2211.15881 [astro-ph.CO].
- [253] H. G. Escudero, J.-L. Kuo, R. E. Keeley, and K. N. Abazajian, Early or phantom dark energy, self-interacting, extra, or massive neutrinos, primordial magnetic fields, or a curved universe: An exploration of possible solutions to the  $H_0$  and  $\sigma_8$  problems, *Phys. Rev. D* **106**, 103517 (2022), arXiv:2208.14435 [astro-ph.CO].
- [254] M. N. Castillo-Santos, A. Hernández-Almada, M. A. García-Aspeitia, and J. Magaña, An exponential equation of state of dark energy in the light of 2018 CMB Planck data, *Phys. Dark Univ.* **40**, 101225 (2023), arXiv:2212.01974 [astro-ph.CO].
- [255] W. Yang, W. Giarè, S. Pan, E. Di Valentino, A. Melchiorri, and J. Silk, Revealing the effects of curvature on the cosmological models, *Phys. Rev. D* **107**, 063509 (2023), arXiv:2210.09865 [astro-ph.CO].
- [256] S. Dahmani, A. Bouali, I. El Bojaddaini, A. Errahmani, and T. Ouali, Smoothing the  $H_0$  tension with a phantom dynamical dark energy model, *Phys. Dark Univ.* **42**, 101266 (2023), arXiv:2301.04200 [astro-ph.CO].
- [257] L. A. Escamilla, W. Giarè, E. Di Valentino, R. C. Nunes, and S. Vagnozzi, The state of the dark energy equation of state circa 2023, *JCAP* **05**, 091, arXiv:2307.14802 [astro-ph.CO].
- [258] M. Rezaei, S. Pan, W. Yang, and D. F. Mota, Evidence of dynamical dark energy in a non-flat universe: current and future observations, *JCAP* **01**, 052, arXiv:2305.18544 [astro-ph.CO].
- [259] L. A. Escamilla, O. Akarsu, E. Di Valentino, and J. A. Vazquez, Model-independent reconstruction of the interacting dark energy kernel: Binned and Gaussian process, *JCAP* **11**, 051, arXiv:2305.16290 [astro-ph.CO].
- [260] J. A. Lozano Torres, Generalized emergent dark energy in the late-time Universe, *Mon. Not. Roy. Astron. Soc.* **533**, 1865 (2024).
- [261] J. K. Singh, P. Singh, E. N. Saridakis, S. Myrzakul, and H. Balhara, New Parametrization of the Dark-Energy Equation of State with a Single Parameter, *Universe* **10**, 246 (2024), arXiv:2304.03783 [gr-qc].
- [262] M. Rezaei, Oscillating Dark Energy in Light of the Latest Observations and Its Impact on the Hubble Tension, *Astrophys. J.* **967**, 2 (2024), arXiv:2403.18968 [astro-ph.CO].
- [263] M. Reyhani, M. Najafi, J. T. Firouzjaee, and E. Di Valentino, Structure formation in various dynamical dark energy scenarios, *Phys. Dark Univ.* **44**, 101477 (2024), arXiv:2403.15202 [astro-ph.CO].
- [264] L. A. Escamilla, E. Özlüker, Ö. Akarsu, E. Di Valentino, and J. A. Vázquez, Improved late-time fits with wavelet

- extensions of  $\Lambda$ CDM, *Mon. Not. Roy. Astron. Soc.* **544**, 836 (2025), [arXiv:2408.12516 \[astro-ph.CO\]](#).
- [265] Ö. Akarsu, M. Caruana, K. F. Dialektopoulos, L. A. Escamilla, E. O. Kahya, and J. Levi Said, Hints of sign-changing scalar field energy density and a transient acceleration phase at  $z \sim 2$  from model-agnostic reconstructions (2026), [arXiv:2602.08928 \[astro-ph.CO\]](#).
- [266] M. Chevallier and D. Polarski, Accelerating universes with scaling dark matter, *Int. J. Mod. Phys. D* **10**, 213 (2001), [arXiv:gr-qc/0009008](#).
- [267] E. V. Linder, Exploring the expansion history of the universe, *Phys. Rev. Lett.* **90**, 091301 (2003), [arXiv:astro-ph/0208512](#).
- [268] T. J. Hoyt, D. Rubin, G. Aldering, S. Perlmutter, A. Cuceu, and R. Gupta, Union3.1: Self-consistent Measurements of Host Galaxy Properties for 2000 Type Ia Supernovae (2026), [arXiv:2601.19424 \[astro-ph.CO\]](#).
- [269] K. Lodha *et al.* (DESI), Extended dark energy analysis using DESI DR2 BAO measurements, *Phys. Rev. D* **112**, 083511 (2025), [arXiv:2503.14743 \[astro-ph.CO\]](#).
- [270] A. G. Adame *et al.* (DESI), DESI 2024 VI: cosmological constraints from the measurements of baryon acoustic oscillations, *JCAP* **02**, 021, [arXiv:2404.03002 \[astro-ph.CO\]](#).
- [271] M. Cortês and A. R. Liddle, Interpreting DESI's evidence for evolving dark energy, *JCAP* **12**, 007, [arXiv:2404.08056 \[astro-ph.CO\]](#).
- [272] D. Shlivko and P. J. Steinhardt, Assessing observational constraints on dark energy, *Phys. Lett. B* **855**, 138826 (2024), [arXiv:2405.03933 \[astro-ph.CO\]](#).
- [273] O. Luongo and M. Muccino, Model-independent cosmographic constraints from DESI 2024, *Astron. Astrophys.* **690**, A40 (2024), [arXiv:2404.07070 \[astro-ph.CO\]](#).
- [274] I. D. Gialamas, G. Hütsi, K. Kannike, A. Racioppi, M. Raidal, M. Vasar, and H. Veermäe, Interpreting DESI 2024 BAO: late-time dynamical dark energy or a local effect? (2024), [arXiv:2406.07533 \[astro-ph.CO\]](#).
- [275] B. R. Dinda, A new diagnostic for the null test of dynamical dark energy in light of DESI 2024 and other BAO data, *JCAP* **09**, 062, [arXiv:2405.06618 \[astro-ph.CO\]](#).
- [276] M. Najafi, S. Pan, E. Di Valentino, and J. T. Firouzjaee, Dynamical dark energy confronted with multiple CMB missions, *Phys. Dark Univ.* **45**, 101539 (2024), [arXiv:2407.14939 \[astro-ph.CO\]](#).
- [277] H. Wang and Y.-S. Piao, Dark energy in light of recent DESI BAO and Hubble tension (2024), [arXiv:2404.18579 \[astro-ph.CO\]](#).
- [278] G. Ye, M. Martinelli, B. Hu, and A. Silvestri, Hints of Nonminimally Coupled Gravity in DESI 2024 Baryon Acoustic Oscillation Measurements, *Phys. Rev. Lett.* **134**, 181002 (2025), [arXiv:2407.15832 \[astro-ph.CO\]](#).
- [279] Y. Tada and T. Terada, Quintessential interpretation of the evolving dark energy in light of DESI observations, *Phys. Rev. D* **109**, L121305 (2024), [arXiv:2404.05722 \[astro-ph.CO\]](#).
- [280] Y. Carloni, O. Luongo, and M. Muccino, Does dark energy really revive using DESI 2024 data?, *Phys. Rev. D* **111**, 023512 (2025), [arXiv:2404.12068 \[astro-ph.CO\]](#).
- [281] C.-G. Park, J. de Cruz Pérez, and B. Ratra, Using non-DESI data to confirm and strengthen the DESI 2024 spatially flat  $w_0w_a$ CDM cosmological parametrization result, *Phys. Rev. D* **110**, 123533 (2024), [arXiv:2405.00502 \[astro-ph.CO\]](#).
- [282] K. Lodha *et al.* (DESI), DESI 2024: Constraints on physics-focused aspects of dark energy using DESI DR1 BAO data, *Phys. Rev. D* **111**, 023532 (2025), [arXiv:2405.13588 \[astro-ph.CO\]](#).
- [283] S. Bhattacharya, G. Borghetto, A. Malhotra, S. Parameswaran, G. Tasinato, and I. Zavala, Cosmological constraints on curved quintessence, *JCAP* **09**, 073, [arXiv:2405.17396 \[astro-ph.CO\]](#).
- [284] O. F. Ramadan, J. Sakstein, and D. Rubin, DESI constraints on exponential quintessence, *Phys. Rev. D* **110**, L041303 (2024), [arXiv:2405.18747 \[astro-ph.CO\]](#).
- [285] S. Pourojaghi, M. Malekjani, and Z. Davari, Cosmological constraints on dark energy parametrizations after DESI 2024: Persistent deviation from standard  $\Lambda$ CDM cosmology (2024), [arXiv:2407.09767 \[astro-ph.CO\]](#).
- [286] W. Giarè, M. Najafi, S. Pan, E. Di Valentino, and J. T. Firouzjaee, Robust preference for Dynamical Dark Energy in DESI BAO and SN measurements, *JCAP* **10**, 035, [arXiv:2407.16689 \[astro-ph.CO\]](#).
- [287] J. a. Rebouças, D. H. F. de Souza, K. Zhong, V. Miranda, and R. Rosenfeld, Investigating late-time dark energy and massive neutrinos in light of DESI Y1 BAO, *JCAP* **02**, 024, [arXiv:2408.14628 \[astro-ph.CO\]](#).
- [288] W. Giarè, Dynamical Dark Energy Beyond Planck? Constraints from multiple CMB probes, DESI BAO and Type-Ia Supernovae (2024), [arXiv:2409.17074 \[astro-ph.CO\]](#).
- [289] C.-G. Park, J. de Cruz Perez, and B. Ratra, Is the  $w_0w_a$ CDM cosmological parameterization evidence for dark energy dynamics partially caused by the excess smoothing of Planck CMB anisotropy data? (2024), [arXiv:2410.13627 \[astro-ph.CO\]](#).
- [290] T.-N. Li, Y.-H. Li, G.-H. Du, P.-J. Wu, L. Feng, J.-F. Zhang, and X. Zhang, Revisiting holographic dark energy after DESI 2024 (2024), [arXiv:2411.08639 \[astro-ph.CO\]](#).
- [291] S. Roy Choudhury and T. Okumura, Updated Cosmological Constraints in Extended Parameter Space with Planck PR4, DESI Baryon Acoustic Oscillations, and Supernovae: Dynamical Dark Energy, Neutrino Masses, Lensing Anomaly, and the Hubble Tension, *Astrophys. J. Lett.* **976**, L11 (2024), [arXiv:2409.13022 \[astro-ph.CO\]](#).
- [292] M. A. Sabogal, Ö. Akarsu, A. Bonilla, E. Di Valentino, and R. C. Nunes, Exploring new physics in the late Universe's expansion through non-parametric inference, *Eur. Phys. J. C* **84**, 703 (2024), [arXiv:2407.04223 \[astro-ph.CO\]](#).
- [293] C. Li, J. Wang, D. Zhang, E. N. Saridakis, and Y.-F. Cai, Quantum gravity meets DESI: dynamical dark energy in light of the trans-Planckian censorship conjecture, *JCAP* **08**, 041, [arXiv:2504.07791 \[astro-ph.CO\]](#).
- [294] W. J. Wolf, C. García-García, and P. G. Ferreira, Robustness of Dark Energy Phenomenology Across Different Parameterizations (2025), [arXiv:2502.04929 \[astro-ph.CO\]](#).
- [295] A. J. Shajib and J. A. Frieman, Evolving dark energy models: Current and forecast constraints (2025), [arXiv:2502.06929 \[astro-ph.CO\]](#).
- [296] W. Giarè, T. Mahassen, E. Di Valentino, and S. Pan, An overview of what current data can (and cannot yet) say about evolving dark energy, *Phys. Dark Univ.* **48**,

- 101906 (2025), [arXiv:2502.10264 \[astro-ph.CO\]](#).
- [297] E. Chaussidon *et al.*, Early time solution as an alternative to the late time evolving dark energy with DESI DR2 BAO (2025), [arXiv:2503.24343 \[astro-ph.CO\]](#).
- [298] D. A. Kessler, L. A. Escamilla, S. Pan, and E. Di Valentino, One-parameter dynamical dark energy: Hints for oscillations (2025), [arXiv:2504.00776 \[astro-ph.CO\]](#).
- [299] Y.-H. Pang, X. Zhang, and Q.-G. Huang, The Impact of the Hubble Tension on the Evidence for Dynamical Dark Energy (2025), [arXiv:2503.21600 \[astro-ph.CO\]](#).
- [300] N. Roy, Dynamical dark energy in the light of DESI 2024 data, *Phys. Dark Univ.* **48**, 101912 (2025), [arXiv:2406.00634 \[astro-ph.CO\]](#).
- [301] S. Roy Choudhury, Cosmology in Extended Parameter Space with DESI DR2 BAO: A  $2\sigma+$  Detection of Non-zero Neutrino Masses with an Update on Dynamical Dark Energy and Lensing Anomaly (2025), [arXiv:2504.15340 \[astro-ph.CO\]](#).
- [302] A. Paliathanasis, Observational constraints on dark energy models with  $\Lambda$  as an equilibrium point, *Phys. Dark Univ.* **48**, 101956 (2025), [arXiv:2502.16221 \[astro-ph.CO\]](#).
- [303] M. Scherer, M. A. Sabogal, R. C. Nunes, and A. De Felice, Challenging  $\Lambda$ CDM:  $5\sigma$  Evidence for a Dynamical Dark Energy Late-Time Transition (2025), [arXiv:2504.20664 \[astro-ph.CO\]](#).
- [304] W. Giarè, Dynamical dark energy beyond Planck? Constraints from multiple CMB probes, DESI BAO, and type-Ia supernovae, *Phys. Rev. D* **112**, 023508 (2025), [arXiv:2409.17074 \[astro-ph.CO\]](#).
- [305] T. Liu, X. Li, and J. Wang, Dynamical Dark Energy in the Crosshairs: A Joint Analysis with DESI, Type Ia Supernovae, and TDCOSMO Constraints, *Astrophys. J.* **988**, 243 (2025), [arXiv:2504.21373 \[astro-ph.CO\]](#).
- [306] E. M. Teixeira, W. Giarè, N. B. Hogg, T. Montandon, A. Poudou, and V. Poulin, Implications of distance duality violation for the  $H_0$  tension and evolving dark energy, *Phys. Rev. D* **112**, 023515 (2025), [arXiv:2504.10464 \[astro-ph.CO\]](#).
- [307] F. B. M. d. Santos, J. Morais, S. Pan, W. Yang, and E. Di Valentino, A New Window on Dynamical Dark Energy: Combining DESI-DR2 BAO with future Gravitational Wave Observations (2025), [arXiv:2504.04646 \[astro-ph.CO\]](#).
- [308] M. A. Sabogal and R. C. Nunes, Robust Evidence for Dynamical Dark Energy from DESI Galaxy-CMB Lensing Cross-Correlation and Geometric Probes (2025), [arXiv:2505.24465 \[astro-ph.CO\]](#).
- [309] H. Cheng, E. Di Valentino, L. A. Escamilla, A. A. Sen, and L. Visinelli, Pressure Parametrization of Dark Energy: First and Second-Order Constraints with Latest Cosmological Data (2025), [arXiv:2505.02932 \[astro-ph.CO\]](#).
- [310] L. Herold and T. Karwal, Bayesian and frequentist perspectives agree on dynamical dark energy (2025), [arXiv:2506.12004 \[astro-ph.CO\]](#).
- [311] H. Cheng, E. Di Valentino, and L. Visinelli, Cosmic Strings as Dynamical Dark Energy: Novel Constraints (2025), [arXiv:2505.22066 \[astro-ph.CO\]](#).
- [312] A. N. Ormondroyd, W. J. Handley, M. P. Hobson, and A. N. Lasenby, Comparison of dynamical dark energy with  $\Lambda$ CDM in light of DESI DR2 (2025), [arXiv:2503.17342 \[astro-ph.CO\]](#).
- [313] E. Silva and R. C. Nunes, Testing Signatures of Phantom Crossing through Full-Shape Galaxy Clustering Analysis (2025), [arXiv:2507.13989 \[astro-ph.CO\]](#).
- [314] M. Ishak and L. Medina-Varela, Is this the fall of the  $\Lambda$ CDM throne? Evidence for dynamical dark energy rising from combinations of different types of datasets (2025), [arXiv:2507.22856 \[astro-ph.CO\]](#).
- [315] E. Fazzari, W. Giarè, and E. Di Valentino, Cosmographic Footprints of Dynamical Dark Energy (2025), [arXiv:2509.16196 \[astro-ph.CO\]](#).
- [316] A. Smith, E. Özlüker, E. Di Valentino, and C. van de Bruck, Dynamical Dark Energy Meets Varying Electron Mass: Implications for Phantom Crossing and the Hubble Constant (2025), [arXiv:2510.21931 \[astro-ph.CO\]](#).
- [317] Z. Zhang, T. Xu, and Y. Chen, Dynamical Dark Energy and the Unresolved Hubble Tension: Multi-model Constraints from DESI 2025 and Other Probes (2025), [arXiv:2512.07281 \[astro-ph.CO\]](#).
- [318] H. Cheng, S. Pan, and E. Di Valentino, Beyond Two Parameters: Revisiting Dark Energy with the Latest Cosmic Probes (2025), [arXiv:2512.09866 \[astro-ph.CO\]](#).
- [319] T. Xu, S. Kumar, Y. Chen, A. J. S. Capistrano, and Ö. Akarsu, Probing Dynamical Dark Energy with Late-Time Data: Evidence, Tensions, and the Limits of the  $w_0w_a$ CDM Framework (2026), [arXiv:2602.11936 \[astro-ph.CO\]](#).
- [320] S. M. Carroll, M. Hoffman, and M. Trodden, Can the dark energy equation-of-state parameter  $w$  be less than  $-1$ ?, *Physical Review D* **68**, 10.1103/physrevd.68.023509 (2003).
- [321] R. R. Caldwell and E. V. Linder, Null Impact of the Null Energy Condition in Current Cosmology, *arXiv preprint* (2025), [arXiv:2511.07526 \[astro-ph.CO\]](#).
- [322] Ö. Akarsu, M. Eingorn, L. Perivolaropoulos, A. E. Yükselci, and A. Zhuk, Dynamical dark energy with AdS-dS transitions vs. Baryon Acoustic Oscillations at  $z = 2.3-2.4$  (2025) [arXiv:2504.07299 \[astro-ph.CO\]](#).
- [323] Ö. Akarsu, E. Di Valentino, J. Vyskočil, E. Yılmaz, A. E. Yükselci, and A. Zhuk, Nonlinear Matter Power Spectrum from relativistic  $N$ -body Simulations:  $\Lambda_s$ CDM versus  $\Lambda$ CDM (2025), [arXiv:2510.18741 \[astro-ph.CO\]](#).
- [324] L. A. Anchordoqui, I. Antoniadis, D. Bielli, A. Chatterbhuti, and H. Isono, Thin-wall vacuum decay in the presence of a compact dimension meets the  $H_0$  and  $S_8$  tensions, *JHEP* **07**, 021, [arXiv:2410.18649 \[hep-th\]](#).
- [325] E. Di Valentino *et al.*, Cosmology Intertwined III:  $f\sigma_8$  and  $S_8$ , *Astropart. Phys.* **131**, 102604 (2021), [arXiv:2008.11285 \[astro-ph.CO\]](#).
- [326] V. Sahni and Y. Shtanov, Brane world models of dark energy, *JCAP* **11**, 014, [arXiv:astro-ph/0202346](#).
- [327] J. A. Vazquez, S. Hee, M. P. Hobson, A. N. Lasenby, M. Ibison, and M. Bridges, Observational constraints on conformal time symmetry, missing matter and double dark energy, *JCAP* **07**, 062, [arXiv:1208.2542 \[astro-ph.CO\]](#).
- [328] T. Delubac *et al.* (BOSS), Baryon acoustic oscillations in the Ly $\alpha$  forest of BOSS DR11 quasars, *Astron. Astrophys.* **574**, A59 (2015), [arXiv:1404.1801 \[astro-ph.CO\]](#).
- [329] V. Sahni, A. Shafieloo, and A. A. Starobinsky, Model independent evidence for dark energy evolution from Baryon Acoustic Oscillations, *Astrophys. J. Lett.* **793**, L40 (2014), [arXiv:1406.2209 \[astro-ph.CO\]](#).

- [330] E. Aubourg *et al.* (BOSS), Cosmological implications of baryon acoustic oscillation measurements, *Phys. Rev. D* **92**, 123516 (2015), [arXiv:1411.1074 \[astro-ph.CO\]](#).
- [331] E. Mörtsell and S. Dhawan, Does the Hubble constant tension call for new physics?, *JCAP* **09**, 025, [arXiv:1801.07260 \[astro-ph.CO\]](#).
- [332] V. Poulin, K. K. Boddy, S. Bird, and M. Kamionkowski, Implications of an extended dark energy cosmology with massive neutrinos for cosmological tensions, *Phys. Rev. D* **97**, 123504 (2018), [arXiv:1803.02474 \[astro-ph.CO\]](#).
- [333] Y. Wang, L. Pogosian, G.-B. Zhao, and A. Zucca, Evolution of dark energy reconstructed from the latest observations, *Astrophys. J. Lett.* **869**, L8 (2018), [arXiv:1807.03772 \[astro-ph.CO\]](#).
- [334] A. Banihashemi, N. Khosravi, and A. H. Shirazi, Phase transition in the dark sector as a proposal to lessen cosmological tensions, *Phys. Rev. D* **101**, 123521 (2020), [arXiv:1808.02472 \[astro-ph.CO\]](#).
- [335] A. Banihashemi, N. Khosravi, and A. H. Shirazi, Ginzburg-Landau Theory of Dark Energy: A Framework to Study Both Temporal and Spatial Cosmological Tensions Simultaneously, *Phys. Rev. D* **99**, 083509 (2019), [arXiv:1810.11007 \[astro-ph.CO\]](#).
- [336] Ö. Akarsu, J. D. Barrow, C. V. R. Board, N. M. Uzun, and J. A. Vazquez, Screening  $\Lambda$  in a new modified gravity model, *Eur. Phys. J. C* **79**, 846 (2019), [arXiv:1903.11519 \[gr-qc\]](#).
- [337] A. Perez, D. Sudarsky, and E. Wilson-Ewing, Resolving the  $H_0$  tension with diffusion, *Gen. Rel. Grav.* **53**, 7 (2021), [arXiv:2001.07536 \[astro-ph.CO\]](#).
- [338] Ö. Akarsu, N. Katirci, S. Kumar, R. C. Nunes, B. Öztürk, and S. Sharma, Rastall gravity extension of the standard  $\Lambda$ CDM model: theoretical features and observational constraints, *Eur. Phys. J. C* **80**, 1050 (2020), [arXiv:2004.04074 \[astro-ph.CO\]](#).
- [339] Ruchika, S. A. Adil, K. Dutta, A. Mukherjee, and A. A. Sen, Observational constraints on axion(s) dark energy with a cosmological constant, *Phys. Dark Univ.* **40**, 101199 (2023), [arXiv:2005.08813 \[astro-ph.CO\]](#).
- [340] A. Paliathanasis and G. Leon, Dynamics of a two scalar field cosmological model with phantom terms, *Class. Quant. Grav.* **38**, 075013 (2021), [arXiv:2009.12874 \[gr-qc\]](#).
- [341] A. Bonilla, S. Kumar, and R. C. Nunes, Measurements of  $H_0$  and reconstruction of the dark energy properties from a model-independent joint analysis, *Eur. Phys. J. C* **81**, 127 (2021), [arXiv:2011.07140 \[astro-ph.CO\]](#).
- [342] G. Acquaviva, Ö. Akarsu, N. Katirci, and J. A. Vazquez, Simple-graduated dark energy and spatial curvature, *Phys. Rev. D* **104**, 023505 (2021), [arXiv:2104.02623 \[astro-ph.CO\]](#).
- [343] S. Bag, V. Sahni, A. Shafieloo, and Y. Shtanov, Phantom Braneworld and the Hubble Tension, *Astrophys. J.* **923**, 212 (2021), [arXiv:2107.03271 \[astro-ph.CO\]](#).
- [344] R. C. Bernardo, D. Grandón, J. Said Levi, and V. H. Cárdenas, Parametric and nonparametric methods hint dark energy evolution, *Phys. Dark Univ.* **36**, 101017 (2022), [arXiv:2111.08289 \[astro-ph.CO\]](#).
- [345] L. A. Escamilla and J. A. Vazquez, Model selection applied to reconstructions of the Dark Energy, *Eur. Phys. J. C* **83**, 251 (2023), [arXiv:2111.10457 \[astro-ph.CO\]](#).
- [346] E. Ozulker, Is the dark energy equation of state parameter singular?, *Phys. Rev. D* **106**, 063509 (2022), [arXiv:2203.04167 \[astro-ph.CO\]](#).
- [347] H. Moshafi, H. Firouzjahi, and A. Talebian, Multiple Transitions in Vacuum Dark Energy and  $H_0$  Tension, *Astrophys. J.* **940**, 121 (2022), [arXiv:2208.05583 \[astro-ph.CO\]](#).
- [348] A. van de Venn, D. Vasak, J. Kirsch, and J. Struckmeier, Torsional dark energy in quadratic gauge gravity, *Eur. Phys. J. C* **83**, 288 (2023), [arXiv:2211.11868 \[gr-qc\]](#).
- [349] M. Malekjani, R. M. Conville, E. Ó. Colgáin, S. Pourojaghi, and M. M. Sheikh-Jabbari, On redshift evolution and negative dark energy density in Pantheon + Supernovae, *Eur. Phys. J. C* **84**, 317 (2024), [arXiv:2301.12725 \[astro-ph.CO\]](#).
- [350] J. A. Vázquez, D. Tamayo, G. Garcia-Arroyo, I. Gómez-Vargas, I. Quiros, and A. A. Sen, Coupled multiscalar field dark energy, *Phys. Rev. D* **109**, 023511 (2024), [arXiv:2305.11396 \[astro-ph.CO\]](#).
- [351] B. Alexandre, S. Gielen, and J. Magueijo, Overall signature of the metric and the cosmological constant, *JCAP* **02**, 036, [arXiv:2306.11502 \[hep-th\]](#).
- [352] S. A. Adil, U. Mukhopadhyay, A. A. Sen, and S. Vagnozzi, Dark energy in light of the early JWST observations: case for a negative cosmological constant?, *JCAP* **10**, 072, [arXiv:2307.12763 \[astro-ph.CO\]](#).
- [353] E. A. Paraskevas and L. Perivolaropoulos, The density of virialized clusters as a probe of dark energy, *Mon. Not. Roy. Astron. Soc.* **531**, 1021 (2024), [arXiv:2308.07046 \[astro-ph.CO\]](#).
- [354] R. Y. Wen, L. T. Hergt, N. Afshordi, and D. Scott, A Glitch in Gravity: Cosmic Lorentz-Violation from Fiery Big Bang to Glacial Heat Death, *Astrophys. Space Sci. Proc.* **61**, 435 (2025), [arXiv:2412.09568 \[astro-ph.CO\]](#).
- [355] A. De Felice, S. Kumar, S. Mukohyama, and R. C. Nunes, Observational bounds on extended minimal theories of massive gravity: new limits on the graviton mass, *JCAP* **04**, 013, [arXiv:2311.10530 \[astro-ph.CO\]](#).
- [356] N. Menci, S. A. Adil, U. Mukhopadhyay, A. A. Sen, and S. Vagnozzi, Negative cosmological constant in the dark energy sector: tests from JWST photometric and spectroscopic observations of high-redshift galaxies, *JCAP* **07**, 072, [arXiv:2401.12659 \[astro-ph.CO\]](#).
- [357] R. Calderon *et al.* (DESI), DESI 2024: reconstructing dark energy using crossing statistics with DESI DR1 BAO data, *JCAP* **10**, 048, [arXiv:2405.04216 \[astro-ph.CO\]](#).
- [358] H. Wang, Z.-Y. Peng, and Y.-S. Piao, Can recent DESI BAO measurements accommodate a negative cosmological constant?, *Phys. Rev. D* **111**, L061306 (2025), [arXiv:2406.03395 \[astro-ph.CO\]](#).
- [359] E. Ó. Colgáin, S. Pourojaghi, and M. M. Sheikh-Jabbari, Implications of DES 5YR SNe Dataset for  $\Lambda$ CDM, *Eur. Phys. J. C* **85**, 286 (2025), [arXiv:2406.06389 \[astro-ph.CO\]](#).
- [360] U. K. Tyagi, S. Haridasu, and S. Basak, Holographic and gravity-thermodynamic approaches in entropic cosmology: Bayesian assessment using late-time data, *Phys. Rev. D* **110**, 063503 (2024), [arXiv:2406.07446 \[astro-ph.CO\]](#).
- [361] V. A. Pai, S. Nelleri, and T. K. Mathew, Dissipative  $\Lambda$ CDM model with causal sign-switching bulk viscous pressure, *Eur. Phys. J. C* **85**, 593 (2025), [arXiv:2409.10919 \[astro-ph.CO\]](#).

- [362] P. Mukherjee, D. Kumar, and A. A. Sen, Quintessential Implications of the presence of AdS in the Dark Energy sector (2025), [arXiv:2501.18335 \[astro-ph.CO\]](#).
- [363] D. Efstratiou and L. Perivolaropoulos, Metastable cosmological constant and gravitational bubbles: Ultralate-time transitions in modified gravity, *Phys. Rev. D* **111**, 123546 (2025), [arXiv:2503.11365 \[gr-qc\]](#).
- [364] A. Gómez-Valent and A. González-Fuentes, Effective Phantom Divide Crossing with Standard and Negative Quintessence (2025), [arXiv:2508.00621 \[astro-ph.CO\]](#).
- [365] H. Wang and Y.-S. Piao, Can the universe experience an AdS landscape since matter-radiation equality?, *Phys. Rev. D* **112**, 083553 (2025), [arXiv:2506.04306 \[gr-qc\]](#).
- [366] D. Tamayo, Thermodynamics of sign-switching dark energy models (2025), [arXiv:2503.16272 \[astro-ph.CO\]](#).
- [367] A. González-Fuentes and A. Gómez-Valent, Reconstruction of dark energy and late-time cosmic expansion using the Weighted Function Regression method (2025), [arXiv:2506.11758 \[astro-ph.CO\]](#).
- [368] M. Bouhmadi-López and B. Ibarra-Uriondo, Cosmological perturbations for smooth sign-switching dark energy models (2025), [arXiv:2506.18992 \[gr-qc\]](#).
- [369] M. Yadav, A. Dixit, A. Pradhan, and M. S. Barak, Empirical validation: Investigating the  $\Lambda$ CDM model with new DESI BAO observations, *JHEAp* **49**, 100453 (2026), [arXiv:2509.26049 \[astro-ph.CO\]](#).
- [370] K. Lehnert, Hitchhiker's Guide to the Swampland: The Cosmologist's Handbook to the string-theoretical Swampland Programme (2025), [arXiv:2509.02632 \[hep-th\]](#).
- [371] H. S. Tan, Inferring Cosmological Parameters with Evidential Physics-Informed Neural Networks, *Universe* **11**, 403 (2025), [arXiv:2509.24327 \[astro-ph.CO\]](#).
- [372] D. Pedrotti, L. A. Escamilla, V. Marra, L. Perivolaropoulos, and S. Vagnozzi, BAO miscalibration cannot rescue late-time solutions to the Hubble tension, *Phys. Rev. D* **113**, 043507 (2026), [arXiv:2510.01974 \[astro-ph.CO\]](#).
- [373] M. Forconi and A. Melchiorri, The impact on non-Gaussianities of the ISW-Lensing correlation in non-standard cosmologies, *Phys. Dark Univ.* **50**, 102126 (2025).
- [374] E. N. Nyergesy, I. G. Márián, A. Trombettoni, and I. Nándori, From negative to positive cosmological constant through decreasing temperature of the Universe: connection with string theory and spacetime foliation results (2025), [arXiv:2510.02244 \[gr-qc\]](#).
- [375] P. A. R. Ade *et al.* (Planck), Planck 2015 results. XIV. Dark energy and modified gravity, *Astron. Astrophys.* **594**, A14 (2016), [arXiv:1502.01590 \[astro-ph.CO\]](#).
- [376] E. V. Linder, The Mirage of  $w=-1$  (2007), [arXiv:0708.0024 \[astro-ph\]](#).
- [377] Y.-F. Cai, E. N. Saridakis, M. R. Setare, and J.-Q. Xia, Quintom Cosmology: Theoretical implications and observations, *Phys. Rept.* **493**, 1 (2010), [arXiv:0909.2776 \[hep-th\]](#).
- [378] S. Vagnozzi, New physics in light of the  $H_0$  tension: An alternative view, *Phys. Rev. D* **102**, 023518 (2020), [arXiv:1907.07569 \[astro-ph.CO\]](#).
- [379] J. Torrado and A. Lewis, Cobaya: Code for Bayesian Analysis of hierarchical physical models, *JCAP* **05**, 057, [arXiv:2005.05290 \[astro-ph.IM\]](#).
- [380] A. Lewis, A. Challinor, and A. Lasenby, Efficient computation of CMB anisotropies in closed FRW models, *Astrophys. J.* **538**, 473 (2000), [arXiv:astro-ph/9911177](#).
- [381] C. Howlett, A. Lewis, A. Hall, and A. Challinor, Cmb power spectrum parameter degeneracies in the era of precision cosmology, *Journal of Cosmology and Astroparticle Physics* **2012** (04), 027–027.
- [382] W. Fang, W. Hu, and A. Lewis, Crossing the Phantom Divide with Parameterized Post-Friedmann Dark Energy, *Phys. Rev. D* **78**, 087303 (2008), [arXiv:0808.3125 \[astro-ph\]](#).
- [383] A. Gelman and D. B. Rubin, Inference from Iterative Simulation Using Multiple Sequences, *Statist. Sci.* **7**, 457 (1992).
- [384] A. Lewis, GetDist: a Python package for analysing Monte Carlo samples, *JCAP* **08**, 025, [arXiv:1910.13970 \[astro-ph.IM\]](#).
- [385] N. Aghanim *et al.* (Planck), Planck 2018 results. V. CMB power spectra and likelihoods, *Astron. Astrophys.* **641**, A5 (2020), [arXiv:1907.12875 \[astro-ph.CO\]](#).
- [386] N. Aghanim *et al.* (Planck), Planck 2018 results. VIII. Gravitational lensing, *Astron. Astrophys.* **641**, A8 (2020), [arXiv:1807.06210 \[astro-ph.CO\]](#).
- [387] G. Efstathiou and S. Gratton, A Detailed Description of the CamSpec Likelihood Pipeline and a Re-analysis of the Planck High Frequency Maps (2019), [arXiv:1910.00483 \[astro-ph.CO\]](#).
- [388] E. Rosenberg, S. Gratton, and G. Efstathiou, CMB power spectra and cosmological parameters from Planck PR4 with CamSpec, *Mon. Not. Roy. Astron. Soc.* **517**, 4620 (2022), [arXiv:2205.10869 \[astro-ph.CO\]](#).
- [389] J. Carron, M. Mirmelstein, and A. Lewis, CMB lensing from Planck PR4 maps, *JCAP* **09**, 039, [arXiv:2206.07773 \[astro-ph.CO\]](#).
- [390] D. H. Weinberg, M. J. Mortonson, D. J. Eisenstein, C. Hirata, A. G. Riess, and E. Rozo, Observational Probes of Cosmic Acceleration, *Phys. Rept.* **530**, 87 (2013), [arXiv:1201.2434 \[astro-ph.CO\]](#).
- [391] T. M. C. Abbott *et al.* (DES), The Dark Energy Survey: Cosmology Results with  $\sim 1500$  New High-redshift Type Ia Supernovae Using the Full 5 yr Data Set, *Astrophys. J. Lett.* **973**, L14 (2024), [arXiv:2401.02929 \[astro-ph.CO\]](#).
- [392] H. Akaike, A new look at the statistical model identification, *IEEE Transactions on Automatic Control* **19**, 716 (1974).
- [393] A. R. Liddle, Information criteria for astrophysical model selection, *Mon. Not. Roy. Astron. Soc.* **377**, L74 (2007), [arXiv:astro-ph/0701113](#).
- [394] A. Heavens, Y. Fantaye, E. Sellentin, H. Eggers, Z. Hosenie, S. Kroon, and A. Mootoivaloo, No evidence for extensions to the standard cosmological model, *Phys. Rev. Lett.* **119**, 101301 (2017), [arXiv:1704.03467 \[astro-ph.CO\]](#).
- [395] A. Heavens, Y. Fantaye, A. Mootoivaloo, H. Eggers, Z. Hosenie, S. Kroon, and E. Sellentin, Marginal Likelihoods from Monte Carlo Markov Chains (2017), [arXiv:1704.03472 \[stat.CO\]](#).
- [396] R. Trotta, Bayes in the sky: Bayesian inference and model selection in cosmology, *Contemp. Phys.* **49**, 71 (2008), [arXiv:0803.4089 \[astro-ph\]](#).
- [397] G. Cowan, K. Cranmer, E. Gross, and O. Vitells, Asymptotic formulae for likelihood-based tests of new physics, *Eur. Phys. J. C* **71**, 1554 (2011), [Erratum: *Eur.Phys.J.C* 73, 2501 (2013)], [arXiv:1007.1727 \[physics.data-an\]](#).

- [398] S. S. Wilks, The Large-Sample Distribution of the Likelihood Ratio for Testing Composite Hypotheses, [Annals Math. Statist.](#) **9**, 60 (1938). 849 (2018).
- [399] W. Handley, fgivenx: A python package for functional posterior plotting, [Journal of Open Source Software](#) **3**,